UNIVERSITY OF ICELAND

University of Akureyri

Improved design of hydroelectric projects. Hydraulic roughness of TBM-bored tunnels.

An experimental study.

Anna Kasprzyk

Katarzyna Filipek

RES | THE SCHOOL *for* RENEWABLE ENERGY SCIENCE

Improved design of hydroelectric projects. Hydraulic roughness of TBM-bored tunnels.

An experimental study.

Anna Kasprzyk

Katarzyna Filipek

A 30 ECTS credit units Master´s thesis

Supervisors

Dr. Kristín Martha Hákonardóttir

Dr. Jónas Elíason

A Master´s thesis was supported by a grant from Iceland, Liechtenstein and Norway through the EEA Financial Mechanism - Project PL0460 in affiliation with

University of Iceland &

University of Akureyri

Akureyri, February 2011

Improved design of hydroelectric project. Hydraulic roughness of TBM-bored tunnels.

An experimental study.

A 30 ECTS credit units Master´s thesis

University of Iceland

Sæmundargötu 2

101 Reykjavík

Phone 525 4000

Fax 552 1331

Email hi@hi.is

University of Akureyri

Nordurslod 2

600 Akureyri, Iceland

Printed in 28.01.2011

at Stell Printing in Akureyri, Iceland

ABSTRACT

The purpose of this thesis is to link head loss coefficients in rough pipes to the physical roughness of the surface through measurements of head loss in fully turbulent flow. It is generally regarded that hydraulic roughness is some function of the height, spacing, density and nature of the physical roughness under consideration. Attempts have been made to link hydraulic roughness to physical roughness of an irregular surface. Those have, however, been incomplete and conducted at flow states which do not allow concrete conclusions to be drawn. Further research on the topic is therefore needed to define a fully mature assessment methodology.

The interior of the pipe were scanned and different methods to convert physical roughness to hydraulic roughness were tested. Two different types of profiles were identified and different methods suggested for each type. The thesis shows connection between the experimental results with measured head loss in hydroelectric projects in operation and deduces hydraulic friction values for different rock types in tunnels excavated with tunnel boring machines. Hydraulic head loss coefficients for different rock types were finally suggested based on the accuracy of the method tested in the pipe flow experiments.

Tunnel boring machine (TBM) technology has not been used for the construction of water tunnels in Poland. However, the methodology implemented for this thesis project offers more accurate head loss estimation, crucial for future investments in Polish HEPs.

PREFACE

This Master's thesis is the final project for receiving the Master of Science degree in Hydropower in affiliation with the University of Iceland and the University of Akureyri. It has been carried out in cooperation with Verkis Company between November 2010 and February 2011.

We specially want to thank our supervisors Dr Kristín Martha Hákonardóttir for her constant advice and support and to Dr Jónas Elíason for his encouragement and special interest in our work.

We would also like to thank our hostess in guest house Baldursbrá Mrs. Evelyne Nihouarn and her husband for their hospitality and kindness during the time we spend in Reykjavik.

Finally we would like to direct our warmest thanks to our parents and whole families and friends for always supporting us.

Thank you!

Akureyri, February 2011

Anna Kasprzyk and Katarzyna Filipek

TABLE OF CONTENTS

List of Figures

List of Tables

List of Symbols

A = pipe's cross-sectional area, m^2

a = amplitude of sinusoid, m

D = pipe's diameter, m

ΔH = pressure head, m

V = tank's volume, m^3

f = Darcy-Weisbach friction factor, dimensionless

g = acceleration due to gravity, m/s^2

HEP = hydroelectric projects

h = roughness height, mm

h_l = head loss due to friction, m

h_s = singular head loss, m

K = coefficient depend on the nature of local resistance, dimensionless

k_s = equivivalent sand grain diameter (Nikuradse), mm

L = length, m

m = hydraulic radius, ft

n = resistance coefficient (Mannings's n), $s/m^{1/3}$

Q = volume rate of flow, m^3/s

R = hydraulic radius, m

Re = Reynold's Number, dimensionless

r_i = range of the laser, m

S = slope of the water surface or the linear hydraulic head loss, dimensionless

t = time, s

T = temperature of water, ℃

TBM = tunnel boring machine

T_n = number of points in series

u = velocity in the flow direction, m/s

$\overline{u}$ = mean velocity, m/s

u_* = shear velocity, m/s

u_R = velocity at the center of the pipe, m/s

λ = wavelength, m

ν = kinematic viscosity, m^2/s

σ = standard deviation, mm

χ = Heerman’s roughness parameter, dimensionless

1 INTRODUCTION

For estimating head loss through tunnel systems in hydroelectric projects (HEP), hydraulic friction factors are used. Incomplete information of technical data and literature on the roughness of unlined tunnel excavated with tunnel boring machines (TBM) has led to the development of an improve methodology to estimate the head loss coefficient along the tunnel and thus a more accurate prediction of the power output of HEP.

Pegram and Pennington (1996) conducted a study which presents the results obtained from a research project carried out at the University of Natal in Durban, South Africa. The paper shows research on hydraulic roughness for the delivery tunnel which is located south of the Lesotho Highlands Water Project. The hydraulic roughness of unlined TBM tunnels (concrete and shotcrete lining, unlined sandstone and granite) was estimated from physical roughness data. All the measurements were based on results provided by scanning strips of tunnel wall surfaces at regular intervals. The representative value of physical roughness height for each measured profile was transformed to hydraulic roughness coefficient and an average value for the different rock types and linings obtained.

Prediction of the hydraulic roughness of the Kárahnnjúkar headrace tunnel was obtained through in situ observations of the tunnel wall surface similar to the Lesotho project in 2005–2007, during the construction of the headrace tunnel. The tunnel was predominantly bored through volcanic rock (basalt) and mainly left unlined. The weakest link in the methodology adopted at Kárahnjúkar involved mapping measured physical roughness on to hydraulic roughness. All the results are shown in a report provided by Kristín Martha Hákonardóttir, Gunnar Tómasson, Joe Kaelin and Björn Stefànsson (Landsvirkjun, 2009).

In the study presented here the relationship between measured physical roughness of tunnel walls and hydraulic roughness is linked through small scale experiments which were carried out by authors of this thesis. Pressure drop through straight pipes of different physical roughness in a fully turbulent flow state is firstly measured directly then calculated from physical roughness profiles. The results are finally compared between the two studies above (Lesotho and Kárahnnjúkar).

This thesis is split into four main parts. Chapter two presents experimental design and method with experimental apparatus. Chapter three shows hydraulic roughness of the pipes calculated from laser scans of the pipe surfaces; hydraulic roughness calculated from measured head loss and compared with hydraulic roughness calculated from the physical roughness data; remarks on the best method for the conversion are concluded. Chapter four provides shows data of head loss measurements in Kárahnjúkar HEPs in operation and a deduction of hydraulic friction factors for different rock types from the data; the comparison between experimental results and deduced data from tunnels in operation; remarks on values of hydraulic roughness for different rock types in TBM bored tunnels.

2 LABORATORY EXPERIMENTS: HEAD LOSS MEASUREMENTS

There are many advantages of HEPs compared with other types of power plants. Most important thing is that water is the renewable source of energy. HEPs don't require any fuel for generation of electricity hence they don't cause any air-pollution and the cost of electricity, produced by them, is more or less constant. They can help in irrigation of farm lands, may prevent from floods or even develop public recreational facilities like water parks, sports or gardens. A Hydropower Plant has a high capital cost but maintenance costs are only minimal when looking at some other sources of energy production.

Hydropower plants convert the energy in moving water to electricity. Their main structures often include dams, reservoirs, turbines, generators, water conveyance tunnels and canals, surge facilities and penstocks (pipes) (Figure 2.1).

The water power of individual projects is determined by several factors, but the most important are head and discharge. In a typical Hydro system the water in the reservoir is considered stored energy. The water in motion, flowing through open control gates and then through a penstock becomes kinetic energy. The head refers to the vertical distance between the water surface and the turbines. It creates pressure at the bottom end of a pipeline which produces the force that drives the turbine. Discharge is the amount of water measured in volume per unit of time carried downhill and through the turbine. When those two factors increase the same will happen with generated electricity.

Head loss refers to the loss of water energy due to along the waterways from the reservoir to the turbines. The head lost slows the water flow and decreases water pressure at the turbines leading to less electricity generated.

The aim of this chapter is to investigate the hydraulic roughness of unlined TBM-bored tunnels walls and to establish corresponding hydraulic friction factors for different rock types. In order to do that, a number of simple experiments were conducted. The experiments involved running water through rough pipes and measuring head loss. The specific description of that process will be discussed further in that chapter.

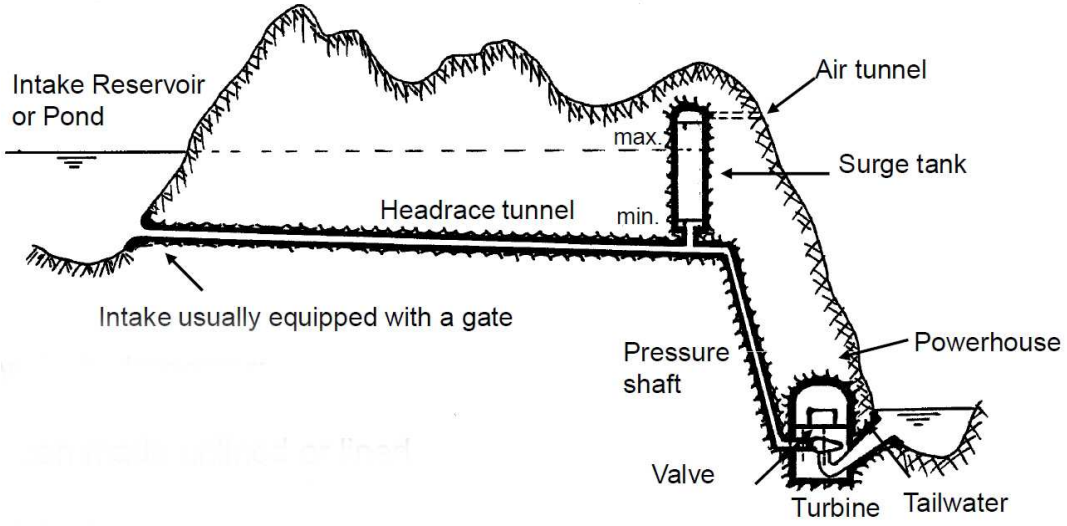

Figure 2.1 The HEP sketch (Leifsson, 2010).

The experiments were carried out in a University of Iceland laboratory in Reykjavik. The main objective of the experiments was to

1) establish a relationship between the rough surface inside the pipes and the measured head loss, and
2) establish a relationship between the surface roughness of the pipes and Nikuradse's equivalent sand grain roughness, k_s and finally obtain the Darcy-Weisbach friction factor, f.

2.1.1 Experimental apparatus

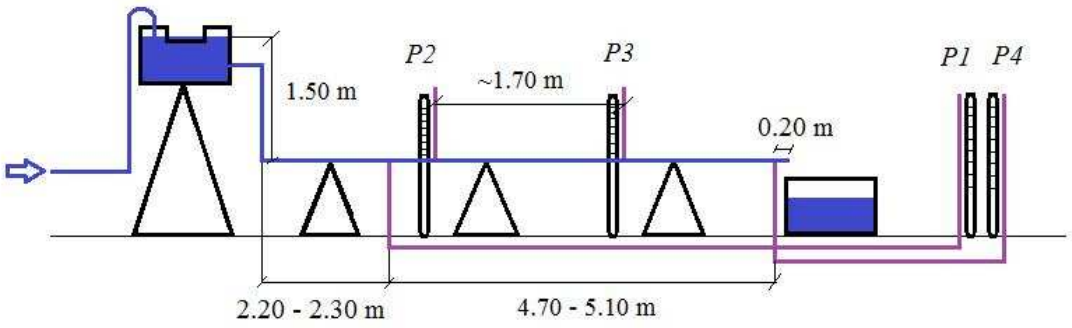

Figure 2.2 The setup sketch.

Water fills up an artificial reservoir and drops ~1.15m, as it's shown in the setup sketch and also in Figure 2.3. The reservoir creates pressure head to drive the water trough different setups of rough pipes.

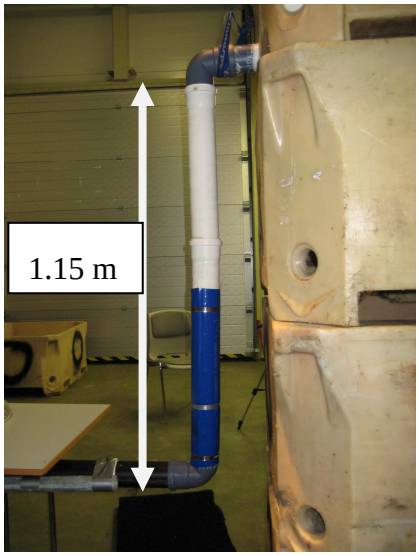

Figure 2.3 Water drop from the artificial reservoir to the actual setup.

Each experimental setup has four pressure tube connections. First tube P_1 (going in the direction of the water flow in the pipes) is connected at a 2.2 - 2.3m distance from the bottom 90˚ smooth bend shown on Figure 2.3. The distance was based on calculations of the developing length of the high Reynolds number flow from the bend. The additional 1.15 vertical meters from the reservoir to the 90˚ bend also stabilize the flow.

The fourth of the pressure tubes P_4 is connected 0.2m from the end of the pipe. It is to avoid an extra disturbance from the outflow. P_1 and P_4 are connected to one manometer shown in Figure 2.4 below.

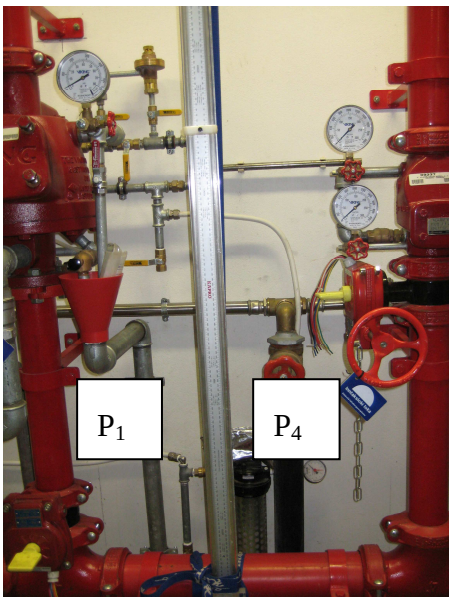

Figure 2.4 Manometer connecting P_1 and P_4 pressure tubes.

The second and the third pressure tube named correspondingly P_2 and P_3 are the pizometers placed at a ~1.7m distance from each other as shown in Figure 2.5.

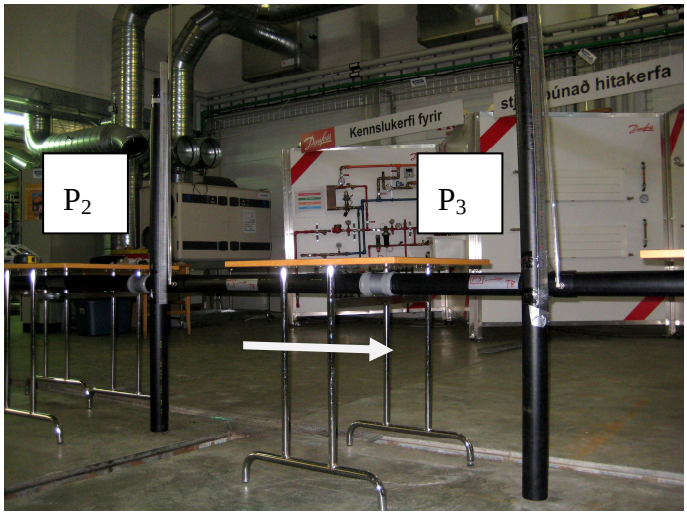

Figure 2.5 Piezometers P_2 and P_3 connected to the setup.

In order to calculate discharge through the pipe system, a 426.6l tank was used at the end of the model (see Figure 2.6). Special grating is installed in the middle of the tank to calm the water surface during filling up in order to get more accurate results and minimize errors.

Figure 2.6 The outflow tank.

Different length between pressure measurements were used in different setups. Their specifics are shown in Table 2-1

Table 2-1 Description of the setups.

Setup name	Description	Total length between P_1 and P_4, m
T1,3	5 PCV smooth pipes	5.04
T7	1 PCV smooth pipe	3.52
T4	5 PCV pipes three times steel brushed inside	5.07
T5	6 PCV pipes three times steel brushed inside with spiral 1 mm deep groove every 14 mm	5.06
T6	6 PCV pipes three times steel brushed inside with spiral 1.5 mm deep groove every 14 mm	5.03
T8	6 PCV pipes three times steel brushed inside with spiral 1 mm deep groove every 7 mm	4.87
T9	6 PCV pipes three times steel brushed inside with two spiral groove; 1.5 mm deep every 7 mm and 2 mm deep every 14 mm	4.74
T10	5 PCV pipes three times steel brushed inside, painted with sand – paint mixture twice and just paint in the end.	5.00

After the experiments two representative pipes from each setup were sent to a workshop and cut in half. The results of that cat are shown in Figure 2.7 and Figure 2.8. Not all of the setups are shown because T1,3 and T7 served as a base for further reshape. Later in time, cut pipes were sent for precise laser scanning to Switzerland.

Figure 2.7 The cross-sections of different pipe setups.

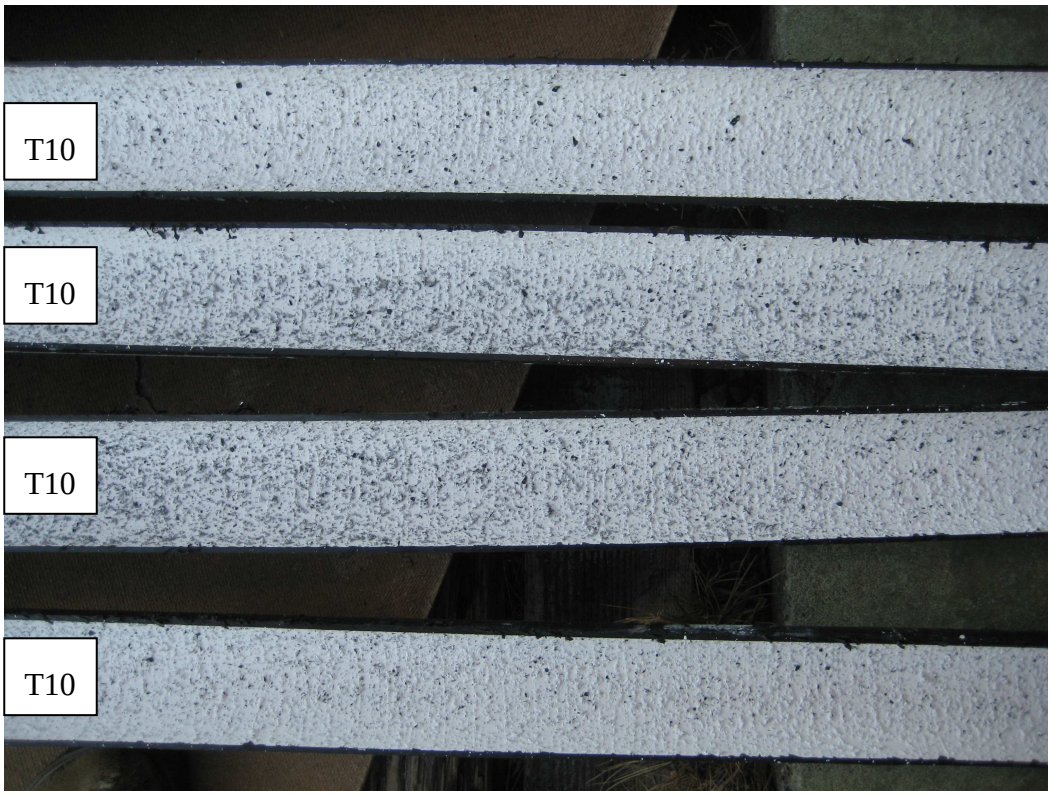

Figure 2.8 The cross-section of T10 setup.

2.1.2 Experimental Technique

In each experiment first thing done was to stabilize water level in the reservoir. This was made by filling the reservoir up until it was full and water started flowing over the spillway and a constant depth was acquired. After doing so, the loss and discharge rate were measured five times per setup to avoid as much human errors as possible. This data as used to calculate average values of the Darcy-Weisbach friction factor, *f*, Nikuradse's equivalent sand grain roughness, k_s and the Manning number, *n* for each pipe setup. All experiments were carried out with rather similar initial conditions and yielded similar results. Average discharge varied from 6 to 8l/s.

2.2 Experimental Observations and Results

Experimental results are shown in appendix A. Reported data is time for discharge calculations of each of the measurement and pressure drop in the manometers.

2.3 Modeling and errors

2.3.1 Modeling

Eight tests and over fifty measurements were conducted over one month period. All of the exact results are shown in appendix A. The initial data for each setup is shown in Table 2-2.

Table 2-2 Initial data for each setup

Symbol	Description	Value	Unit
ΔH	pressure head	1.536	m
V	tank's volume	0.4266	m^3
D	pipe's diameter	0.0692	m
A	pipe's cross-sectional area	0.003759	m^2
T	temperature of water	1ºC	ºC
υ	kinematic viscosity	$1.734 \cdot 10^{-6}$	m^2/s

Flow in pipes may be either laminar or turbulent. Laminar flow occurs when the paths of individual fluid particles flow in parallel layers, with no crossing one another. Turbulent flow is chaotic, random with different paths of fluid particles.

The state of flow of fluid is given by the Reynolds Number, which measures the ratio of internal forces to viscous forces in the fluid (Table 2-3)

$$\mathrm{Re} = \frac{Du}{\nu}$$

Equation 2-1

where:

Re = Reynolds number

D = diameter of conduit [m]

υ = kinematic viscosity [m^2/s]

Laminar flow occurs for *Re* < 2000, turbulent for *Re* > 3000-5000.

Discharge of the flow is calculated (Table 2-3) from the volume of the tank shown in Figure 2.6 and the measured time of filling of the tank.

$$Q = \frac{V}{T},$$

Equation 2-2

where:

Q = discharge [l/s]

V = volume of the tank [l]

T = time of each measurement [s]

Velocity of the flow is given by the ratio between discharge and pipe's cross-sectional area (Table 2-3)

$$u = \frac{Q}{A},$$

Equation 2-3

where:

u = mean velocity of fluid [m/s]

A = cross-sectional area of a pipe [m^2]

Table 2-3 Average values of discharge, velocity and Reynolds number for each setup.

Set	***Q* [m^3/s]**	***u*[m/s]**	***Re* [-]**
T7	0.0082	2.2	$8.5 \cdot 10^4$
T1,3	0.0078	2.1	$8.1 \cdot 10^4$
T4	0.0073	1.9	$7.6 \cdot 10^4 \cdot$
T5	0.0068	1.8	$7.1 \cdot 10^4$
T6	0.0063	1.7	$6.6 \cdot 10^4$
T8	0.0068	1.8	$7.1 \cdot 10^4$
T9	0.0071	1.9	$7.4 \cdot 10^4$
T10	0.0057	1.6	$6.1 \cdot 10^4$

A number of experiments were carried out with rather similar initial conditions and yielded similar results.

The smallest value of flow rate was observed in T10. That is because the interior of the pipe was covered with paint and sand and it was relatively rough. The highest flow speed appeared in set T7 with a completely smooth pipe.

Reynold's Number in each test showed that flow through pipes was fully turbulent.

In designing water tunnels many factors need to be known and expected hydraulic resistance is one of them. It is possible to calculate the resistance (see Table 2-4) due to wall friction knowing the diameter, flow rate and head loss along a pipe stretch of length *L*. This dependence is given by the Darcy – Weisbach equation

$$h_f = f \frac{L}{D} \frac{u^2}{2g},$$

Equation 2-4

where:

h_f = head loss due to friction [m]

f = Darcy – Weisbach friction factor [-]

L = length between manometers [m]

A single pipe system may have many minor losses. Since all are correlated with $u^2/2g$, where g is acceleration due to gravity, they can be summed into single total system loss if the pipe has constant diameter:

$$\Delta H = h_f + \sum h_s = \frac{u^2}{2g}\left(f\frac{L}{D} + \sum_j K_j \right),$$

Equation 2-5

where:

ΔH = pressure head [m]

h_s = singular head loss [m]

K = coefficient depend on the nature of local resistance

$$h_s = \sum_j K_j \frac{u^2}{2g},$$

Equation 2-6

K is non-dimensional factor, like f, and is often correlated with the raw size of the pipe.

Singular losses occur at the connections between the pipes. The coefficient at each connection was calculated by comparing set T1,3 with T7.

Set T1,3 consists of five smooth pipes with four connections, while set T7 consist of a six meters long smooth pipe.

Coefficient depend on the nature of local resistance, K is equal to 0.0302.

The frictional losses, h_f are the difference between measured pressure loss (observed data) and a sum of all singular losses for each setup (see Table 2-4)

Table 2-4 Average values of head losses and friction factor for each setup.

Set	**h_f [m]**	**Friction factor [-]**
T4	0.3802	0.0271
T5	0.4593	0.0378
T6	0.4799	0.0462
T8	0.4404	0.0378
T9	0.3775	0.0301
T10	0.3775	0.0604

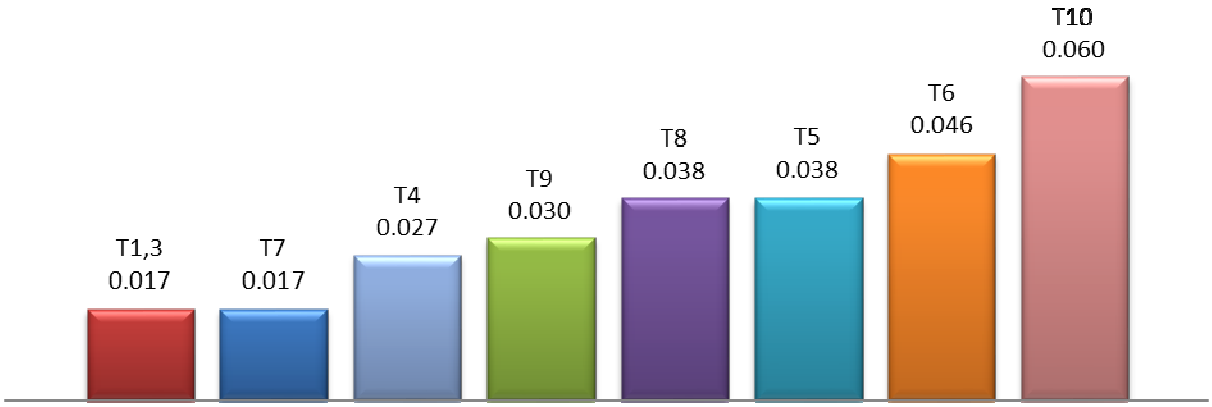

Figure 2.9 Comparison of friction factor for each setup.

In this study, it was found that the accuracy of the measurements were acceptable. Comparison between friction factor measured for a smooth pipe and given from the manufacturer was made. Smooth pipe (T7) friction factor was the smallest, equal to 0.01713 which was almost four times less in comparison with T10 friction factor. Tests T8 and T5 obtained almost the same value (Figure 2.9).

Manning's formula is often used as an hydraulic resistance equation and it can be alternative to Darcy – Weisbach one.

The Manning number is defined by:

$$v = \frac{1}{n} R^{\frac{2}{3}} S^{\frac{1}{2}},$$

Equation 2-7

where:

R = hydraulic radius [m]

S = slope of the water surface or the linear hydraulic head loss [-]

Manning n depends on conduit's diameter and on surface roughness. For a closed conduit flowing full at high Re Manning's n and Darcy – Weisbach f are related by the equation:

$$n = \left(\frac{D}{4}\right)^{1/6} \sqrt{\frac{f}{8g}},$$

Equation 2-8

where:

n = resistance coefficient (Mannings's n) [s/m$^{1/3}$]

Table 2-5 Average values of manning's n for each setup.

Set	Manning Value [s/m$^{1/3}$]
T4	0.0094
T5	0.0112
T6	0.0123
T8	0.0112
T9	0.0101
T10	0.0141

Manning's values are in range between 0.009 s/m$^{1/3}$ and 0.014 s/m$^{1/3}$ (Table 2-5). Most of the literature presents that roughness of tunnels constructed using drill and blast methods is bigger than those for TBM- bored tunnels. Further discussion about Manning's value is presented in chapter three.

Another equation which is related to Darcy – Weisbach friction factor is the Colebrook – White equation. It is possible with knowing *f, D* and *Re* to calculate Nikuradse's equivalent sand grain diameter (Table 2-6). This value is a linear dimension representative of the entire roughness and is a hydraulic resistance parameter (next to *f* and *n*), as opposed to some physical roughness measurement which can be read directly off conduit wall.

$$\frac{1}{\sqrt{f}} = -4\log_{10}\left(\frac{k_s}{3.71d} + \frac{1.26}{\mathrm{Re}\sqrt{f}}\right),$$

Equation 2-9

where:

k_s = Nikuradse's equivalent grain diameter [mm]

Table 2-6 Average values of k_s and relative roughness for each setup.

Set	k_s[mm]	Relative roughness k_s/D
T4	0.18	0.0027
T5	0.64	0.0093
T6	1.16	0.0168
T8	0.63	0.0092
T9	0.31	0.0045
T10	2.28	0.0336

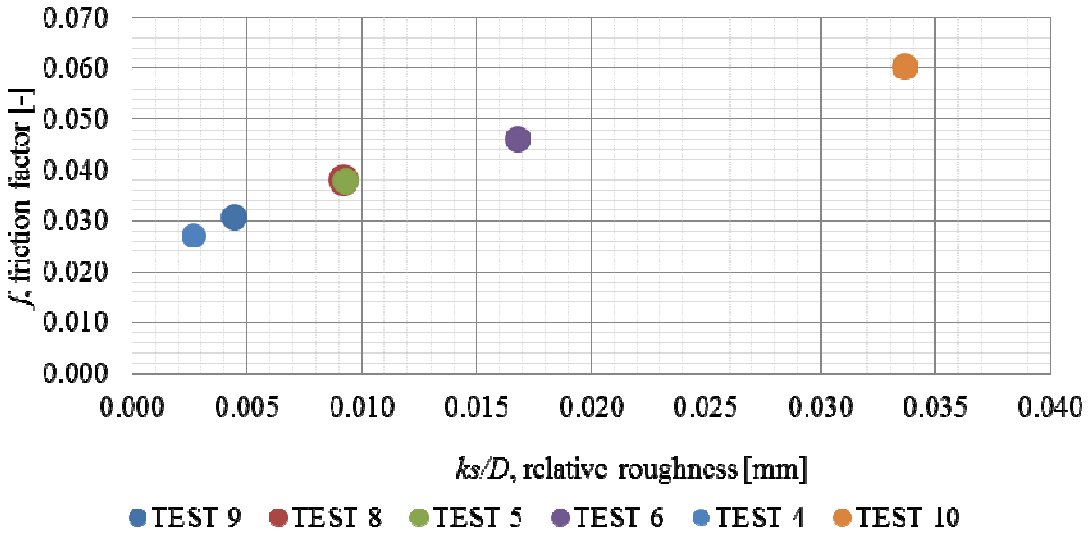

Figure 2.10 Comparison of friction factors versus relative roughness for all sets.

The roughness measure k_s is the equivalent, average diameter of the bumps on the pipe wall if they are uniformly distributed on the wall. Relative roughness k_s/D is therefore the size of the bumps compared to the diameter of the pipe. Perfectly smooth pipes should have roughness of zero (setup T7).

The relationship between the friction factor, *f* and equivalent sand grain roughness present Figure 2.10.

To simplify the design procedure the Colebrook – White equation can be shown as a chart. In 1944 Moody prepared that kind of figure. Given relative roughness (ratio between Nikuradse's equivalent grain diameter and diameter of conduit) and *Re* number, Darcy – Weisbach friction factor can be read off directly (Figure 2.11).

The Moody diagram specifies that for fully turbulent flow *f* becomes constant and continues to increase with decreasing *Re*. This assumption is shown in given results.

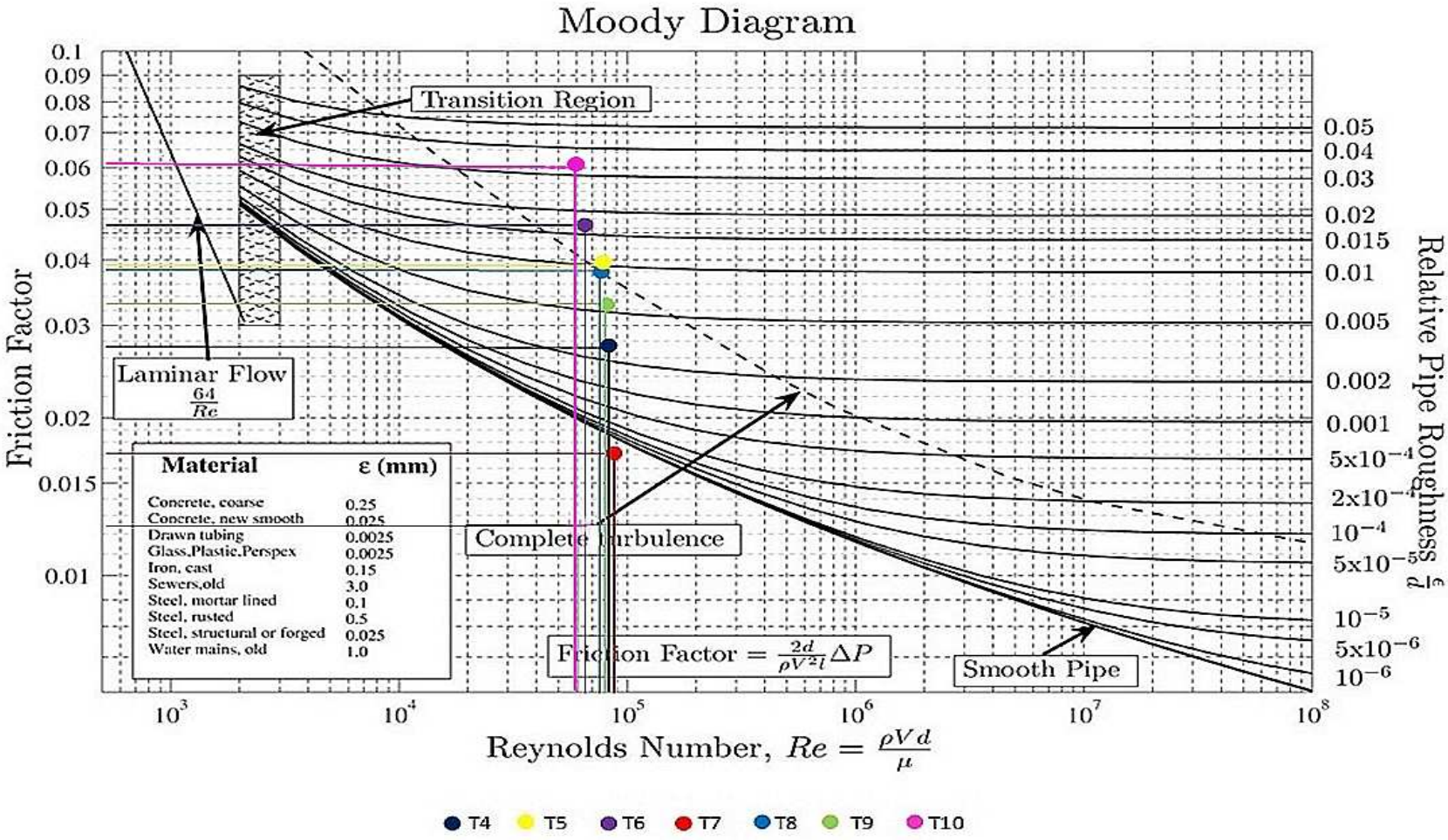

Figure 2.11 Moody diagram with selected set.

2.3.2 Errors

Any measuring instrument will be accurate only to a certain extent and only if it has been calibrated. This is true for the measuring instruments used in this Master Thesis Project. In the experiment four types sources of measurements and instrument errors were identified.

The manometers were used for pressure drop measurement experiments and it is estimated to be on the order of ± 1mm manometer height of water column in a 1000mm column, or 0.1%. This resulted from the human error in reading manometers.

An overflow tank in the setup outflow was used to measure the volume of water over a certain time. The volume measurement method involves only the human error in setting the clock, along with the accuracy of the weighting scale. It is estimated that the uncertainty related to the flow measurement is quite low, approximately below 1%.

For measuring diameter and length of the pipes were used respectively micrometer and tape measure (errors equal to ΔD = 0.001m and ΔL = 0.01m).

For calculating velocity (Δu) errors differences between the highest and lowest results in each test were found. For all tests error variance within 0.1% and 0.9%. The same method was used to calculate head pressure errors (Δh), which variance in a range between 0.1% and 0.6%.

In order to calculate the error in the hydraulic friction factor f, the following equation involving all errors mentioned above was derived from Equation 2-10

$$\Delta f = \frac{2gD}{Lu^2}\sqrt{\frac{1}{h_f}\Delta h_f + \frac{1}{d}\Delta D + \frac{1}{L}\Delta L + \frac{2}{u}\Delta u}$$

Equation 2-10

List of errors for each test is shown in a Table 2-7.

A friction factor was calculated from pressure manometers at two different distances. Between P_1 and P_4 and also between P_2 and P_3. Both of the results were within 5-15% of each other.

Figure 2.12 to Figure 2.17 show friction factors with errors for each of the measurement in each set calculated for P_1-P_4, except tests T1,3 and T7 which were used only for calibrating the model.

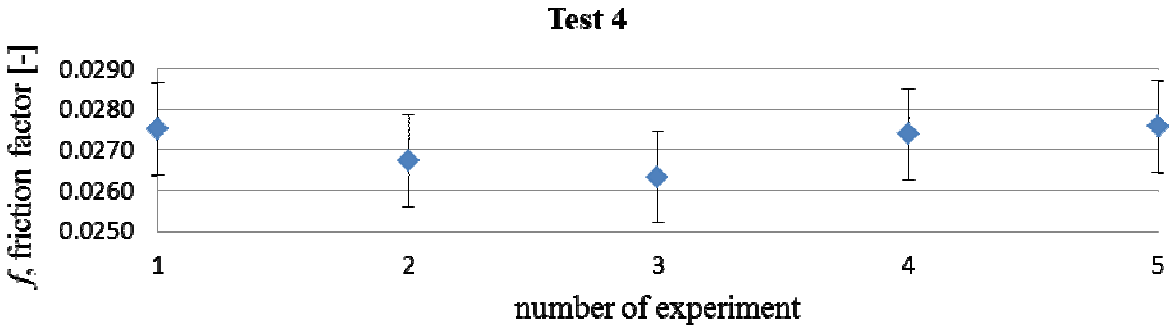

Figure 2.12 Friction factor with error bars for each measurement (no. 1-5) in TEST 4.

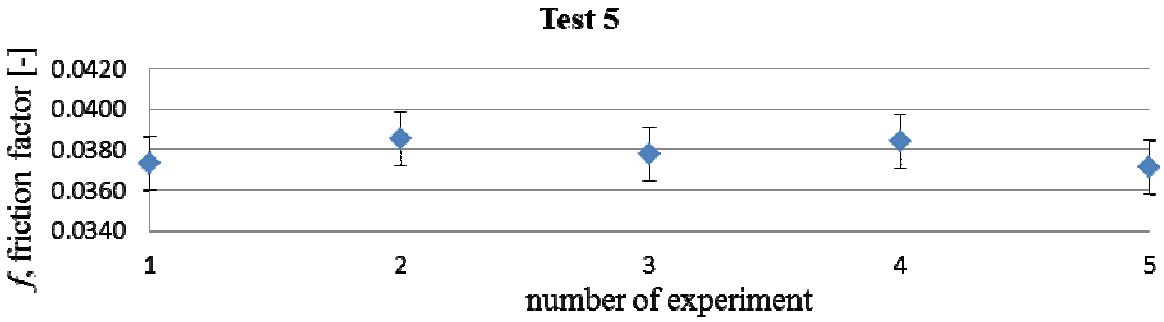

Figure 2.13 Friction factor with error bars for each measurement (no. 1-5) in TEST 5.

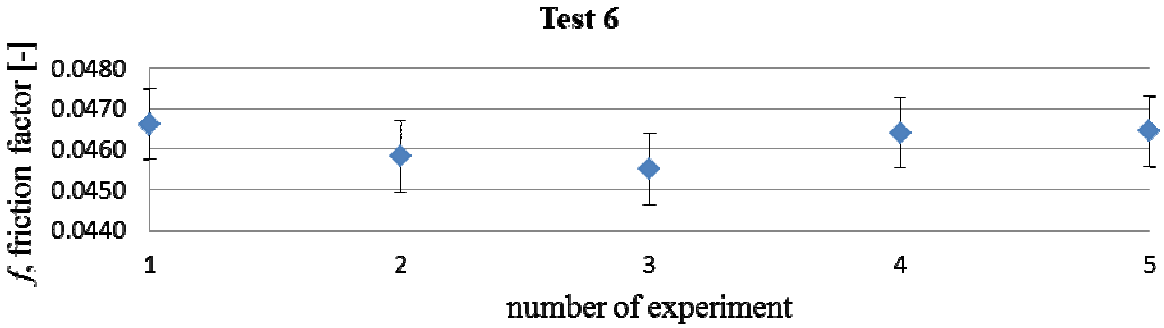

Figure 2.14 Friction factor with error bars for each measurement (no. 1-5) in TEST 6.

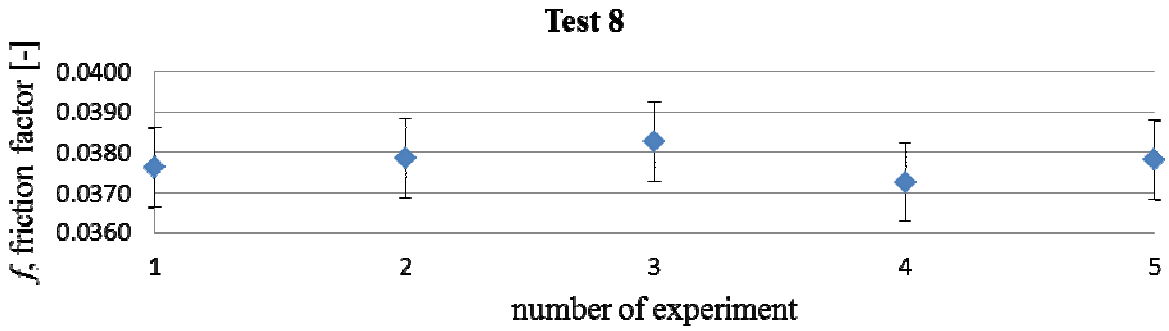

Figure 2.15 Friction factor with error bars for each measurement (no. 1-5) in TEST 8.

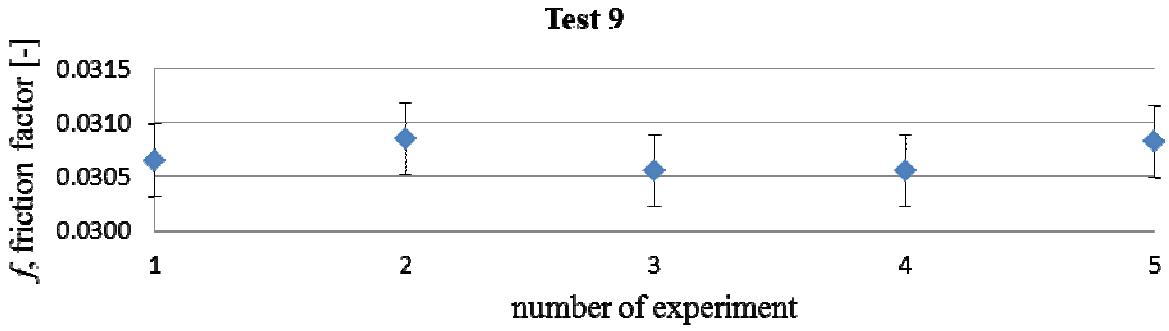

Figure 2.16 Friction factor with error bars for each measurement (no. 1-5) in TEST 9.

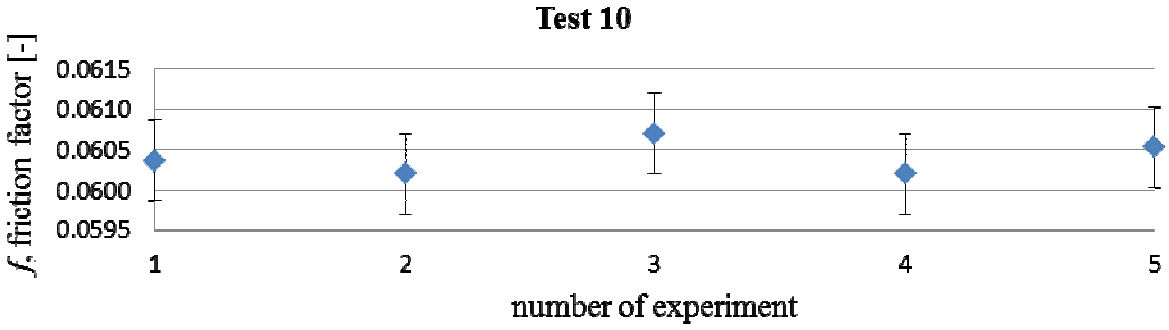

Figure 2.17 Friction factor with error bars for each measurement (no. 1-5) in TEST 10.

The experimental results contain a lot of errors not only due to equipment but also human errors. During experimental measurements some small leakages (not seen then) or any other type of mistake may have occurred.

Table 2-7 List of errors for each setup.

Type of error	Accuracy
ΔD	0.0001 m
ΔL	0.0010 m
TEST 4	
Δu	0.040 m/s
Δh_f	0.0019 m
Δf	0.0011
TEST 5	
Δu	0.032 m/s
Δh_f	0.0007 m
Δf	0.0013
TEST 6	
Δu	0.015 m/s
Δh_f	0.0031 m
Δf	0.0009
TEST 8	
Δu	0.023 m/s
Δh_f	0.0019 m
Δf	0.0010
TEST 9	
Δu	0.009 m/s
Δh_f	0.0016 m
Δf	0.0003
TEST 10	
Δu	0.006 m/s
Δh_f	0.000095
Δf	0.0005

2.4 Conclusions

The experiments were designed to test first, how the distance between distinct irregularities and second, the depth/height of the irregularities changed the hydraulic friction in rough turbulent pipe flow.

In the Figure 2.9 it is observed that T10 setup has the highest friction factor, f=0.060, of all of the experimental results. The interior of the pipe was covered by a mixture of paint and sand (see Figure 2.8) which occurred to be the most flow resistant. Furthermore all reported data for this test (time for discharge, pressure drop in the manometers) were almost the same in each measurement. The head pressure error for T10 (Δh) occurred very small comparing to other tests as it is relevant to the velocity of the flow and pressure measurements.

Setups T6 and T5 are placed accordingly on the second and third positions. Both of them had the same spiral inside (see Figure 2.7); the difference was the depth of the slit (see Table 2-1). It was to be expected that the T6 setup, with 1.5mm deep groove, yielded higher friction factor value, than T5 with only 1.0mm deep groove.

On the fourth place, as shown in Figure 2.9, setup T8 is placed, with slightly smaller friction factor than T5. The spiral inside T8 setup was twice compacted as in T5. The reason why those two friction factor values differ so little could be that the turbulence caused in one groove in T8 was overlapping turbulence in the next one yielding smaller friction factor as a result. Comparison of tests T8 and T5 shows that the 7mm distance between the grooves is too small to cause changes and in the future experiments this distance should be grater.

In the friction factor comparison (Figure 2.9) T9 setup is located on the fifth place. This setup has two different spirals inside the pipe. As seen in the Figure 2.7 the grooves may not be as deep as they were supposed to be (see Table 2-1) what would explain this distant position in the comparison.

T4 setup yielded friction factor value f=0.027, smaller than T9, which locates it on the seventh place, when comparing to the other setups results. This test interior was the closest to the smooth pipe and that's why it's located just before smooth pipe setups like T7 and T1,3.

3 LASER SCANS: PHYSICAL ROUGHNESS TO HYDRAULIC ROUGHNESS

3.1 Introduction

The physical roughness of the artificially roughened PCV pipes was measured accurately with a laser distance-measuring apparatus. The aim of this chapter is to link the hydraulic roughness to measured physical roughness (roughness height, *h*) of an irregular surface, and thus establish a link between hydraulic resistance and psychical roughness in pipe flow at high Reynolds number (full turbulence).

3.1.1 Theory

There are at least three numbers defining hydraulic roughness. These are the: linear dimension representative of the entire roughness, termed Nikuradse's equivalent sand grain diameter, k_s, the Darcy-Weisbach friction factor, *f*, and the Manning number, *n*.

The Colebrook-White equation links both: Darcy-Weisbach friction factor, *f* and Nikuradse's equivalent sand grain roughness, k_s and is given by Equation 2-9 the Manning number is defined in Equation 2-7 the Manning number and the Darcy-Weisbach friction factor are related by Equation 2-8.

There is no clear method of linking hydraulic roughness to physical roughness of an irregular surface. Many attempts were made in the past and many various methods were proposed. The best way to establish the required link is to obtain a value of k_s as a function of the height, spacing, density and nature of the physical roughness. An attempt to obtain the required link is presented in the chapter by comparing measurements of physical roughness and measured hydraulic roughness (see chapter 2).

3.1.2 Relationship between physical roughness and hydraulic roughness

In 1968 **Heerman** presented a method for calculating the hydraulic friction factor, *f*, from the standard deviation of physical roughness data. He establish a relationship between a roughness parameter χ (defined by himself) and the one-dimensional standard deviation, σ, by

$$\chi = 12.9\sigma^{1.66},$$

Equation 3-1

where σ is a standard deviation in feet.

Because the roughness parameter χ is connected with the mean velocity, $\bar{u}$ by the universal log law for the velocity distribution in rough turbulent flow, this equation can be presented as

$$\frac{\bar{u}}{u_*} = 6.06 \log_{10}\left(\frac{m}{\chi}\right),$$

Equation 3-2

where m is the hydraulic radius in feet and u_* is the shear velocity = $(\tau_0/\rho)^{1/2}$.

When comparing the above equation to the universal log law for the velocity distribution in a pipe

$$\frac{\bar{u}}{u_*} = (2\pi)^{1/2} \ln\left(\frac{y}{y_0}\right),$$

Equation 3-3

it can be observed that χ is related to the distance from the boundary, y_0, which means that for this velocity distribution the log low expression tends to zero.

By merging above equations for conduits full yields

$$\frac{\bar{u}}{u_*} = \sqrt{\frac{2}{f}} = 6.06 \log_{10}\left(\frac{D}{51.6\sigma^{1.66}}\right),$$

Equation 3-4

Because D and σ in the equation above are given in feet when rearranged and changed in to the metric units gives

$$\frac{1}{\sqrt{f}} = 4.285 \log_{10}\left(\frac{D}{\sigma^{1.66}}\right) - 8.798,$$

Equation 3-5

This equation, according to Heerman's suggestions may be used in estimating f directly from the standard deviation of a physical roughness data set.

Heerman tested his equation on pipe flow at Re close to 10^4. The equation may be limited by the upper range of Reynolds numbers tested. The maximum value for Re that he used was slightly more than $3 \cdot 10^4$ which is not clear if the flow may still have been in the transition zone between laminar and fully turbulent, rough flow.

The biggest advantage of Heerman's method is that it obtains a complete description of the surface roughness by the standard deviation only of a rough surface and no separate spacing parameter is used (Pengram and Penington, 1996).

In **this study**, particular case of turbulent flow in close conduits is examined. Because the universal log law is invalid near the center of closed conduits flowing full, following equation was derived, taking the linear variation of shear stress over a section into account, which is valid for the main body of the flow

$$u = u_* \sqrt{2\pi} \left(2z + \ln \left| \frac{z-1}{z+1} \right| \right) + u_R ,$$

Equation 3-6

where u is a velocity of fluid particle, u_* is a shear velocity, z is a substitution for $z = \sqrt{1 - \frac{y}{R}}$ with respect to y at any radius r < R and u_R is a velocity at the center of the pipe.

The above equation is a full velocity distribution for turbulent flow in a circular pipe and it holds trough the flow, except for a very thin region near the wall, called the viscous sublayer. Using the model of cylindrical eddies at the bed, in which equivalent sand grain roughness equals to twice roughness height, $k_s=2h$, yields an equation for friction factor for fully developed, rough turbulent flow.

$$\frac{1}{\sqrt{f}} = 4.08 \log_{10} \left(\frac{D}{k_s} \right) + 1.82 .$$

Equation 3-7

This equation can be rewritten in the different constant terms and shown as

$$\frac{1}{\sqrt{f}} = 4 \log_{10} \left(\frac{D}{k_s} \right) + 2.28 .$$

Equation 3-8

The above equation was developed to fit experimental data. When doing so major question appeared, what k_s value should be used in order to yield correct f value. LeCocq and Martin suggested that $k_s=h$ and it has been also suggested from other source that $k_s=2h$ could be a good answer.

After knowing what k_s values would be used other question appears, how should be h measured. Two methods have been proposed.

First from the mean range corresponding to wavelength

$$h_\lambda = \frac{1}{T_n - \lambda} \sum_{i=1}^{T_n - \lambda} r_i \,,$$

Equation 3-9

where T_n is a number of points in series, λ is a wavelength and r_i is a range.

Using the equation above physical roughness data may be represented by a set of dominant or significant wavelengths and their associated mean ranges.

Second from the standard deviation (independent from λ)

$$a = \sqrt{2}\sigma$$
$$h_\sigma = 2a = 2.83\sigma$$

Equation 3-10

where a is an amplitude of sinusoid fitted through the physical roughness data.

The equation above may be used to define the effective height of a random surface with variance σ^2.

To decide which value of k_s should be further used, five different methods were suggested to estimate the hydraulic roughness of each roughness profile.

A: Heerman's method used to calculate the Darcy-Weisbach friction factor from the standard deviation of the roughness data (Pegram and Pennington, 1996).

B: Nikuradse's equivalent sand grain roughness is assumed equal to the amplitude of the equivalent sinusoid of the roughness data, h_σ. The amplitude is a linear function of the standard deviation (Pegram and Pennington, 1996).

C: Nikuradse's equivalent sand grain roughness is assumed twice the amplitude of the equivalent sinusoid of the roughness data (Pegram and Pennington, 1996).

D: Nikuradse's equivalent sand grain roughness is assumed equal to the mean range height, h_λ calculated from the centroidal wave length of the roughness data (Pegram and Pennington, 1996).

E: Nikuradse's equivalent sand grain roughness is assumed equal to twice the mean range height calculated from the centroidal wave length of the roughness data as in method D (Pegram and Pennington, 1996).

Two other methods, which aren't to be used in that study, but are worth mentioning, are discussed below.

Morris (1954 and 1959) suggested one of the rational methods of calculating friction factor, *f*, using physical roughness dimensions for five different flow types that he firstly identified. For a very variable surface roughness when more types of flow are produced Morris suggested that friction factor for each type may be added together and gave the obvious *f* for the surface as a whole. This may only happened if the wake effects of the different roughness do not interfere with each other. Because of that limitation methods suggested by Morris were found to be unsuitable for this study (Pegram and Pennington, 1996).

LeCocq and Martin in 1976 were investigating Echaillon Tunnel in France to find a relationship between physical roughness and hydraulic resistance. They suggested that the parameters which most affect the hydraulic resistance of tunnel walls are the roughness height, h, and concentration, γ.

By analyzing 21 roughness data sets LeCocq and Martin got the concentration value to be slightly higher than γ=0.05. By studying effect of the concentration this value implies that equivalent sand grain diameter, k_s, is taken to be equal to physical roughness height, h.

LeCocq and Martin had made a lot of estimations which not all of them are clear. On the basis of estimated h they also estimated Manning's number, n. These values varied from n=0.0147s/m$^{1/3}$ to n= 0.0154s/m$^{1/3}$, and an average value of n=0.0150s/m$^{1/3}$ was chosen to be the representative one (Pegram and Pennington, 1996).

3.2 Laser scans of pipe surfaces

The laser distance measurements unit for TBM bored tunnels are first used and developed in South Africa by the Department of Civil Engineering, University of Natal, Durban and the South African Water Research commission (WRC). This apparatus uses a laser distance measuring device to read physical roughness, which is then converted to digital form stored in a computer.

After finishing the experiments in the laboratory in Reykjavik pipes were first, sent to a workshop and cut lengthways, second they were sent to be scanned to Switzerland. One pipe from each setup was scanned in the high precision laser scanner, since all of the pipes had been roughened in the same way. However, two pipes (four pipe halfs) from experiment T10 were scanned because a visual inspection showed differences between pipes in the setup.

The laser scans depend on a reflection from the wall. In order to avoid measuring errors every investigated area was covered by matt white spray-paint before scanning as shown in Figure 3.1 below (Pegram and Pennington, 1996).

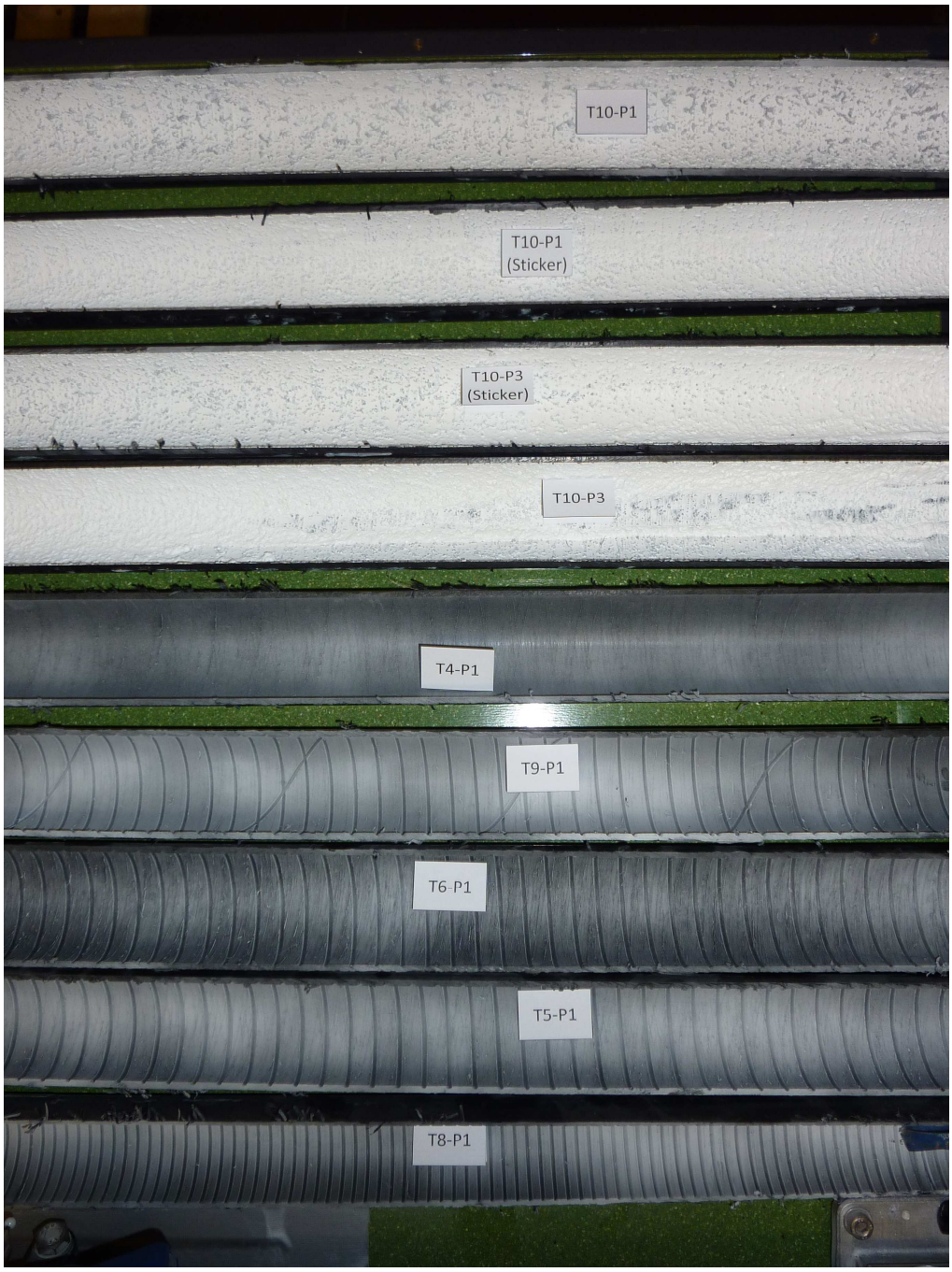

Figure 3.1 The cross-sections of different pipes painted matt spray-paint before scanning.

A 4cm wide slice and approximate 1m long of each pipe half was scanned (see Figure 3.2) and four profiles with 1cm distance were extracted from each scan. The laser scanner generated forty computer text files.

Figure 3.2 Laser scanning machine during work.

3.3 Results

Methods A to D (described in §3.1.1) were used to calculate values of Nikuradses equivalent sand grain roughness for each profile, and an average value for each pipe was calculated

For the computations a special script in program R version 2.12.0 was used. The script can be found in Appendix B. The program generated two files for each run. First file outputted the results as a text file and second as three plots. The plots show: roughness data plotted as a function of length in the flow direction, the power spectrum, C_{xx} plotted as a function of the frequency of the data and mean range height, h_{λ} plotted as a function of the wavelength of the roughness data.

In the appendix B it can be observed that pipes were slightly bended while the mapping is based on a horizontal surface. In order to get all computations right the most horizontal fragments were analyzed. The final, horizontal fragments can be seen below in Figure 3.3 to Figure 3.30.

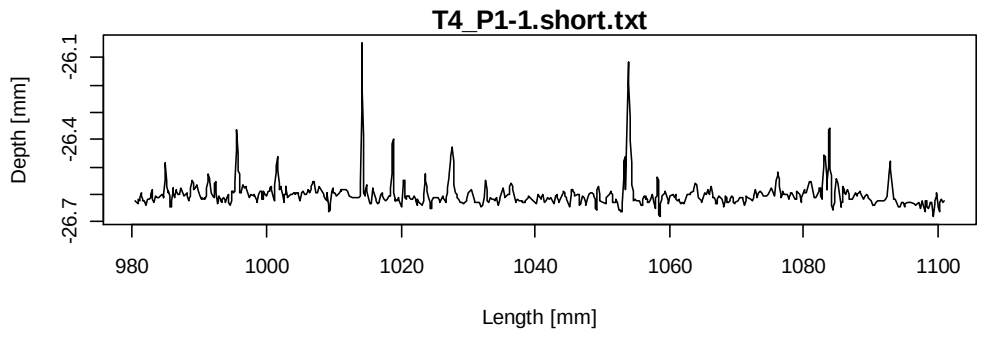

Figure 3.3 Depth – length shorted profile for T4, first run.

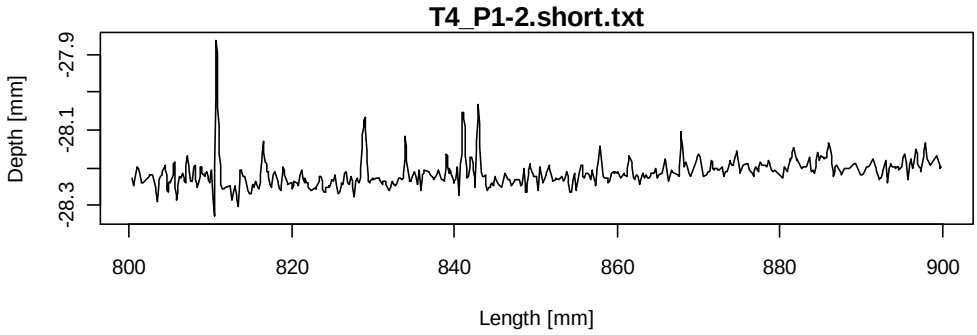

Figure 3.4 Depth – length shorted profile for T4, second run.

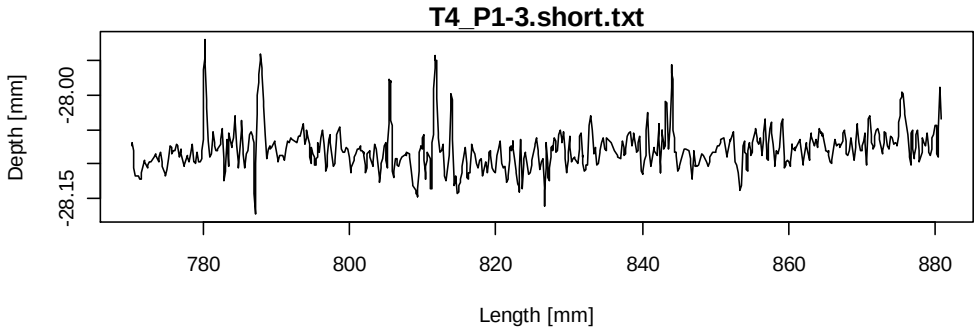

Figure 3.5 Depth – length shorted profile for T4, third run.

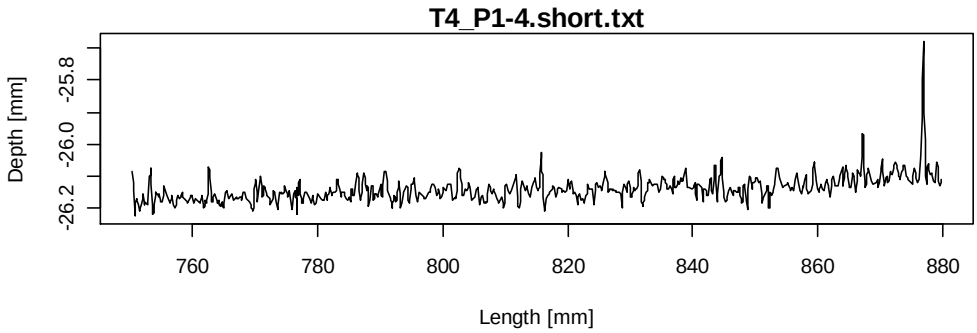

Figure 3.6 Depth – length shorted profile for T4, fourth run.

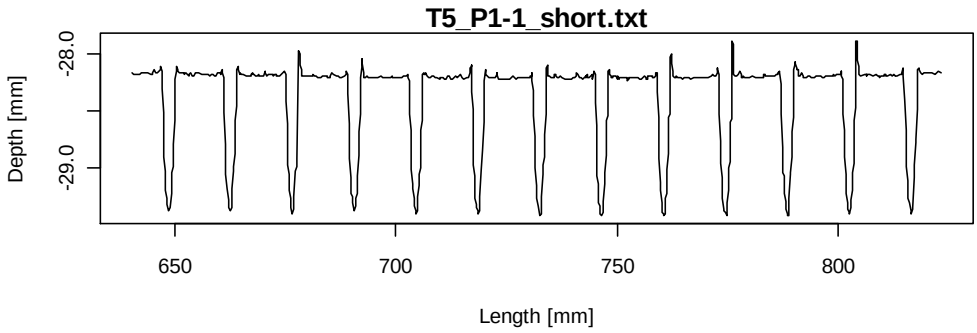

Figure 3.7 Depth – length shorted profile for T5, first run.

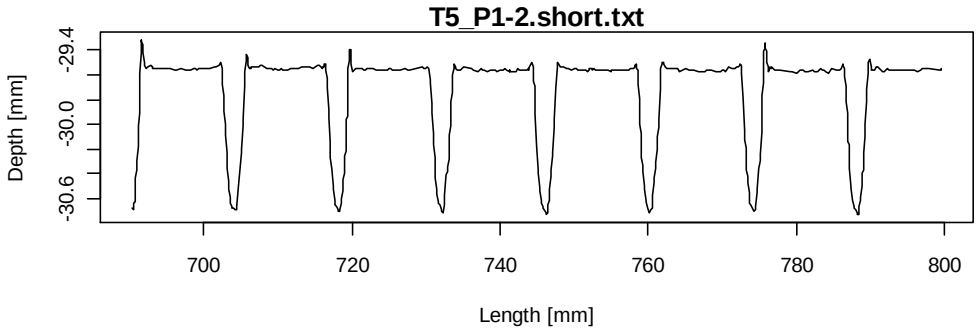

Figure 3.8 Depth – length shorted profile for T5, second run.

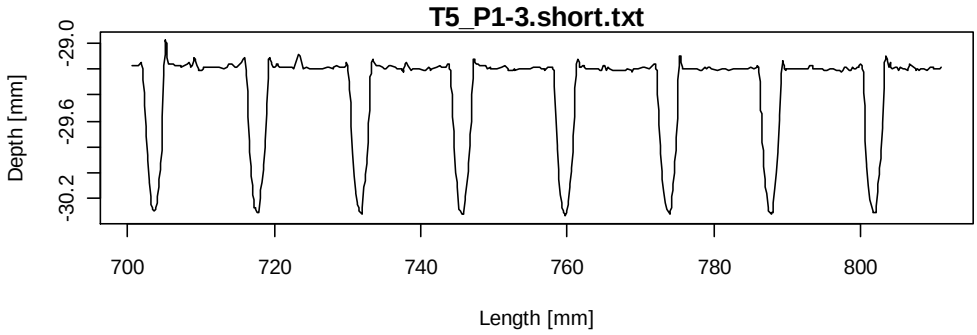

Figure 3.9 Depth – length shorted profile for T5, third run.

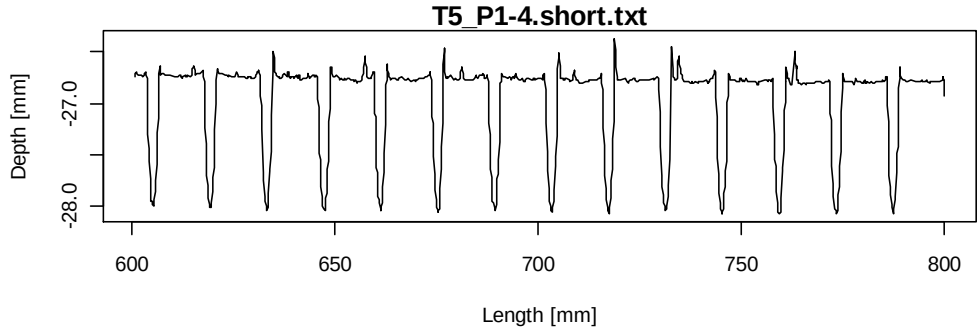

Figure 3.10 Depth – length shorted profile for T5, fourth run.

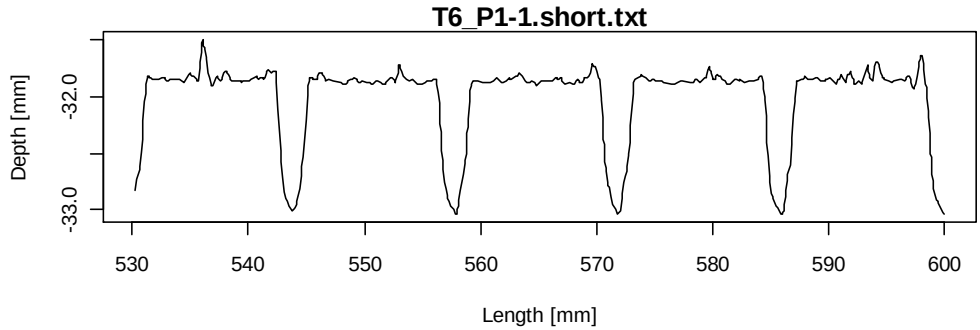

Figure 3.11 Depth – length shorted profile for T6, first run.

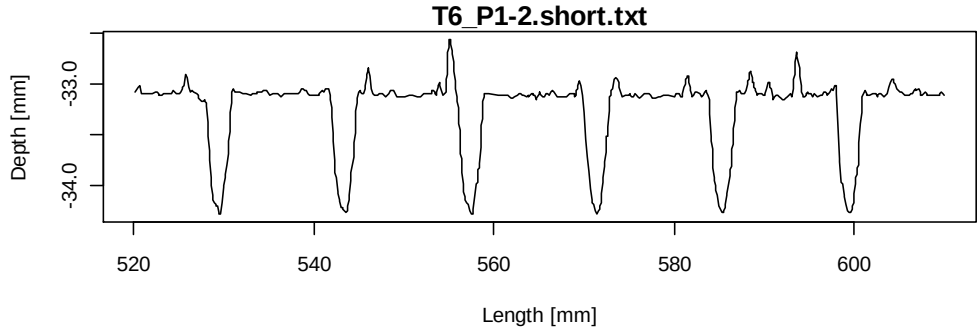

Figure 3.12 Depth – length shorted profile for T6, second run.

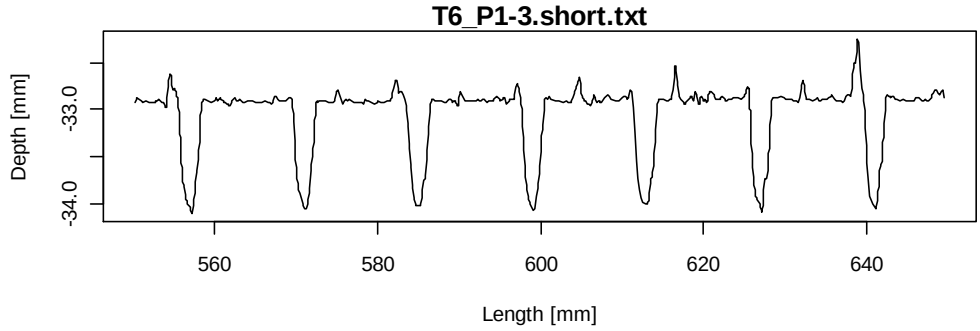

Figure 3.13 Depth – length shorted profile for T6, third run.

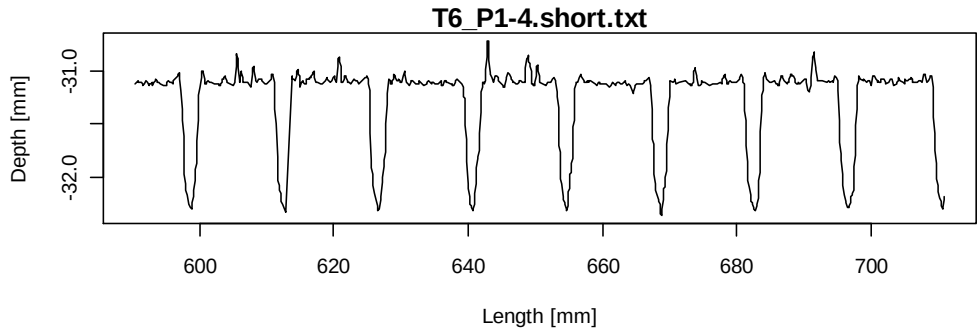

Figure 3.14 Depth – length shorted profile for T6, fourth run.

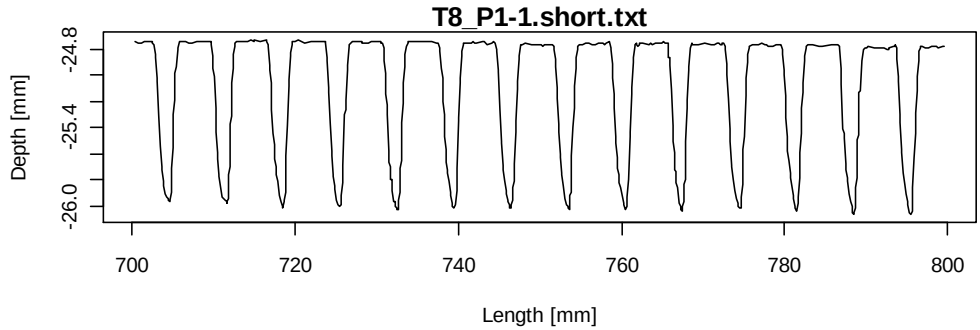

Figure 3.15 Depth – length shorted profile for T8, first run.

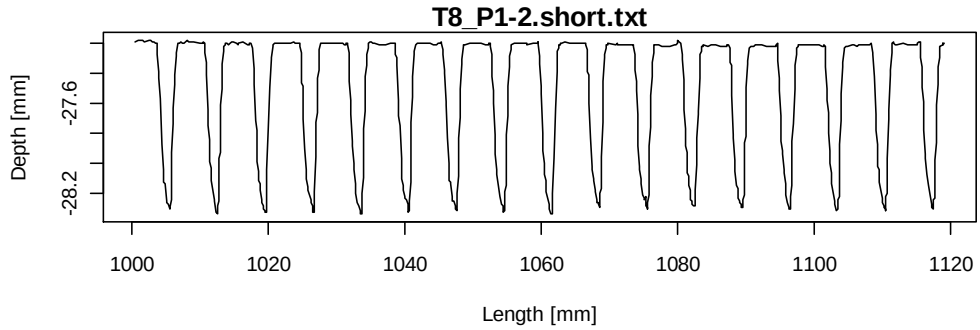

Figure 3.16 Depth – length shorted profile for T8, second run.

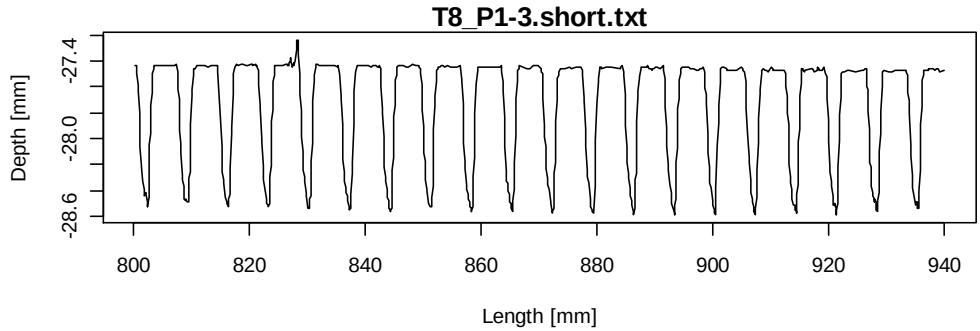

Figure 3.17 Depth – length shorted profile for T8, third run.

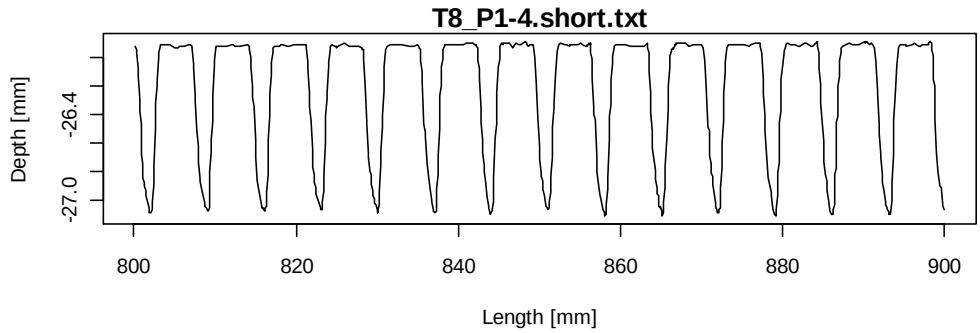

Figure 3.18 Depth – length shorted profile for T8, fourth run.

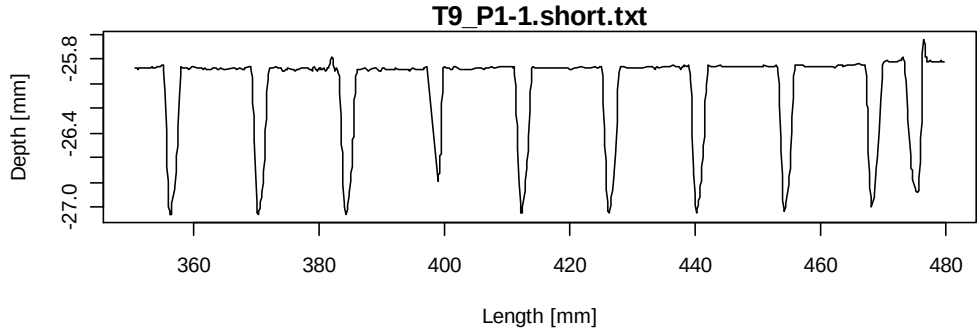

Figure 3.19 Depth – length shorted profile for T9, first run.

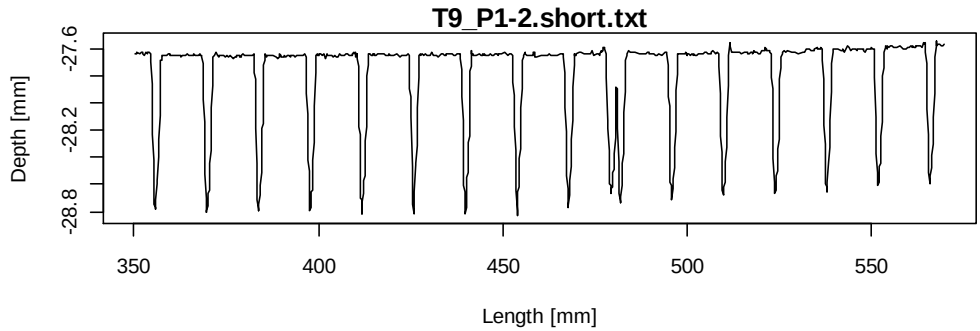

Figure 3.20 Depth – length shorted profile for T9, second run.

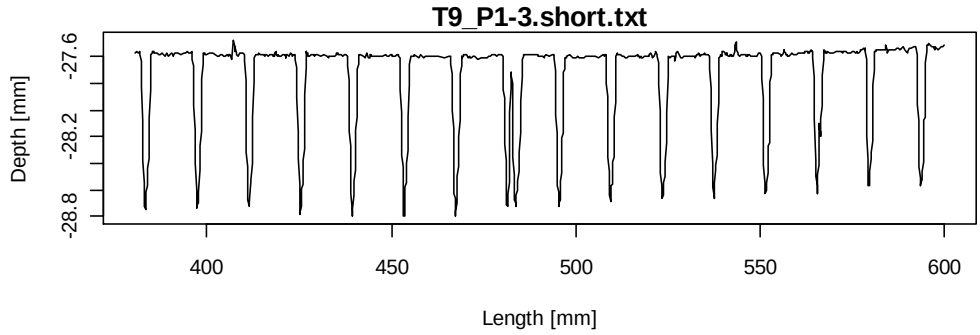

Figure 3.21 Depth – length shorted profile for T9, third run.

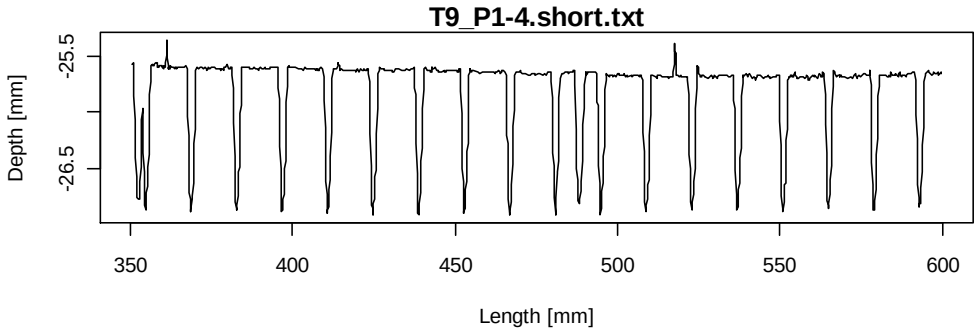

Figure 3.22 Depth – length shorted profile for T9, fourth run.

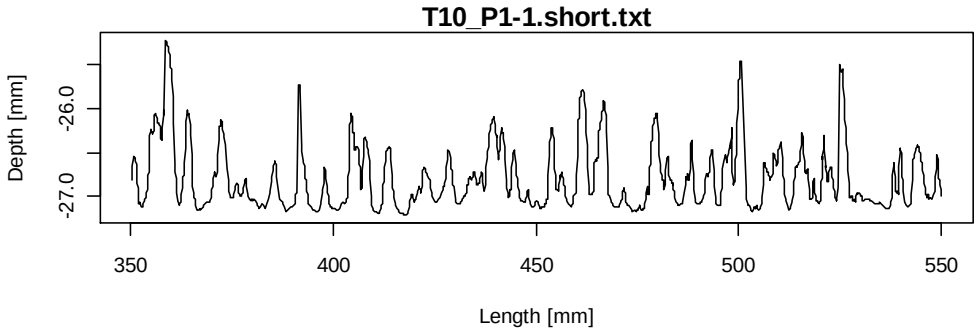

Figure 3.23 Depth – length shorted profile for T10, first pipe, first run.

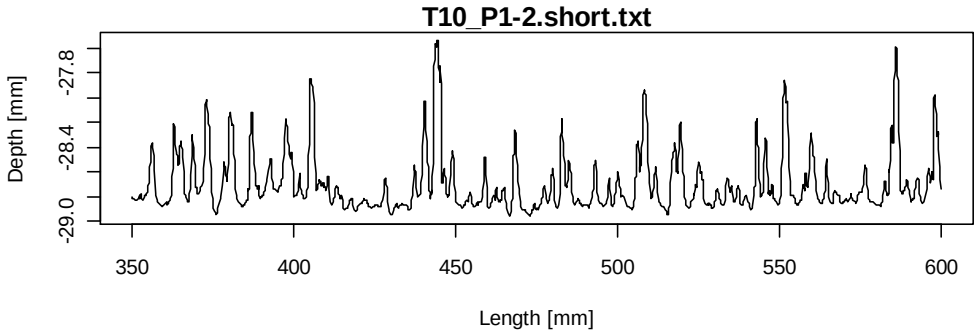

Figure 3.24 Depth – length shorted profile for T10, first pipe, second run.

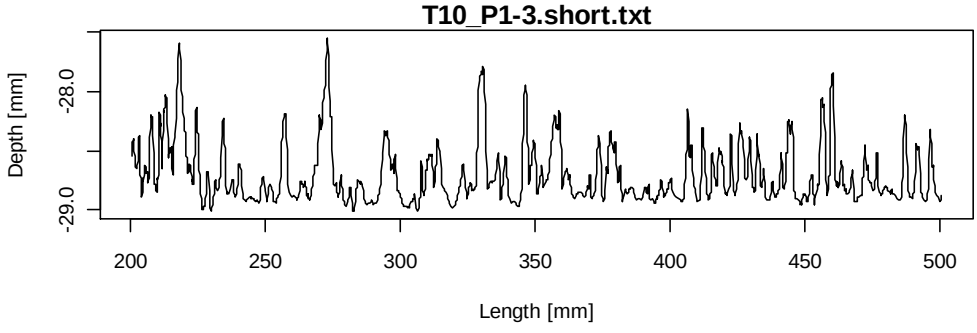

Figure 3.25 Depth – length shorted profile for T10, first pipe, third run.

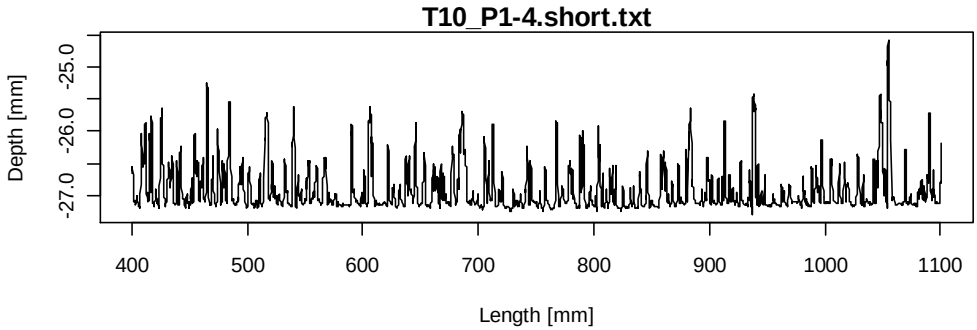

Figure 3.26 Depth – length shorted profile for T10, first pipe, fourth run.

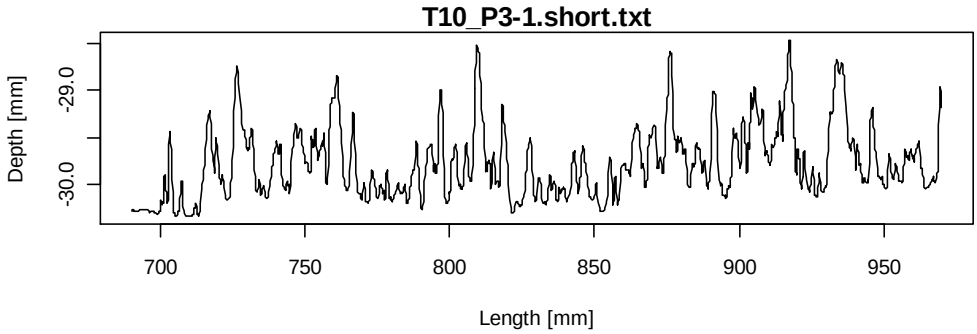

Figure 3.27 Depth – length shorted profile for T10, third pipe, first run.

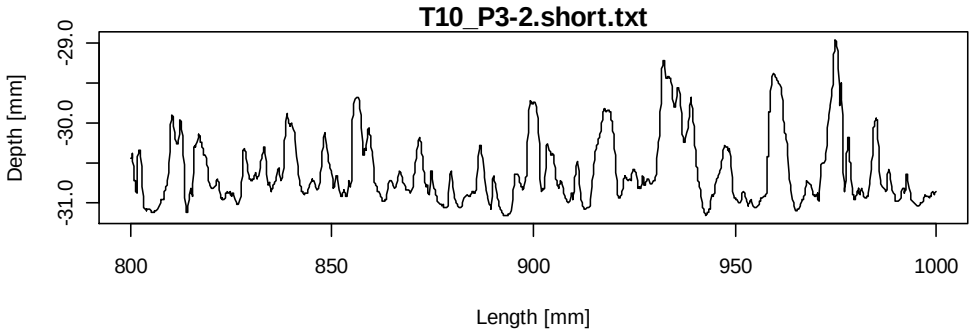

Figure 3.28 Depth – length shorted profile for T10, third pipe, second run.

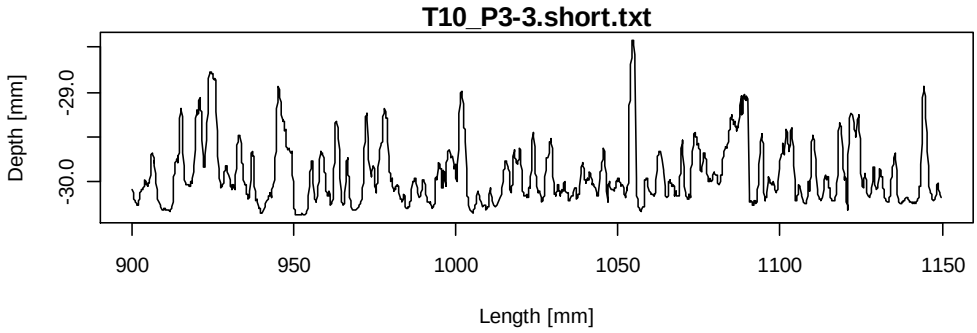

Figure 3.29 Depth – length shorted profile for T10, third pipe, third run.

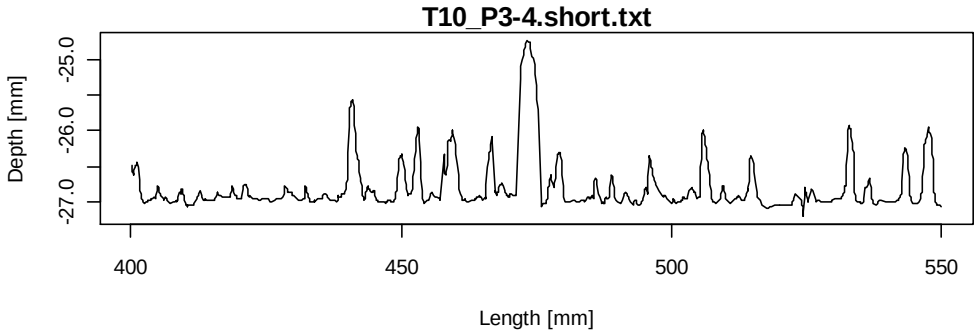

Figure 3.30 Depth – length shorted profile for T10, third pipe, fourth run.

Together with the plots above, all sets of calculations and more precise graphs were produced. Exact program computations and the plots can be found in Appendix B.

In the Table 3-1below average values for each setup are given as a results for program computations.

Table 3-1 Computations with average values for each setup.

	T4	T5	T6	T8	T9	T10
Number of data points	827.5	894.75	773	796.5	1108.75	1641.229
Spacing of data points, delta [mm]=	0.028104	0.036746	0.023174	0.027939	0.049895	0.047689
N=	4096	4096	4096	4096	4096	4096
Reynolds tala=	76176.92	70893.1	65797.23	70893.1	73754.3	61443.26

Nyquist frequency [mm-1]=	17.9	14.6	22.4	19.4	10.6	12.9
Lowest frequency [mm-1]=	0.0087	0.0071	0.0109	0.0089	0.0052	0.0063
Centroidal frequency [mm-1]=	0.52	0.16	0.17	0.20	0.17	0.14

Signal variance [mm]=	0.002229	0.184376	0.161478	0.211388	0.173765	0.132217
h_sigma [mm]=2*sqrt(2*Var)	0.130891	1.21346	1.1364	1.298962	1.178179	1.013799

Centroidal wavelength: lambda_c [mm]	1.955433	6.131906	5.89091	4.913259	5.895072	7.183789
h_lambda_c [mm]=	0.081209	0.780892	0.825852	1.095923	0.679734	0.786862

(Multiplied by 4, see script in the Appendix B)						
A: Darcy-Weisbach friction factor, *f*=	0.013691	0.038556	0.037067	0.040199	0.037875	0.03491
B: Darcy-Weisbach friction factor, *f*=	0.022978	0.046199	0.045092	0.047394	0.045695	0.043505
C: Darcy-Weisbach friction factor, *f*=	0.027831	0.060955	0.059282	0.062773	0.060192	0.056927

D: Darcy-Weisbach friction factor, *f*=	0.020378	0.03941	0.040199	0.044485	0.037609	0.039718
E: Darcy-Weisbach friction factor, *f*=	0.024393	0.050843	0.051998	0.05837	0.048212	0.051321

B: Roughness, k_s=*h*_sigma [mm]=	0.130891	1.21346	1.1364	1.298962	1.178179	1.013799
C: Roughness, k_s=*2h*_sigma [mm]=	0.261782	2.426921	2.272799	2.597924	2.356358	2.027598
D: Roughness, k_s=*h*_lambda_c [mm]=	0.081209	0.780892	0.825852	1.095923	0.679734	0.786862
E: Roughness, k_s=*2h*_lambda_c [mm]=	0.162418	1.561785	1.651705	2.191846	1.359468	1.573724

A: Manning number, *n*	0.006709	0.011265	0.011047	0.011503	0.011166	0.010665
B: Manning number, *n*	0.008694	0.012332	0.012184	0.012491	0.012265	0.011915
C: Manning number, *n*	0.009568	0.014165	0.01397	0.014375	0.014077	0.013627
D: Manning number, *n*	0.00819	0.011389	0.011503	0.012101	0.011126	0.011383
E: Manning number, *n*	0.00896	0.012935	0.013082	0.013861	0.012597	0.012936

A: 1/Manning number, *M*	149.25	88.5	90.5	87	89.75	94.125
B: 1/Manning number, *M*	115	81	82	80.25	81.75	84.02083
C: 1/Manning number, *M*	104.75	70.75	71.75	69.5	71	73.45833
D: 1/Manning number, *M*	122.25	87.75	87	82.5	90	88
E: 1/Manning number, *M*	111.75	77.25	76.25	72.5	79.25	77.41667

It should be noted that the best fitting method for mapping is not consistently the same in all the setups. The method showing the lowest friction factor is method A and the highest factors are method C. In Figure 3.31 to Figure 3.36 the comparison for each setup is presented. The comparison applies to experimental *f* values with error bars and calculations of *f* for each method based on the laser scans.

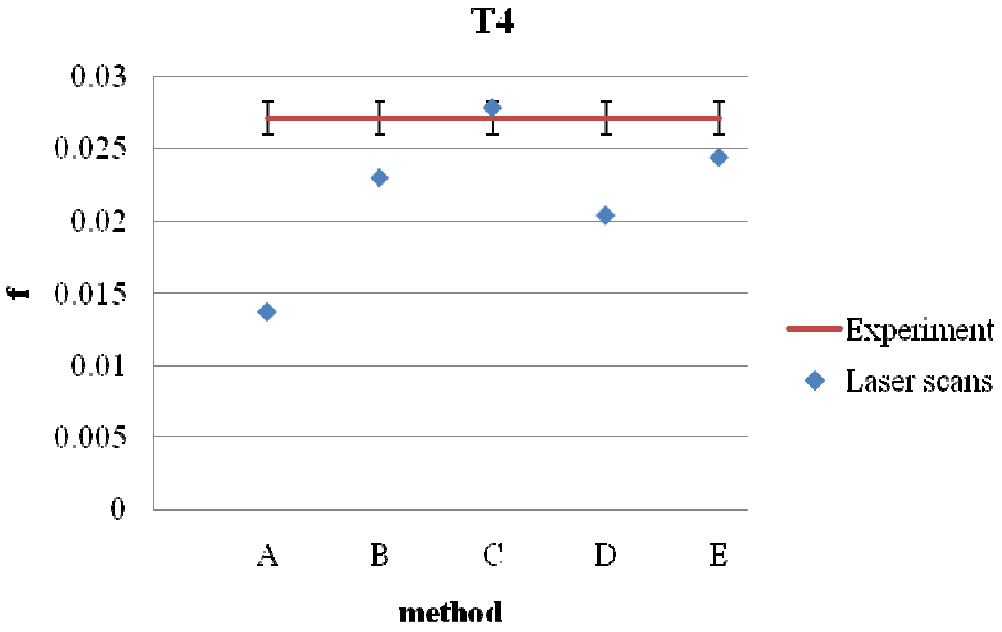

Figure 3.31 Comparison of experimental f with calculated values for each method for T4.

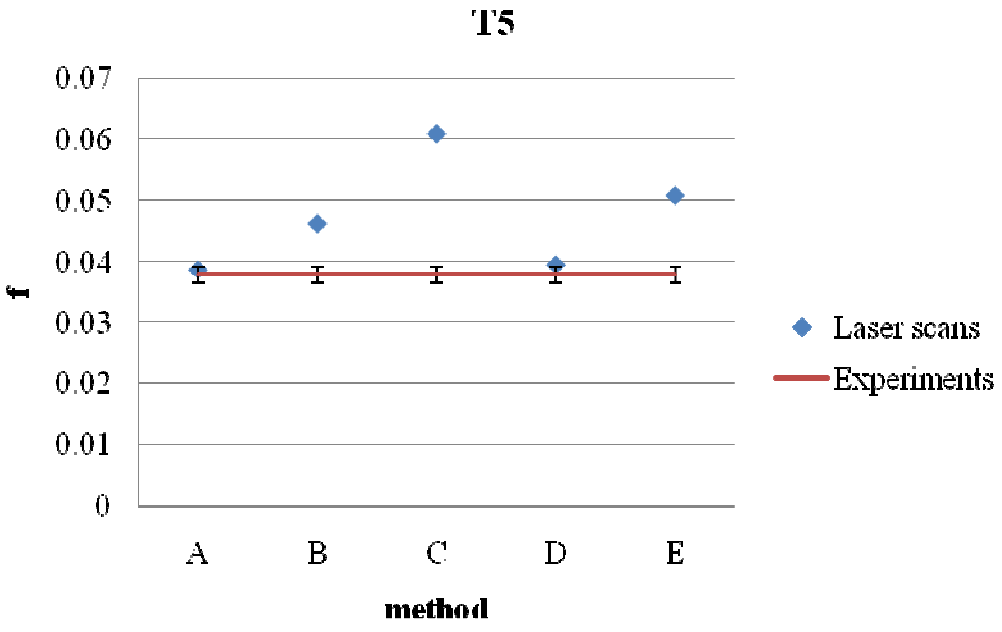

Figure 3.32 Comparison of experimental f with calculated values for each method for T5.

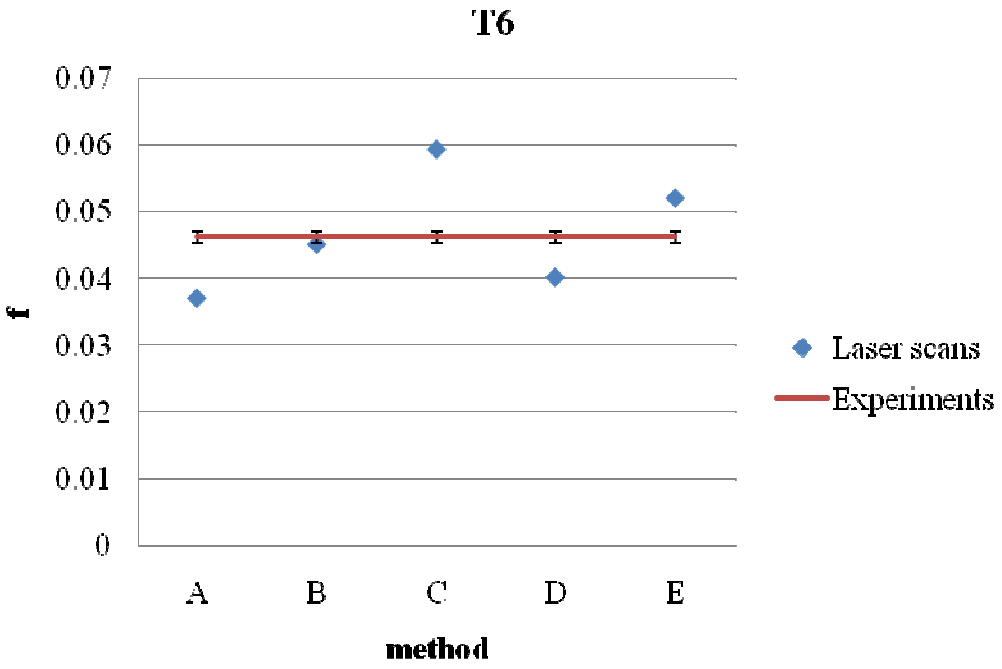

Figure 3.33 Comparison of experimental f with calculated values for each method for T6.

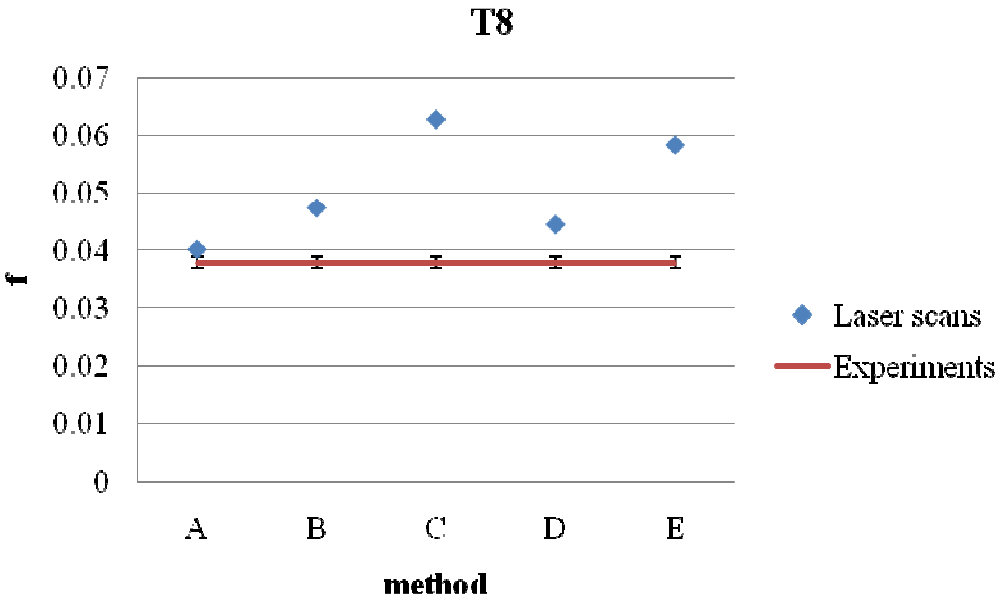

Figure 3.34 Comparison of experimental f with calculated values for each method for T8.

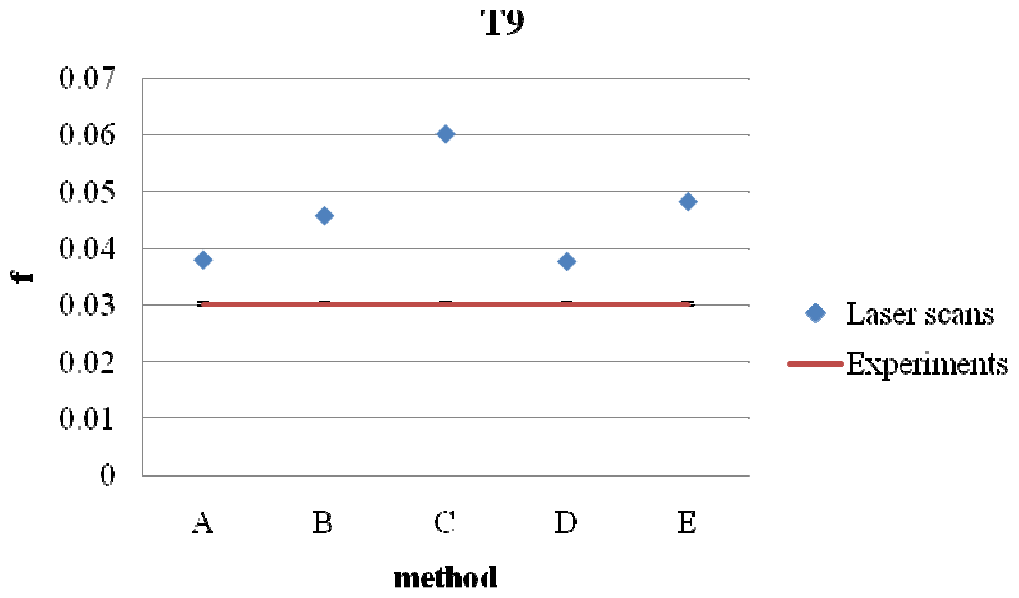

Figure 3.35 Comparison of experimental f with calculated values for each method for T9.

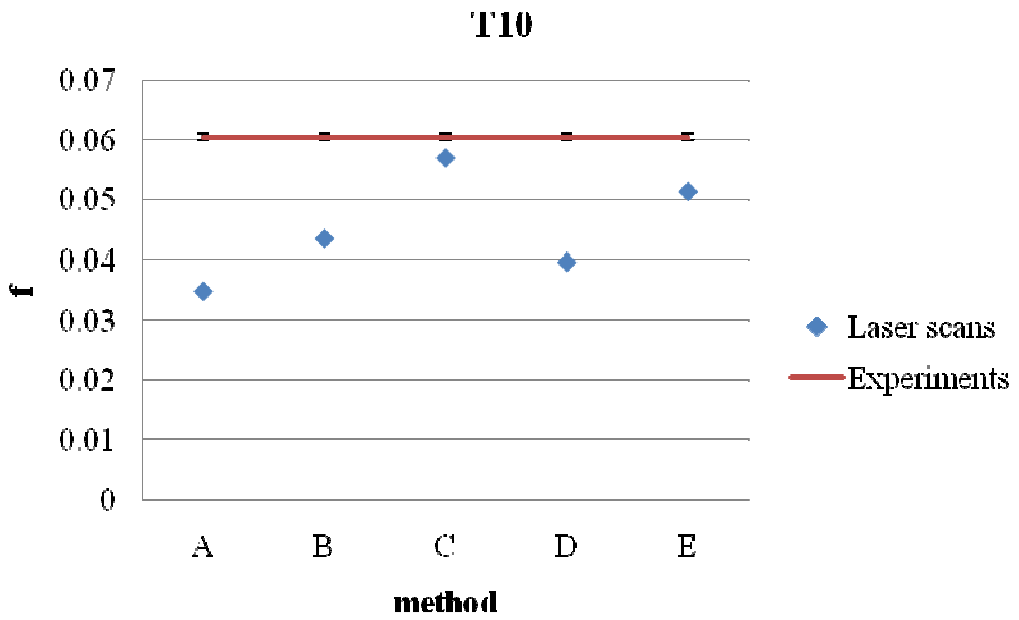

Figure 3.36 Comparison of experimental f with calculated values for each method for T10.

In Figure 3.37 to Figure 3.42 the friction factors calculated from each method are shown on the Moody Diagrams and compared with the experimental value (red dot) below.

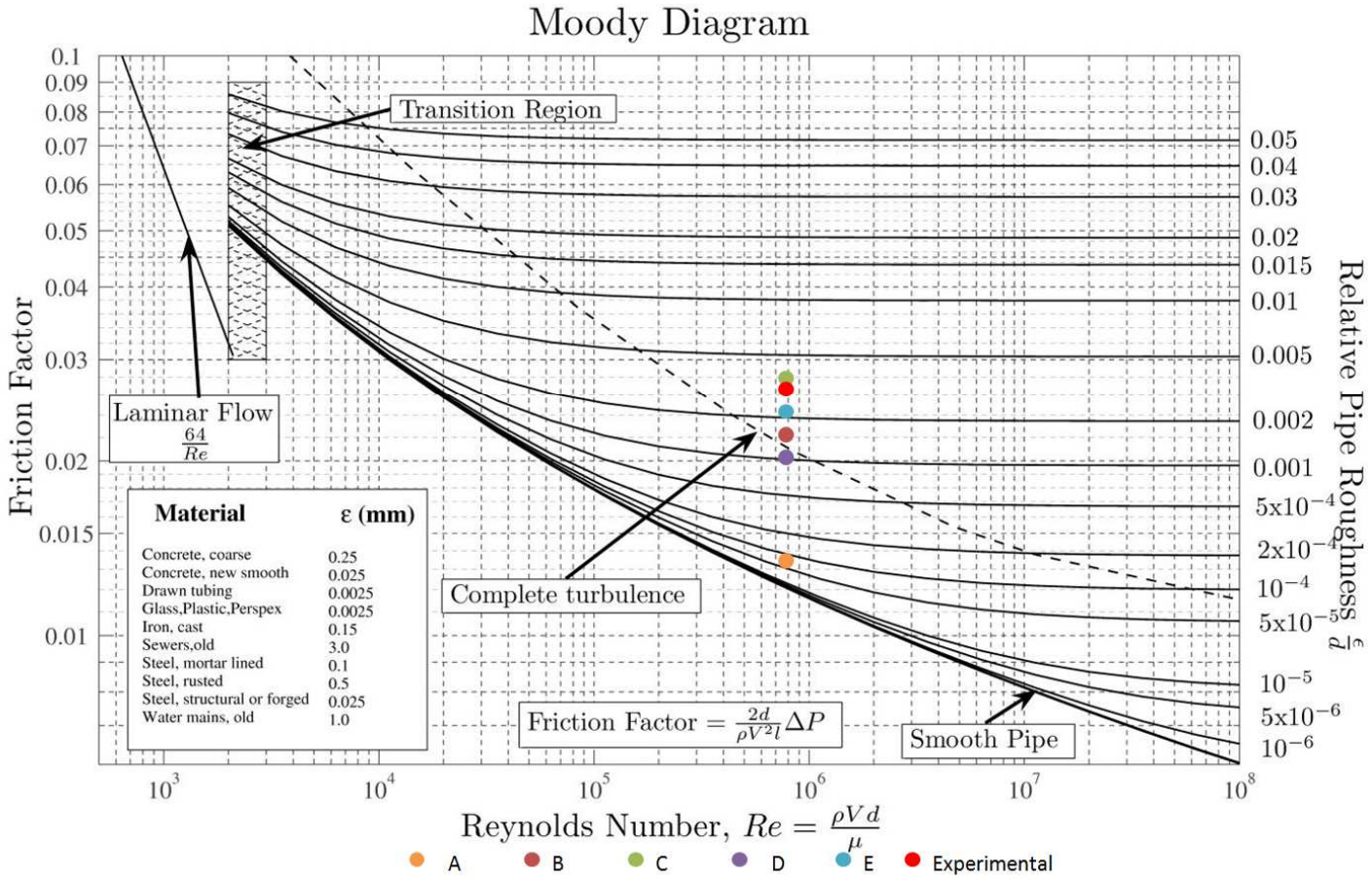

Figure 3.37 Moody diagram showing f results of each method for T4 set.

T5

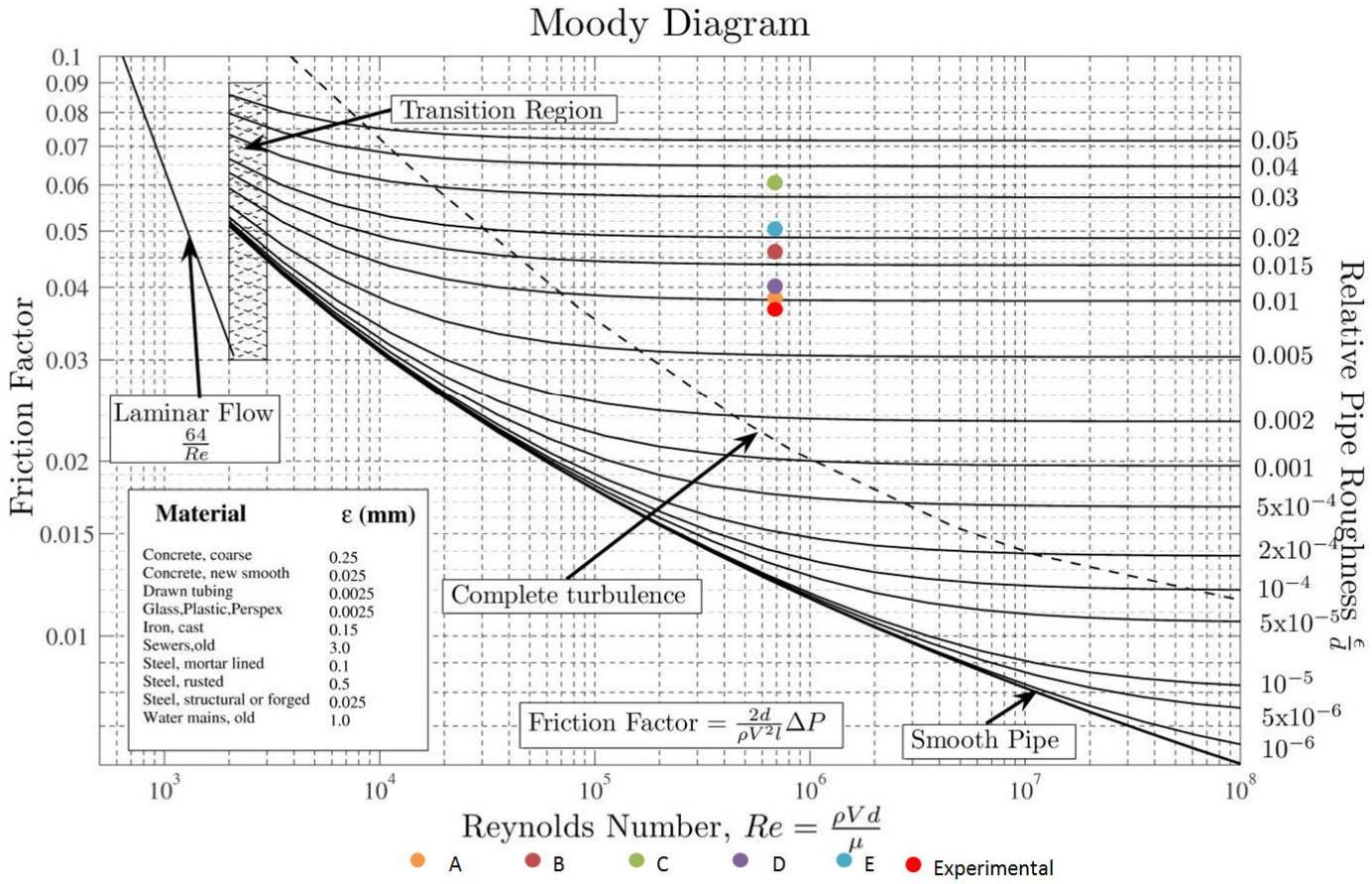

Figure 3.38 Moody diagram showing f results of each method for T5 set.

T6

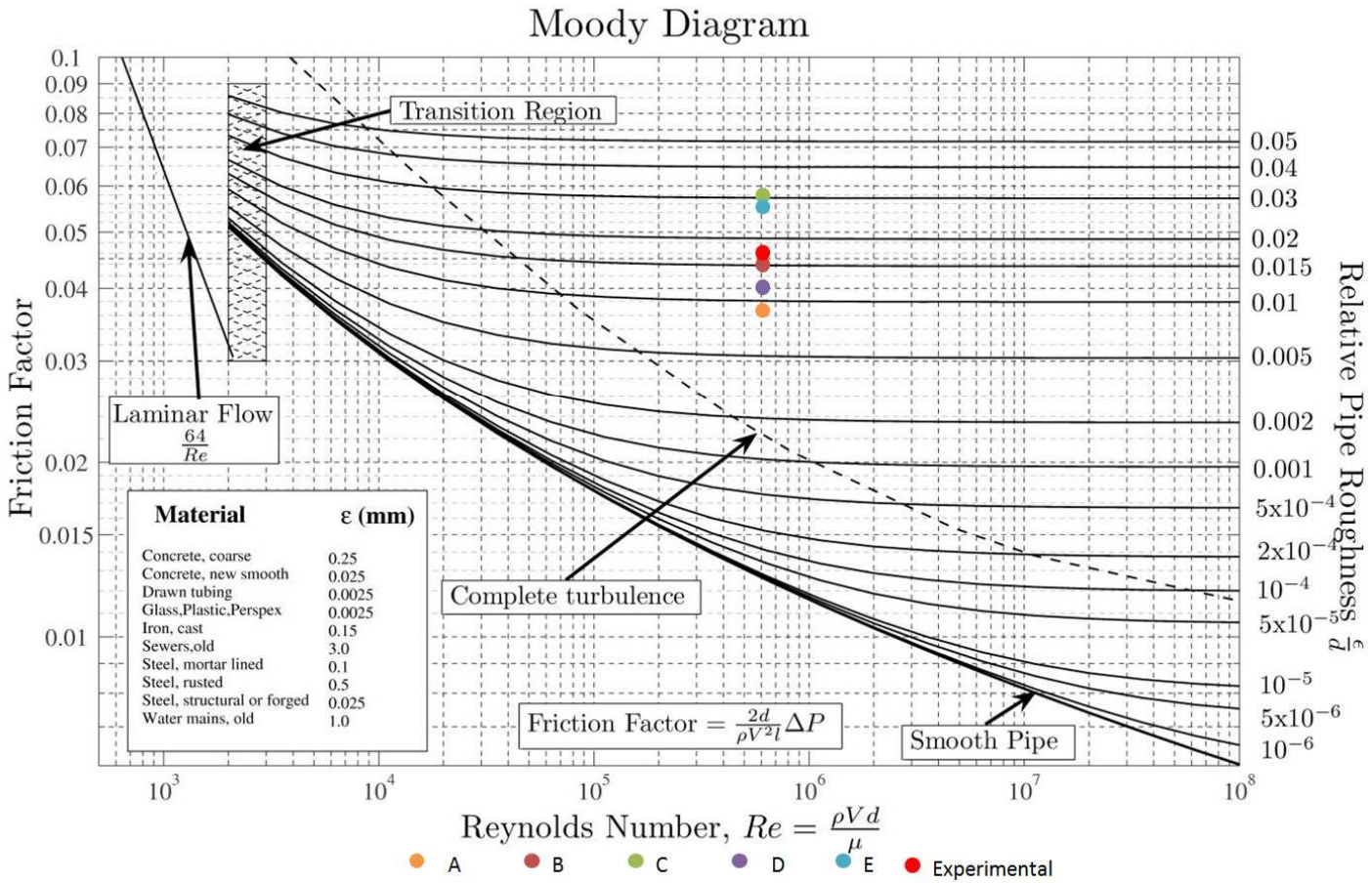

Figure 3.39 Moody diagram showing f results of each method for T6 set.

T8

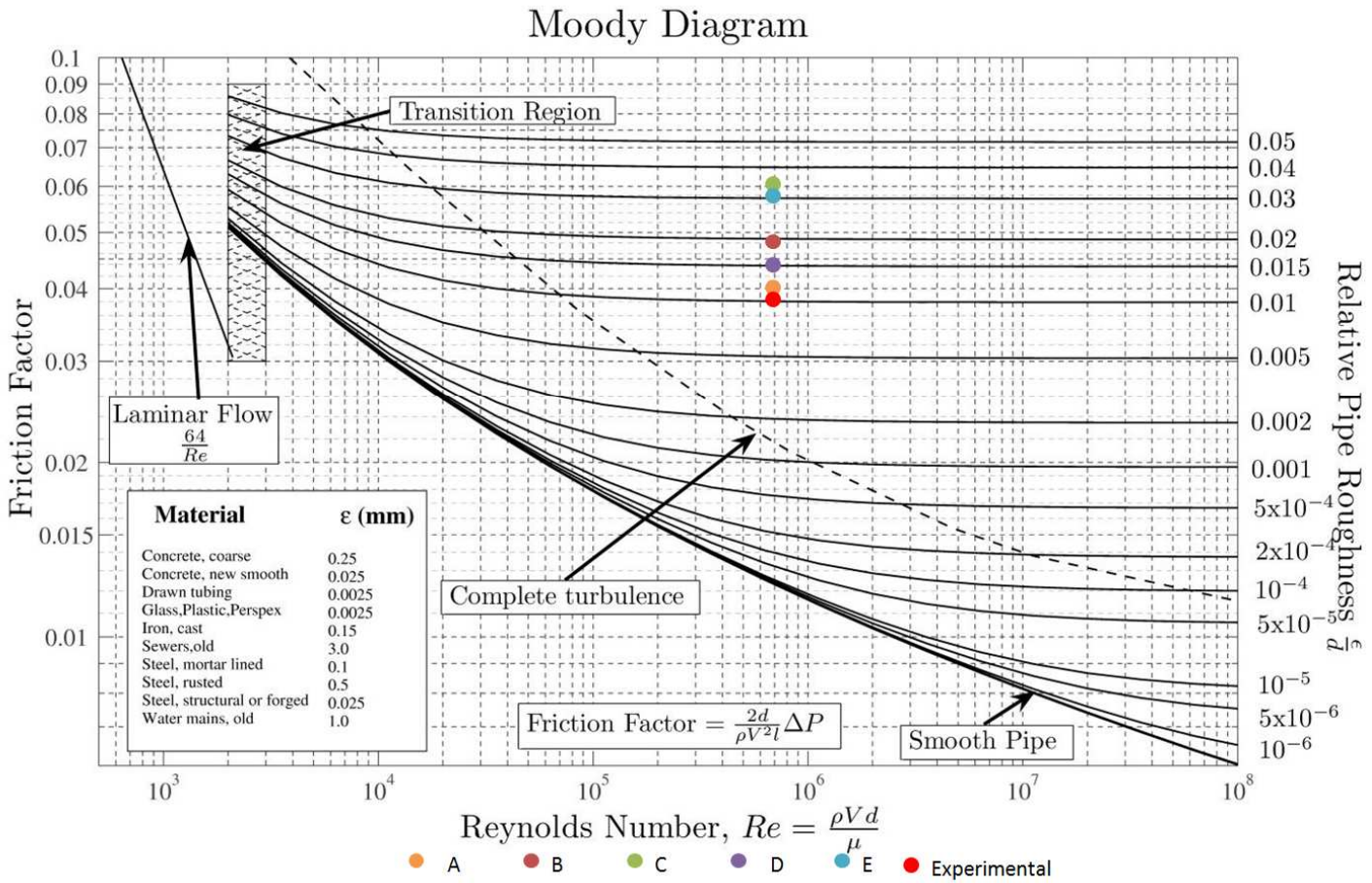

Figure 3.40 Moody diagram showing f results of each method for T8 set.

T9

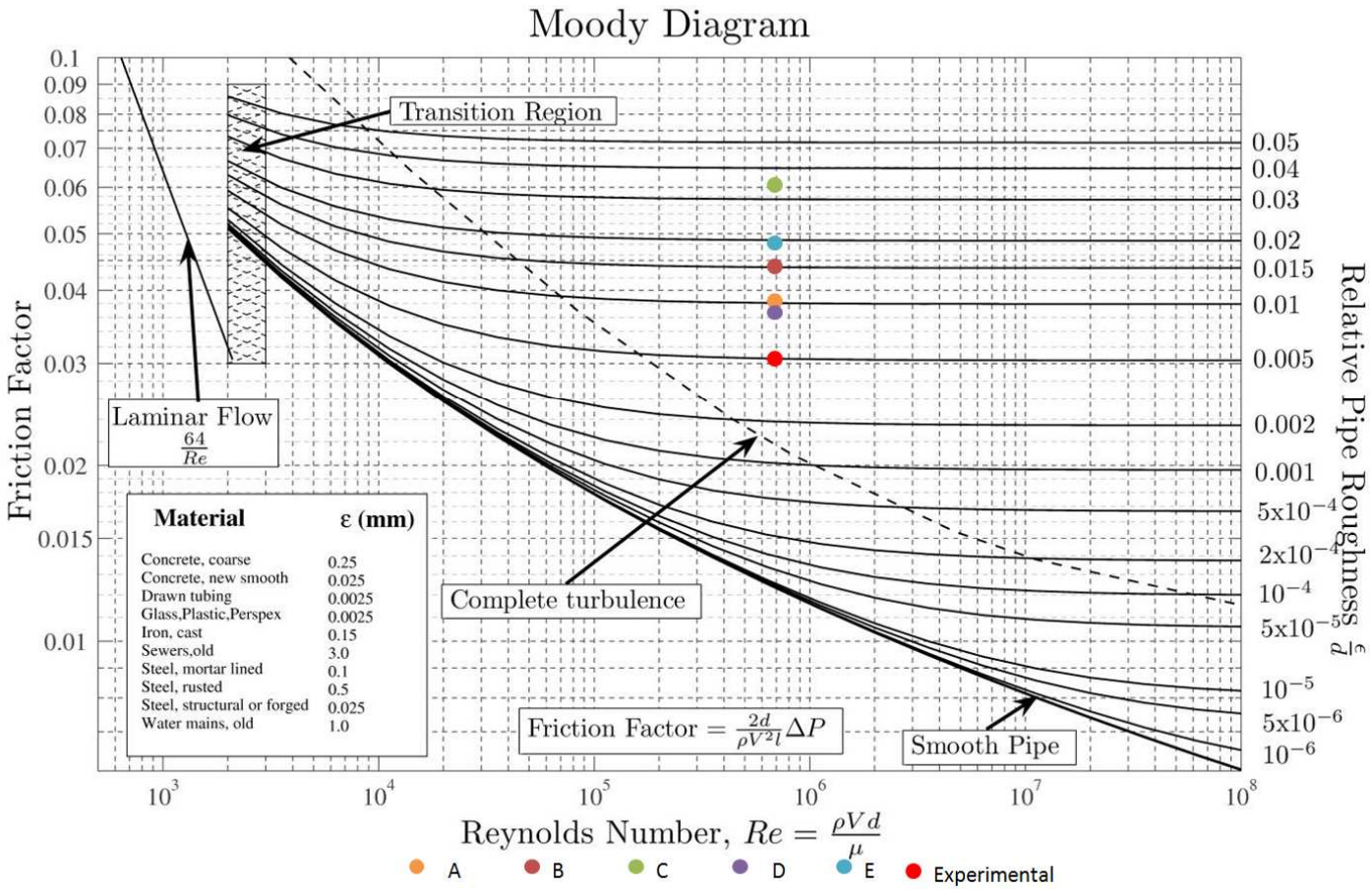

Figure 3.41 Moody diagram showing f results of each method for T9 set.

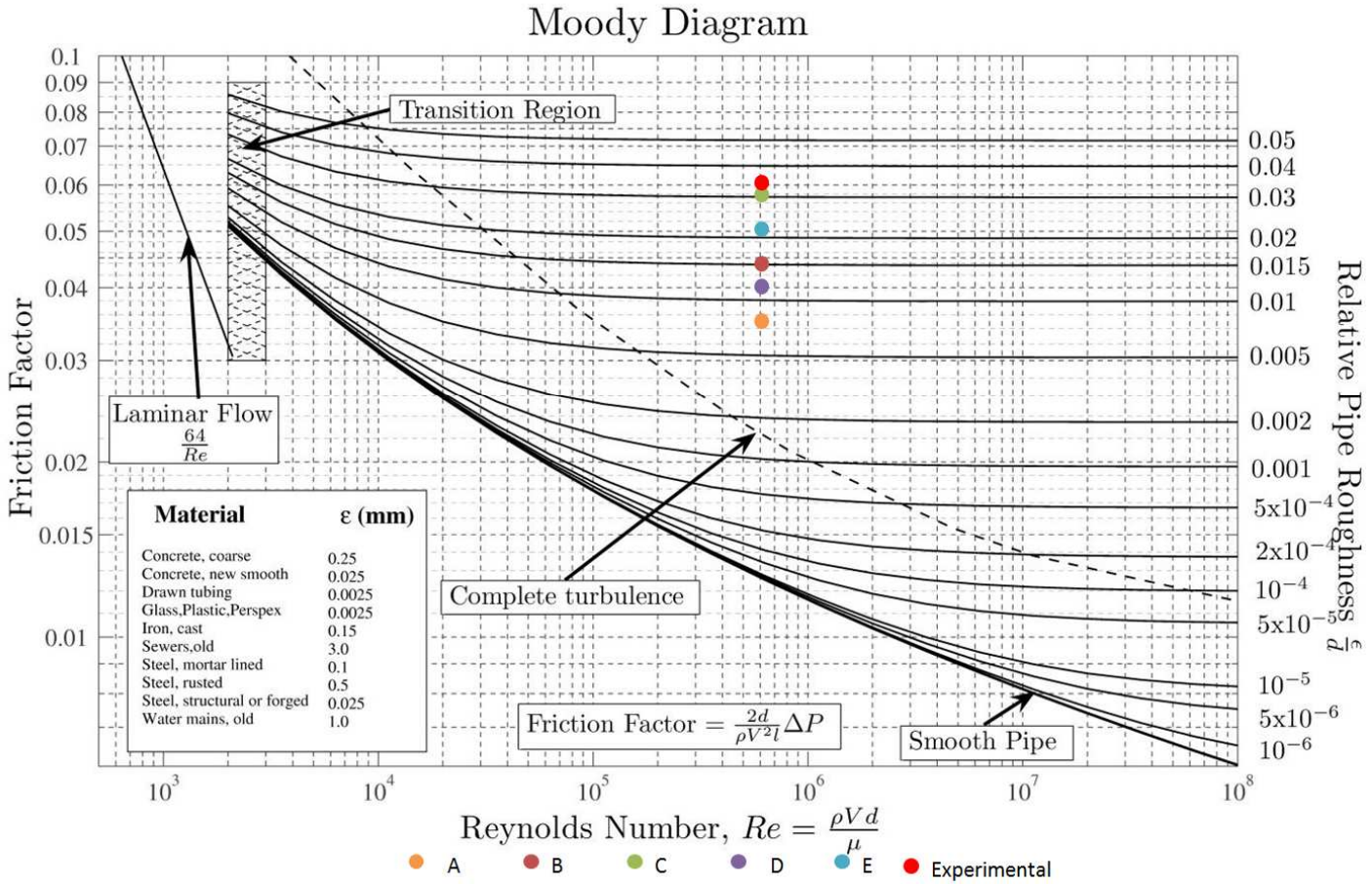

Figure 3.42 Moody diagram showing f results of each method for T10 set.

3.4 Conclusions

A number of different techniques for describing surface roughness were presented. These were all used in establishing links between physical and hydraulic roughness. To have a better visual look at the results and to choose the best fitting method, additional tables are shown below.

Table 3-2 Comparison of experimental values for f with values for each method.

	T4	T5	T6	T8	T9	T10
Experimental D-W friction factor, *f*=	**0.027** ± 0.0011	**0.038** ± 0.0013	**0.046** ± 0.0008	**0.038** ± 0.0010	**0.030** ± 0.0003	**0.060** ± 0.0005
A: Darcy-Weisbach friction factor, *f*=	0.014	0.039	0.037	0.040	0.038	0.035
B: Darcy-Weisbach friction factor, *f*=	0.023	0.046	0.045	0.047	0.046	0.044
C: Darcy-Weisbach friction factor, *f*=	0.028	0.061	0.059	0.063	0.060	0.057
D: Darcy-Weisbach friction factor, *f*=	0.020	0.039	0.040	0.044	0.038	0.040
E: Darcy-Weisbach friction factor, *f*=	0.024	0.051	0.052	0.058	0.048	0.051

In the Table 3-2 values marked **pink** are the values from the experiments, **violet** colour are the closest to the measured values and by **green** colour second choice values were marked. In the Table 3-3 modify results from Table 3-2 are shown.

Table 3-3 The best fitting methods for each setup

	T4	T5	T6	T8	T9	T10
First - the best fit	C	A	B	A	**D**	C
Second – to best fit	E	**D**	**D**	**D**	A	E

In this study, two basic methods for calculating *f* from physical boundary roughness measurements have been used. The first A was Heerman's who suggested using standard deviation and the second by using the Colebrook-White equation. According to the second one there were four proposals B, C, D and E as to how k_s and h are related (see §3.1.1). The two statistics used in the roughness height estimations, namely the mean range and the standard deviation yield comparable results. However, it was found that by rearranging the constant term in the Colebrook-White equation method A or D ($k=h_\lambda$) gives better

agreement with the experimental data than C ($k_s=2h_\sigma$), E ($k_s=2h_\lambda$) or B ($k_s=h_\sigma$). Because the variance is a quadratic function it is more likely to stand out in the data then the linear mean range when the surface has deep anomalies (cuts). For this reason, the mean range estimate of h is preferred to that of the variance.

Methods C and E, using double the k_s-values of B and D respectively, were found to mainly overestimate laser data values for f. This would mean that the assumption that $k_s=2h$ is not correct, and that the best estimator for hydraulic resistance would be using method D or A. However, Heerman's method was found to be inaccurate because of the flow types that were found in tested PCV pipes.

From the testing of methods over the six different surface types, the method of choice for T5, T6, T8 and T9 setups for the calculation of f from physical boundary roughness measurements is method D. However, the best fitting method for experimental sets: T4 and T10 with finer surface roughness than the other sets is method E.

4 COMPARISON BETWEEN EXPERIMENTAL RESULTS AND DEDUCED DATA FROM TUNNELS IN OPERATION

4.1 Collecting data of head loss measurements in Kárahnnjúkar HEP, Iceland and deduction of hydraulic friction factors for different rock types from the data

The first phase of the study was a literature analysis. Information on frictional losses in fluid flow in closed conduits was gathered. The focus was on finding values for equivalent sand grain roughness for different types of geology of TBM bored water conveyance tunnels.

A methodology based on recent publications was developed to predict the tunnel roughness of the Kárahnnjúkar headrace tunnel. Accurate calculations and measurements were carried out over a period of two years, during the construction of the tunnel, and published in a report provided by Landsvirkjun, Iceland's national power company (Hakonardottir, Tómasson, Kaelin and Stefansson, 2009) used in this chapter.

The history of rock TBMs started and was developed in XIXth century with the beginning of history of long tunnels. Rapid improvements in technology permitted TBMs to overcome strong, abrasive rock. They began to spread their range into harder and harder rock and to allow enlarged penetration rates and at larger diameters as time went on. TBMs cannot alone provide economic tunnel excavation, when dealing with difficult ground. To avoid problems it is necessary to have project coordination, management and planning while using the most suitable method and equipment. For optimal performance of proper selected TBMs intact rock properties together with rock mass characteristic should be well investigated (Pelizza, 1998).

The Kárahnnjúkar Hydroelectric Project is located on the east coast of Iceland. The generated electricity of 690 MW is supplying an aluminum smelter located close by. The project, named after the nearby Mountain Kárahnjúkur, involves damming the Jökulsá á Dal River and the Jökulsá í Fljótsdal river with five dams, creating three reservoirs (Figure 4.1).

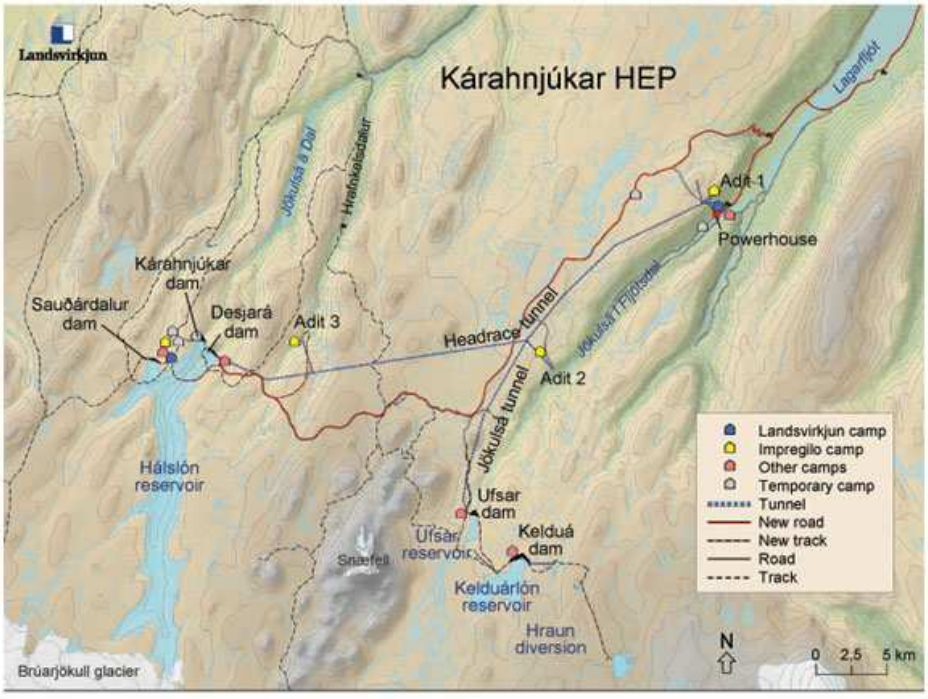

Figure 4.1 The Kárahnjúkar Project Structures and Reservoirs on East of Iceland (Hakonardottir, Tómasson, Kaelin and Stefansson, 2009).

Water from the reservoirs is diverted through 73km of underground water tunnels and down two 420m long vertical penstocks towards six Francis' turbines. The headrace tunnel from Hálslón reservoir is 40 km long. Almost 90% of the tunnel is excavated by TBM (Figure 4.2). The gross head of HEP is 600m. The tunnels were designed for discharge equal to 144 m^3/s.

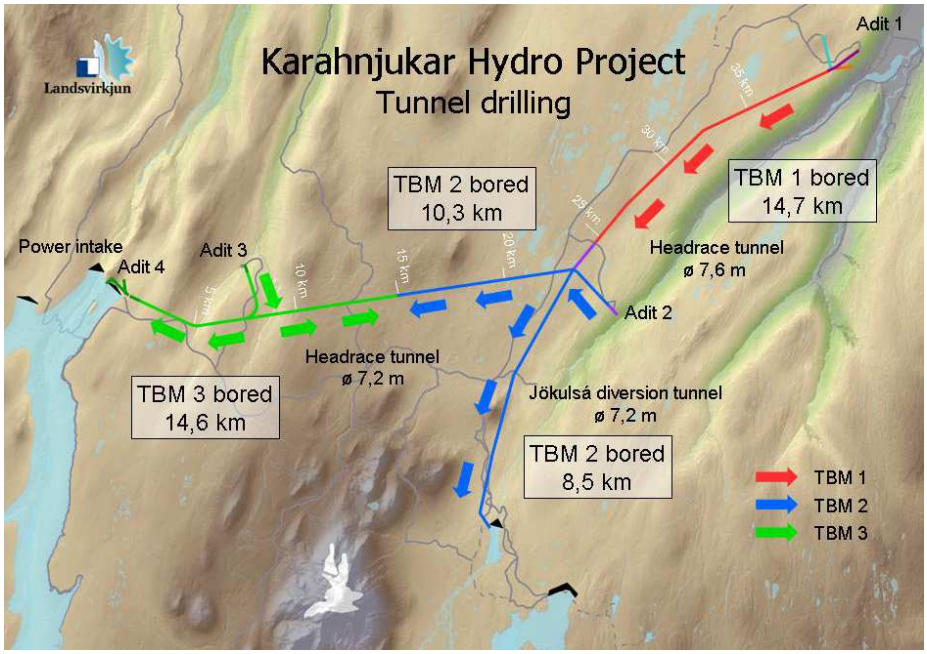

Figure 4.2 Paths taken by the three TBMs and their performance of Kárahnjukar HEP (Hakonardottir, Tómasson, Kaelin and Stefansson, 2009).

Design criteria for the Kárahnnjúkar headrace tunnel were based on investigations of existing friction factors and roughness data from various sources such as university research, published literature and data from hydropower operating plants. Kárahnnjúkar HEP is mostly excavated through highly heterogeneous basaltic rock, and the roughness of the tunnel was expected to be larger than for sandstone.

The frictional head loss of the TBM bored Kárahnnjúkar headrace tunnel involved systematic visual inspections of the tunnel walls. The inspected surfaces were classified into one of 15 categories by its intact small scale roughness and larger scale rock features such as joints and pockets. The intact roughness categories are smooth, medium and rough. The classification into three categories was based on measurements of the average maximum deviation of the surface from a straight bar. Almost 65% of the tunnel is excavated through basalt and the other 35% of the tunnel is excavated through sedimentary rock formations (mostly sandstone and conglomerate, some tuff and siltstone). The tunnel is mostly unlined, but some 9km of the tunnel walls are shotcreted and small portions are lined with concrete. The shotcreted part is approximately 33% smooth, 50% medium and 17% rough. 25% of the unlined tunnel surfaces were smooth, 62% were medium and 13% rough.

The tunnel wall surfaces were scanned with a high accuracy laser scanner (see chapter 3) and roughness profiles for each roughness category were produced (Figure 4.3).

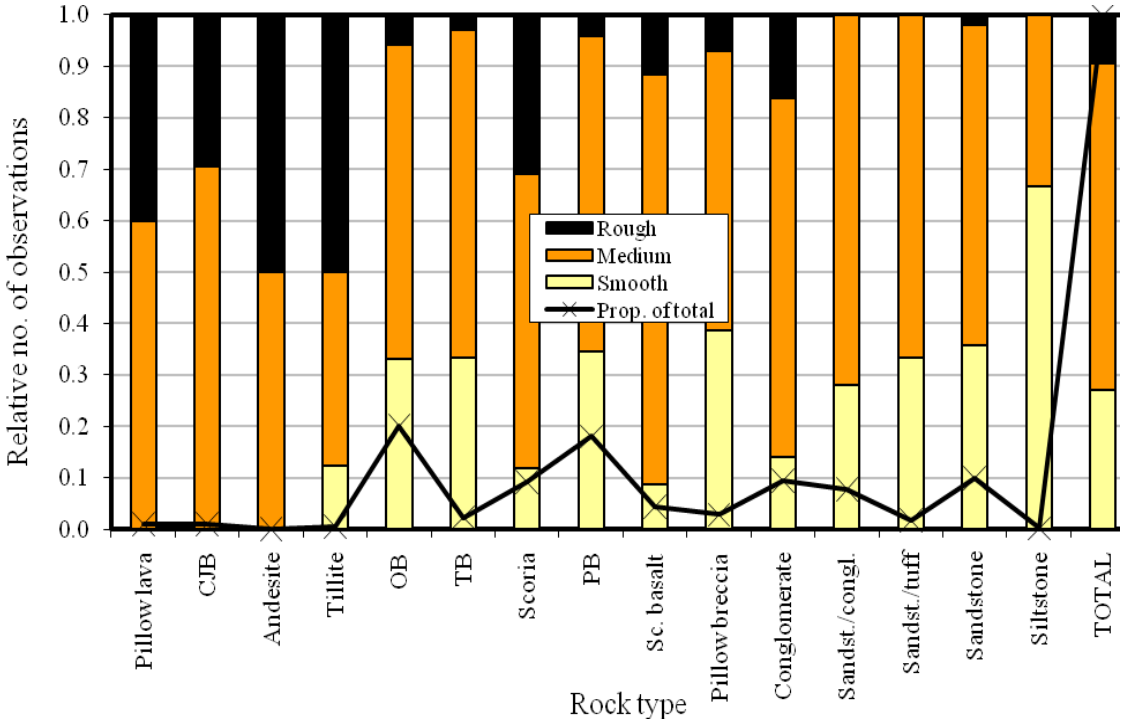

Figure 4.3 The surface roughness at 628 locations as a function of rock type and the proportion of each rock type within the tunnel. Sh: shotcrete, Gr: granite, Sa: sandstone, PB: porphyritic basalt, OB: olivine basalt, TB: tholeitic basalt, Sc. basalt: scoracious basalt, CJB: cube jointed basalt. Also shown are values obtained by Pegram and Pennington (1996) for granite and sandstone for comparison (Hakonardottir, Tómasson, Kaelin and Stefansson, 2009).

Each roughness profile was processed leading to one representative value of the physical roughness height for each profile. The physical roughness height of each roughness profile was transformed to a hydraulic roughness coefficient using method D for each roughness and joint category (see chapter 3 for description of method D).

Figure 4.4 shows rock types and joints along the different tunnel stretches. It is based on categorization at 628 locations for the different types of geology in the tunnel. The rock type with largest proportion of rough surfaces are pillow lava, cube jointed basalt and andesite (almost half of the surfaces are rough) next in order are tillite, scoria, pillow breccia, scoracious basalt and conglomerate. The rock types with the largest proportion of smooth surfaces are: siltstone, sandstone/tuff, and sandstone/conglomerate.

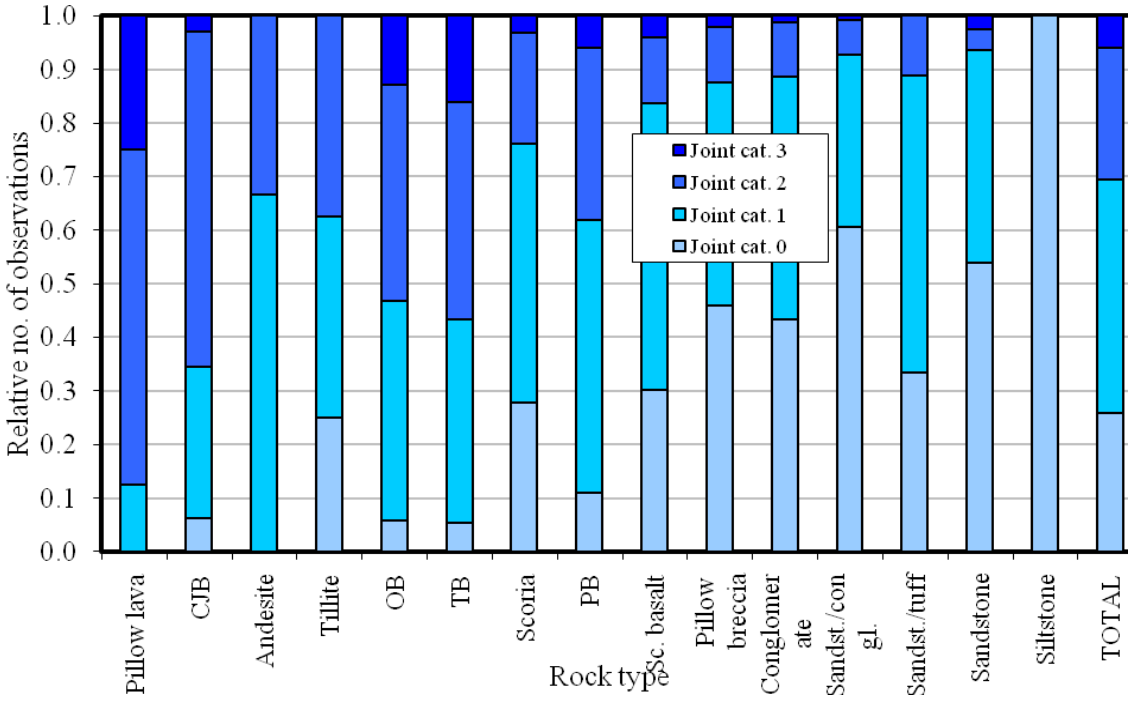

Figure 4.4 Rock types and joints(Hakonardottir, Tómasson, Kaelin and Stefansson, 2009).

The equivalent sand grain roughness for each rock type in the tunnel was derived based on the head loss contribution of the 15 categories (see Figure 4.5).

The average roughness value of each rock type should be most accurate for the rock types that are most common in the tunnel. The igneous rock formations in the tunnel were considerably rougher than the sedimentary rock. For porphyritic basalt the equivalent sand grain roughness was approximately 7.5mm; for olivine basalt almost 8.5mm – due to occurrences of larger joints. The scoria and scoracious basalt was of medium roughness 7-9 mm; pillow lava and cube jointed basalt in the range 15-19mm. The sedimentary formations of dilstone, sandstone, tuff and conglomerates were smoother with some occurrences of mainly shallow pockets with equivalent roughness values in the range 3-6 mm. similar values were for sandstone and granite.

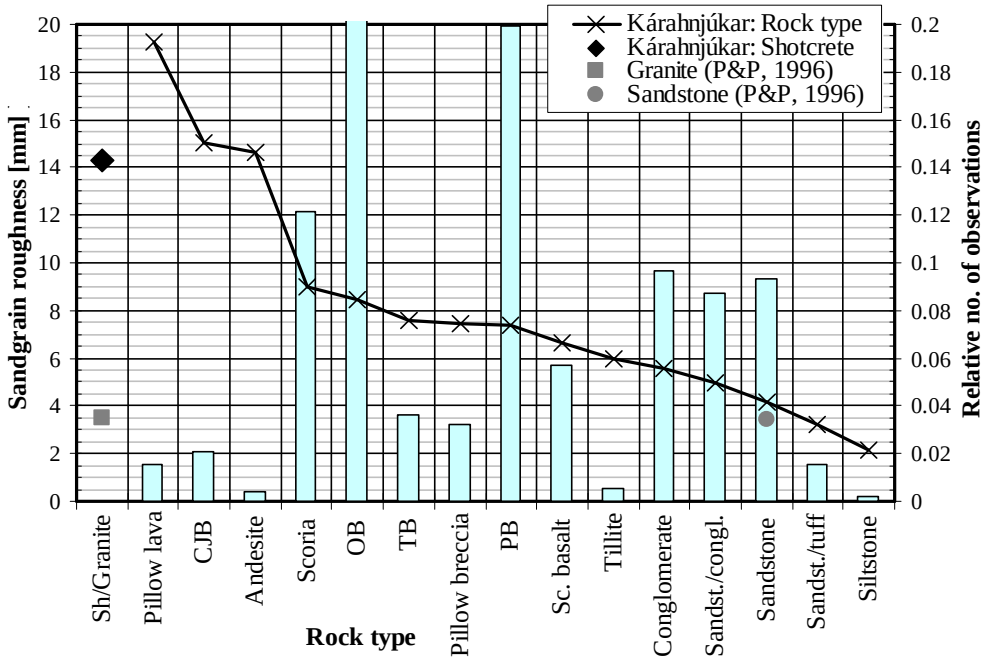

Figure 4.5 Nikuradse´s equivalent sandgrain roughness, k_s as a function of rock type (solid black line) and the relative amount of each rock type in the tunnel, prior to tunnel lining (blue columns). (Hakonardottir, Tómasson, Kaelin and Stefansson, 2009).

4.2 Calculations of friction factor for Kárahnnjúkar HEP, Iceland

Seven pressure sensors are located along the Kárahnnjúkar headrace tunnel. Five of them are in pressure gauges (AV01-AV04). Two sensors are fixed to the ceiling, close to the surge shaft and one in the surge tunnel (VST). Additional pressure measurements are connected to the power station's control and monitoring system.

The total length of TBM bored tunnels is 35488m and excavated with drill and blast method - 1704m (Table 4-1).

Table 4-1 The tunnel stretches between measurement locations in Kárahnnjúkar HEP (Hakonardottir, Tómasson, Kaelin and Stefansson, 2009).

Tunnel reach	Length of TBM bored section[m]	Length of Drill and Blast section [m]	Diameter [m]
AVO1-AVO2	5106	136	7.2
AVO2-AVO3	6832	23.4	7.2
AVO3-AVO4	8847	1282.3	7.2
AVO4-VST	14703	262.7	7.4

The most heavily jointed rock types, mostly shotcreted, are in stretch AV01-AV02 therefore it should have the highest value of friction factor, *f* (see chapter 2). For AV02-AV03 stretch smaller joints were observed and with higher proportion of the smooth rock surfaces. Mostly consist of porphyritic basalt scoria, olivine basalts and conglomerate. AV03-AV04 consists mostly of the same types of rock as AV02-AV03 but is slightly less rough. The rock in AV04-VST stretch is mostly porphyritic basalt, sandstone, scoria and olivine basalt. Shotcrete lining was roughest along AV01-AV02 than elsewhere in the headrace tunnel and the smoothest along AV04-VST (see Figure 4.6)

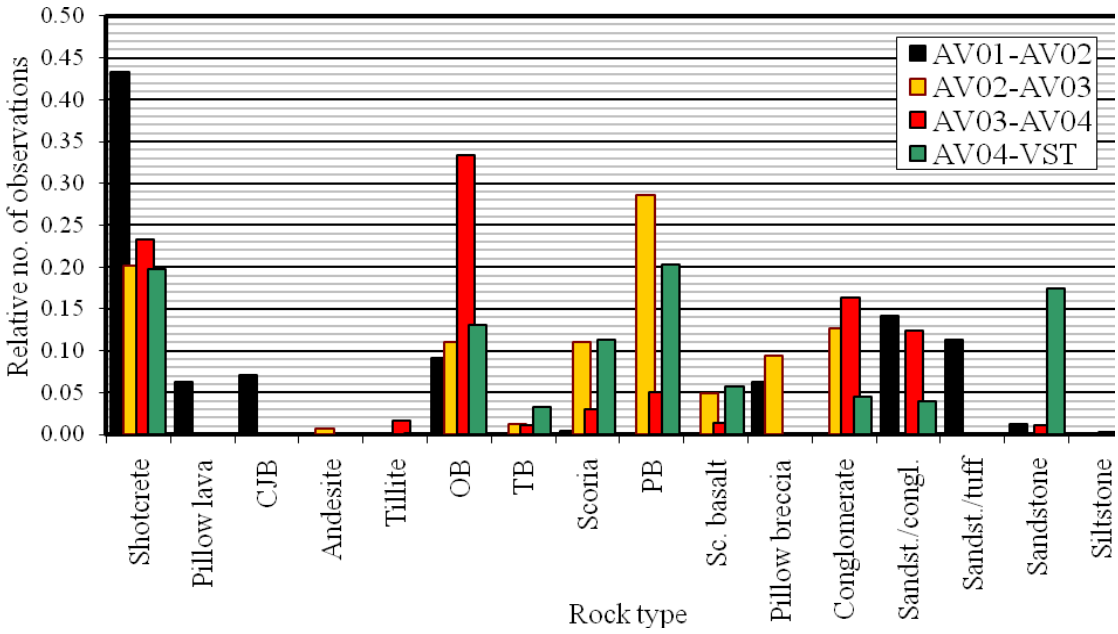

Figure 4.6 Rock type along each tunnel section.

Frictional head losses corresponding to the design discharge rates through the tunnel (Q=144 m^3/s), were calculated for each roughness category using the friction factors given by the Colebrook-White formula and the Darcy-Weisbach (see Equation 2-4 and Equation 2-9).

The measured frictional head losses along the TBM bored tunnel stretches were compared with the calculated for discharge through the tunnel Q=120 m^3/s frictional head losses along the same stretches (from laser measurements) as shown in Table 4-2.

$$H_L = h_f + h_{d\&b} + h_k$$

Equation 4-1

where:

H_L = the total head loss along the stretch [m]

h_f = the frictional loss along TBM bored stretches [m]

$h_{d\&b}$ = the frictional loss along drilled & blasted stretches

h_k = minor losses (singular losses) [m]

Table 4-2 Measured and calculated frictional head losses in each tunnel stretch, for Q=120 m^3/s.

TBM tunnel stretch	Measured head losses, h_f [m]	Calculated head losses h_{fc} [m]
AVO1-AVO2	6	8
AVO2-AVO3	10	9
AVO3-AVO4	11	13
AVO4-VST	15	14

The position of the first pressure sensor is 2000 m lower than the Hálslón reservoir and the measured pressure head there is approximately 595m a. s. l. The differences between calculated and measured results vary in range of 5 to 27%. Head losses between AV01and AV02 as well AV03- AV04 are overestimated, while AV02-AV03 and AV04-VST are slightly underestimated (Figure 4.7).

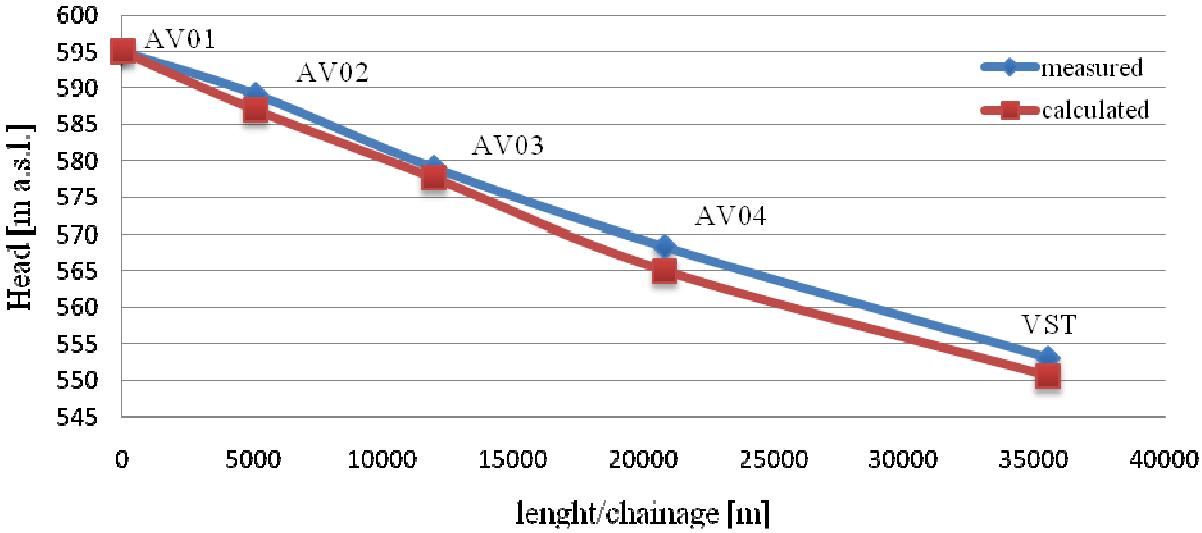

Figure 4.7 The calculated (h_k, $h_{d\&b}$) and measured (H_d) head losses in Kárahnnjúkar HEP.

The specific head losses for shotcrete sections with heavily fractured rocks (AV01-AV02) are not well determined. This tunnel has the smallest amount of smooth surfaces and the largest amount of rough surfaces. Heavily jointed rock may slightly decrease the internal diameter of the tunnel leading to slightly lower flow velocity and thus head loss for constant friction factors.

AV04 – VST have greater diameter consequently there are higher velocity and higher specific head losses. The calculated average head losses along AV04-VST are approximately the same as the measured head losses. The difference between two results was 5%. This stretch is made mostly of smooth surfaces (sandstone, conglomerate) with relatively small values of roughness to other tunnel stretches as shown in Figure 4.6.

For whole tunnel length (from AV01 to VST) the difference in measured (42m) and calculated (44m) head losses varys approximately in 5%.

The hydraulic roughness for each stretch of the headrace tunnel was calculated and refers to equations and is shown in Figure 4.8

.

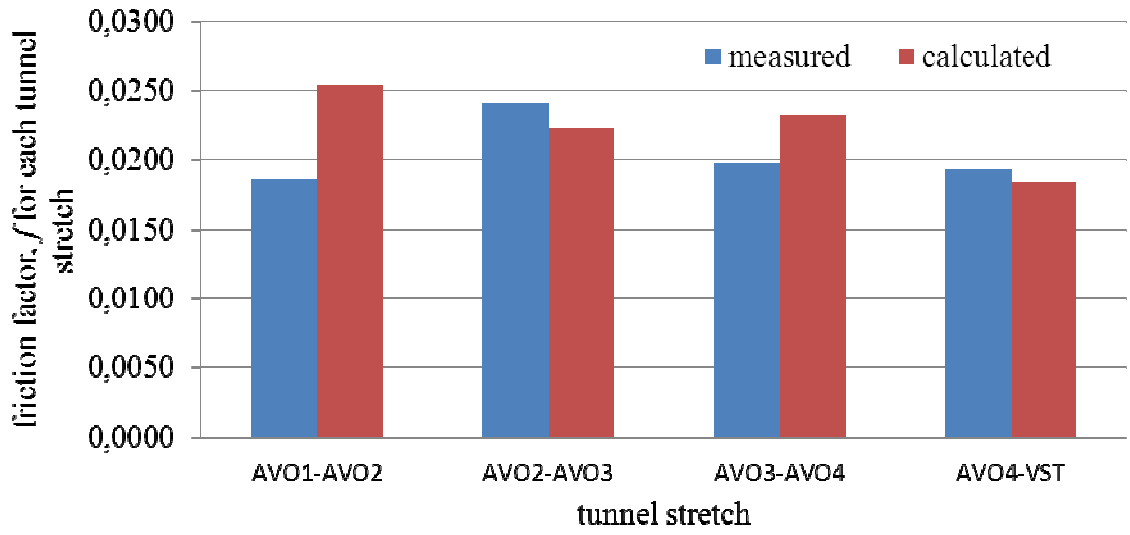

Figure 4.8 Comparison of measured and calculated friction factors, f for each tunnel stretch.

Measured and calculated values of friction factor differ noticeable. For first two stretches the difference reaches over 30% but only 5% for AV04 – VST.

According to results given by laser scans the roughest stretch is AV01 - AV02 not AV02 – AV03 as the measurements present. The difference is related, the same way, to measurements of head loss for this stretch of the tunnel.

AV02-AV03 and AV03-AV04 have slightly different calculated friction factors. Both stretches have the largest proportion of smooth rock surfaces and much less on average rough rock formation. They have a similar amount of shotcrete in the tunnel, but the shotcrete along AV02-AV03 was observed to be slightly smoother.

The smallest value of friction factor, f is for AV04-VST.

The diversity of the rock wall surface creates limitations. Shotcreted tunnels, rough or heavily jointed unlined surfaces can be hard to define. When surface roughness increases and the joints getting deeper the variance from an average value also gets grater. For tunnels where predicted is high friction factor it is suggested to make more laser scans of surfaces to get accurate average value of the physical roughness or to think about methodology of conversion from physical roughness to hydraulic roughness to predict overestimates results for that kind of surfaces.

4.3 Conclusions

Data of head loss measurements in Kárahnjúkar HEPs in operation and a deduction of hydraulic friction factors for different rock types from the data were delivered. The comparison between experimental results and deduced data from tunnels in operation was

made and remarks on values of hydraulic roughness for different rock types in TBM bored tunnels were shown.

A verification of hydraulic friction values was obtained by measurements of actual head losses at four different locations along the headrace tunnel. The measurements provided verification of estimated head losses through tunnel stretches passing through many different rock formations but did not provide direct verification of estimated roughness of individual rock types.

The investigation reveals that measured results for head losses and friction factors are not reliable when it comes to measurements of heavily, abrasive, jointed rocks. Methodology presented in thesis consists of many errors, which can be reduced by making more effective tests.

Laser scans provide accurate rock surface characterization, but there is shown that for smooth or medium surfaces results as well for whole tunnel lenght the calculated results are comparable with the measured ones.

It was identified how for specific types of rock head losses through the tunnel may behave. The measurements provide important information about values of roughness for different types of geology of TBM bored water conveyance tunnels. Further research including laboratory tests and laser measurements may improve methods for estimating head loss of unlined tunnels, excavated with tunnel boring machines water conveyance tunnels which will leads to the improvement of accurate prediction of the power output of HEPs.

5 HYDROELECTRIC PROJECTS IN POLAND

5.1 Introduction

Water power engineering in Poland plays only a minor part in general power production due to the lack of proper conditions to build water power plants as well as high construction costs. There are no good hydrological and geographical conditions for the development of hydropower or construction of large hydroelectric power stations. This potential is limited due to small mountain area, high permeability of soils or insufficient rainfall.

Poland has a moderate climate with both maritime and continental elements. This is due to humid Atlantic air which collides over its territory with dry air from the Eurasian interior. As the results weather tends to be capricious and the seasons differ with regard to rainfall (therefore small Polish water potential occurs in not to heavy rain falls).

The Polish landscape is very diverse. Many elements have formed it over a period of a million years. The lowlands stretch all over the central and northern parts of the country. Only in southern parts is alpine landscape with the Carpathian Mountains. Largely flat lie of the land and soils with large permeability are not optional conditions for the design of HEPs.

The domestic reserves of hydro energy are mainly concentrated in the Vistula River basin or in Odra River and the rivers of Pomerania. Approximately 80% of the Vistula river and its tributaries with a focus on the lower part of the river with more than 40 % hydropower capacity, in the top part of 25% and in median of 15%. The Odra river basin is about 18% of the national technical capacity, the rest are other Polish rivers.

The Polish hydro-energy reserves are estimated at 13.7 TWh/year (about 0.1% of world reserves). At present Poland uses only 12% of its hydro-energy reserves, which amounts to 7.3% of installed power in the country's power energy system. In comparison, France uses almost 100%, Norway 84%, and Germany 80% of their water reserves. According to the statistics at the end of 1999, at 34,200MW installed capacity in the Polish Power System installed hydroelectric power is about 2200MW, which represents less than 6.5 % of the total installed capacity.

5.2 Current HEPs

Nowadays there are about 590 HEPs in Poland. Most of them are small hydropower plants with power output of less than 5MW. Only eighteen polish hydropower plants have the output of more than 5MW. The biggest Hydroelectric project in Poland is called Zarnowiec no. 1 in Figure 5.1 (4 x Francis turbine, each 179MW), Porabka Zar no. 2 in Figure 5.1 (500 MW), Solina no. 3 in Figure 5.1 (200MW), Włocławek no. 4 in Figure 5.1 (162 MW) and Żydowo no. 5 in Figure 5.1 (150MW) (Mikulski, 2004).

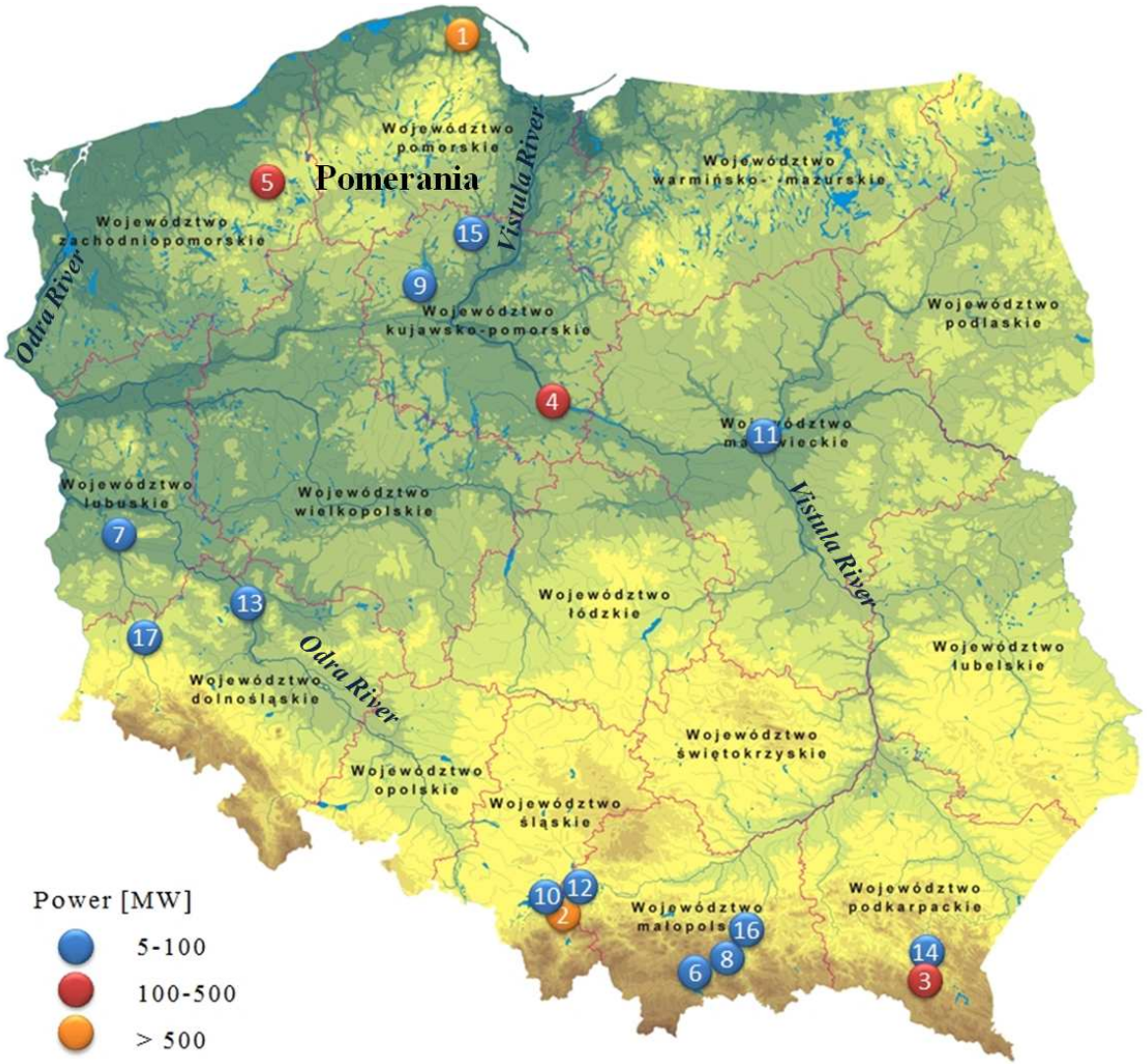

Figure 5.1 Locations of Power Plants in Poland

Table 5-1 List of Polish Hydropower Plants *(Mikulski, 2004).*

Number	Name	River	Year	Power (in MW)
1	Żarnowiec	Żarnowiec Lake	1982	716
2	Porąbka Żar	Soła	1979	500
3	Solina	Soła	2003	200
4	Włocławek	Vistula	1970	162
5	Żydowo	Kamienna Lake Kwieckie Lake	1971	151
6	Czorsztyn – Niedzica Sromowce Wyżne	Dunajec	1997	92.1
7	Dychów	Bóbr	1936	79.5
8	Rożnów	Dunajec	1941	50
9	Koronowo	Brda	1961	26
10	Tresna	Soła	1967	21
11	Dębe	Narew	1963	20
12	Porąbka	Soła	1953	12.6
13	Brzeg Dolny/ Wały Śląskie	Odra	1958	9.8
14	Myczkowce	San	1962	8.3
15	Żur	Wda	1929	8.0
16	Czchów	Dunajec	1951	8.0
17	Pilchowice	Bóbr	1912	7.5
18	Bielkowo	Radunia	1925	7.2

Zarnowiec is an example of a typical pumped – storage power plant. The intake of the HEP is totally artificial and has volume equal to 13.6 million cubic metres. The outtake is Zarnowiec Lake with 122 hectares of surface. Penstock creates four steel pipelines of 1.1km in length.

Figure 5.2 Zarnowiec Hydro Power Plant.

The power plants in Porabka – Zar and Zydowo are pumped storage plants as well.

The water storage station in Solina contains of two classic reversible turbines with the total power output of 136MW until year 2003 when modernization of a project was made and the installed power has increased up to 200MW.

Figure 5.3 Solina Hydro Power Plant.

In 1997 the newest power plant started to operate. Project is located in Niedzica on the Dunajec River. It has two turbines, each 46MW power output.

Figure 5.4 Niedzica Hydro Power Plant

5.3 Future development

Based on data contained in the "Polish Energy Policy until 2030" available with attachments on the website of the Ministry of Economy in 2006 water power was used in almost 50% compared to other types of renewable energy sources. In 2030 instead of water power, wind energy will take that place with nearly 50 % share in electricity demand of the final gross of other renewable sources.

In current economic and legal context of Polish hydro power plant development of this source of energy is unlikely to increase. There are great difficulties with constriction of medium and large HEPs due to:

- high capital cost ranging in billions of euros,
- limited government spending on renewables power resources,
- poor recognition of benefits associated with flood control provided by the dams,
- strong opposition of environmental organizations.

Polish government needs to ensure a stable share in production and purchase of renewable energy companies engaged in electricity trading. It will be helpful if there were clearly defined and stable prices and tax preferences with clear Energy Law and Water Law. Further support should be active supporting of new technical research and the promotion of effective solutions.

5.4 Tunnel Boring Machines in Poland

It is only cost effective to use TBMs to bore tunnels when the tunnels exceed a certain length. Up until the present TBMs have not been used for the construction of tunnels in Poland.

However, there is one and first upcoming TBM project planned in Poland. In Warsaw, the capital of Poland, Czajka Sewage Treatment Plant is waiting for a specially designed Tunnel Boring Machine in order to drill a tunnel under Vistula River. The main task of that tunnel is to drain sewage from the left bank of the river to the Czajka treatment. TBM diameter will be 4.5 meters. The tunnel will be placed 10 meters under the bottom of the Vistula River, and its length will be close to 1400 meters. The whole achievement is so important because the capital will finally stop polluting the Baltic Sea, and currently sewage from the left-bank of Warsaw goes to the Czajka Plant.

In applying this new technology sewage treatment sector overtook the Warsaw Metro which is under construction now. Next year it is planned to use 70 meters long TBM to drill a central part of the second Metro line (Szolucha, 2011).

6 FINAL CONCLUSIONS

High tunnel roughness can significantly reduce the efficiency of hydroelectric station. Every percentage point saved in head losses equals in more economic benefits for hydropower plants. It also means more benefits to the clients. It is important to gather knowledge about tunnel roughness to modify operational rules for the hydropower systems. The methodology implemented for this thesis project offers more accurate head loss estimation, crucial for future investments in HEPs.

For understanding and estimating the surface roughness of lined and especially unlined tunnel walls direct measurements with a laser may be needed. The study presented here identify the most suitable method for transforming the measured physical roughness to hydraulic roughness and suggests values of hydraulic roughness of different rock types counted in the volcanic headrace tunnel of the Kárahnjúkar HEP, in Iceland.

The experimental design and method with experimental apparatus were derived. The hydraulic roughness of the pipes was calculated from hydraulic roughness calculated from measured head loss and compared with hydraulic roughness calculated from the physical roughness data. Laser scans of the pipe surfaces were taken. Observations on the best method for the conversion were established. The comparison between experimental results and deduced data from tunnels in operation; remarks on values of hydraulic roughness for different rock types in TBM bored tunnels were described.

The experiments showed that the presented model work well, with not very significant mistake to laser measurements of the same surface. However, for further, accurate results measurements need to be derived with different Reynolds number and values of the discharge. This will be served only with other sets of pipes with different diameters and roughness.

Many lessons were learned from the flow testing instrumentation and consequent data analysis. Testing had provided a baseline set of results, not only for future design criteria, but also for future testing of rock surfaces. This is particularly important, as the knowledge of the effect of a relationship between the rough surface inside the pipes and the measured head loss in a conduit is somewhat limited.

Most important thing is to improve the accuracy of linking the scanned data of wall roughness to the actual equivalent sand grain roughness, as this is independent of tunnel diameter.

Major economic benefits may result, which will affect future water projects and, certainly, the further development of TBM technology in such countries as Poland.

Poland has a fair experience in HEPs but even greater potential for improvement due to aging assets. TBMs weren’t ever used for HEPs in Poland, mostly because of poor hydrological and geographical conditions. However, it is just a matter of time, when many benefits of this technology will be seen and it’ll become more popular, starting from Czajka Sewage Treatment Plant. This study may become a base for improving design of Hydroelectric project in Poland and give useful information about hydraulic roughness of TBM-bored tunnels.

REFERENCES

Boeriu, P. and V. Doandes 1997. ‘A new method for in situ determination of the roughness coefficient of the hydropower plant tunnels’ , *Hydropower '97*, Broch, Lysne, Flatabø & Helland-Hansen (eds). Balkema, Rotterdam, pp. 575-580.

Garnayak, M.K. 2001. *Hydraulic head losses in an unlined pressure tunnel of a high head power plant. Theoretical approach and comparison with the measured values. Case Study of 2x72 MW Chimay Hydropower Project, Peru,* Postgraduate Diploma project. *LCH, EPFL* pp. 14, 2001.

Hákonardóttir, K.M., Tomasson, G.G. og Stefansson, B. 2009. ‘The hydraulic roughness of TBM tunnels in basaltic and sedimentary rock: Measurements of headlosses in the Kárahnjúkar HEP, Iceland’, *The International Journal on Hydropower & Dams,* Hydro 2009, Lyon, France.

Hákonardóttir, K.M., Tomasson, G.G. & Stefansson, B. 2009. ‘The hydraulic roughness of unlined and shotcreted TBM-bored tunnels in volcanic rock: In-situ observations and measurements at Kárahnjúkar Iceland’ - *Tunnelling and Underground Space Technology*, In press, doi:10.1016/j.tust.2009.07.007.

Landsvirkjun, February 2009. *Kárahnjúkar Waterways. Roughness measurements and headloss calculations*, Report RE-KMH-001-R1.

Leifsson, Þ.S. ‘HYDRO604: Waterways lectures. Hydraulic design static flow’, paper presented to the students of University of Iceland and University of Akureyri (Hydropower specialization 2011), 9-13 September.

Mikulski, Z. 2004. ‘The development of the utilisation of water power in Poland’, *Miscellanea Geographica*, Warsaw 2004, Vol.11.

Pegram, G.G.S. and M.S. Pennington, 1996. *A method for estimating the hydraulic roughness of unlined bored tunnels*”, Report to the Water Research Commission by the Department of Civil Engineering, University of Natal, WRC Report No 579/1/96. ISBN No. 1 86845 219 0.

Pelizza, S. 1998. *TBM Bored long rock tunnels*, vieved 23 january 2011, *http://www.ita-aites.org/fileadmin/filemounts/general/pdf/ItaAssociation/WhatIsITA/CommemorativeBook/pelizza.pdf*, PDF file.

Stutsman, R.D. 1987. Asce, M. ‘TBM Tunnel Friction Values for the Kerckhoff 2 Project’, *Water Power ’87*, pp. 1710-1725.

Szolucha, P. 2011. ‘Oczyszczalnia Czajka szybsza od Warszawskiego Metra’, *Polska,* viewed 23 january 2011, <http://www.polskatimes.pl/aktualnosci/356098,oczyszczalnia-czajka-szybsza-od-warszawskiego-metra,id,t.html>.

Viljoen, B.C. and J.R. Metcalf, 1999. ‘Commissioning of the LHWP Delivery Tunnel: Overview of Work Done and Results Obtained’, *Tunnelling and Underground Space Technology*, Vol. 14, No. 1, pp. 37 - 54.

Appendix A

Table A-1 Observed data for TEST 1,3

Measur.	**P1**	P2	P 3	**P 4**	t	P 2-P 3	P 2-P 3	**P 1-P 4**	**P 1-P 4**
no.	**mmH2O**	mmH2O	mmH2O	**mmH2O**	s	mmH20	mH2O	**mmH20**	**mH2O**
1	**854.2**	435.8	325.5	**563.2**	53.92	110.3	0.11	**291.0**	**0.29**
2	**854.6**	427.8	321.8	**562.8**	55.14	106.0	0.11	**291.8**	**0.29**
3	**853.6**	431.3	323.8	**563.4**	55.26	107.5	0.11	**290.2**	**0.29**
4	**853.2**	435.8	327.3	**562.8**	54.38	108.5	0.11	**290.4**	**0.29**
5	**852.4**	434.8	328.3	**563.2**	56.11	106.5	0.11	**289.2**	**0.29**
average	**853.6**	433.1	325.3	**563.1**	54.96	107.8	0.11	**290.5**	**0.29**

Table A-2 Calculations for TEST 1,3, part 1

						goal seek		
Q	Q	U	ks	ks/D	ks/D * Re	f	to C-W	hf
l/sek	m3/sek	m/sek	mm	-	-	-	equation	m
7.91	0.00791	2.10			12	0.018	0	0.097877
7.74	0.00774	2.06			12	0.018	0	0.094529
7.72	0.00772	2.05	0.01	0.0001	12	0.018	0	0.094119
7.84	0.00784	2.09			12	0.018	0	0.097190
7.60	0.00760	2.02			11	0.018	0	0.091289
7.76	0.00776	2.06	0.01	0.0001	12	0.018	0	0.095001

Table A-3 Calculations for TEST 1,3, part 2

3 connections between manometers P1 and P4										
for L1-L4					**for L2-L3**					
hf	**f 1**	**ks**	**ks/D**	**ks/D * Re**	**hf**	**f 2**	ks	ks/D	ks/D * Re	%f
m	-	**mm**	**-**	**-**	**m**	-	mm	-	-	
0.271	**0.016**	**-0.03**	**0**	**-33**	**0.103**	**0.019**	0.004	0.00006	5	13%
0.272	**0.017**	**-0.02**	**0**	**-23**	**0.100**	**0.019**	0.005	0.00007	6	9%
0.271	**0.017**	**-0.02**	**0**	**-23**	**0.101**	**0.020**	0.010	0.00015	12	11%
0.270	**0.017**	**-0.03**	**0**	**-30**	**0.102**	**0.019**	0.004	0.00006	5	12%
0.270	**0.018**	**-0.01**	**0**	**-17**	**0.100**	**0.020**	0.017	0.00024	19	11%
0.271	**0.017**	**-0.02**	**0**	**-25**	**0.101**	**0.019**	0.008	0.00012	9	11%

Table A-4 Observed data for TEST 4

Measur.	**P1**	P2	P 3	**P 4**	t	P 2-P 3	P 2-P 3	P 1-P 4	P 1-P 4
no.	**mmH2O**	mmH2O	mmH2O	**mmH2O**	s	mmH20	mH2O	mmH20	mH2O
1	**852.0**	484.5	369.5	**454.4**	58.90	115.0	0.12	397.6	0.40
2	**850.4**	482.0	367.8	**453.0**	58.10	114.3	0.11	397.4	0.40
3	**850.0**	486.5	371.0	**452.8**	57.70	115.5	0.12	397.2	0.40
4	**850.0**	478.8	368.8	**453.0**	58.80	110.0	0.11	397.0	0.40
5	**849.4**	484.0	372.3	**451.0**	58.90	111.8	0.11	398.4	0.40
average	**850.4**	483.2	369.9	**452.8**	58.48	113.3	0.11	397.5	0.40

Table A-5 Calculations for TEST 4

3 connections between manometers P1 and P4													
			for P1-P4					for P2-P3					
Q	Q	U	**h_f**	**f 1**	**k_s**	**k_s/D**	**k_s/D * Re**	**h_f**	f 2	k_s	k_s/D	k_s/D * Re	%f
l/sek	m³/sek	m/sek	**m**	-	**mm**	**-**	**-**	**m**	-	mm	-	-	
7.24	0.00724	1.93	**0.381**	**0.028**	**0.20**	**0.003**	**216**	0.109	0.024	0.09	0.001	95	14%
7.34	0.00734	1.95	**0.380**	**0.027**	**0.17**	**0.003**	**192**	0.108	0.023	0.07	0.001	76	15%
7.39	0.00739	1.97	**0.379**	**0.026**	**0.16**	**0.002**	**180**	0.110	0.023	0.07	0.001	75	14%
7.26	0.00726	1.93	**0.380**	**0.027**	**0.19**	**0.003**	**211**	0.104	0.022	0.06	0.001	66	18%
7.24	0.00724	1.93	**0.381**	**0.028**	**0.20**	**0.003**	**218**	0.106	0.023	0.07	0.001	77	17%
7.30	0.00730	1.94	**0.380**	**0.027**	**0.18**	**0.003**	**203**	0.108	0.023	0.07	0.001	78	16%

Table A-6 Observed data for TEST 5

Measur.	**P1**	P2	P 3	**P 4**	t	P 2-P 3	P 2-P 3	P 1-P 4	P 1-P 4
no.	**mmH2O**	mmH2O	mmH2O	**mmH2O**	s	mmH20	mH2O	mmH20	mH2O
1	**863.8**	548.5	381.8	**384.0**	62.40	166.8	0.17	479.8	0.48
2	**863.2**	548.0	381.3	**384.0**	63.40	166.8	0.17	479.2	0.48
3	**863.0**	544.5	379.3	**384.0**	62.80	165.3	0.17	479.0	0.48
4	**863.0**	545.5	379.3	**383.8**	63.30	166.3	0.17	479.2	0.48
5	**863.0**	547.5	379.0	**383.8**	62.30	168.5	0.17	479.2	0.48
average	**863.2**	546.8	380.1	**383.9**	62.84	166.7	0.17	479.3	0.48

Table A-7 Calculations for TEST 5

Q	Q	U	**h_f**	**f 1**	**k_s**	**k_s/D**	**k_s/D * Re**	h_f	f 2	k_s	k_s/D	k_s/D * Re	%f
l/sek	m^3/sek	m/sek	**m**	-	**mm**	**-**	**-**	m	-	mm	-	-	
6.84	0.00684	1.82	**0.460**	**0.037**	**0.62**	**0.009**	**636**	0.162	0.039	0.72	0.010	738	5%
6.73	0.00673	1.79	**0.460**	**0.039**	**0.68**	**0.010**	**692**	0.162	0.040	0.79	0.011	803	5%
6.79	0.00679	1.81	**0.459**	**0.038**	**0.64**	**0.009**	**655**	0.160	0.039	0.72	0.010	742	4%
6.74	0.00674	1.79	**0.459**	**0.038**	**0.67**	**0.010**	**686**	0.161	0.040	0.78	0.011	789	4%
6.85	0.00685	1.82	**0.459**	**0.037**	**0.61**	**0.009**	**627**	0.163	0.039	0.73	0.011	757	6%
6.79	0.00679	1.81	**0.459**	**0.038**	**0.64**	**0.009**	**659**	0.162	0.040	0.75	0.011	766	5%

Table A-8 Observed data for TEST 6

Measur.	**P1**	P2	P 3	**P 4**	t	P 2-P 3	P 2-P 3	P 1-P 4	P 1-P 4
no.	**mmH_2O**	mmH_2O	mmH_2O	**mmH_2O**	s	mmH_20	mH_2O	mmH_20	mH_2O
1	**891.8**	541.8	368.0	**392.8**	67.90	173.8	0.17	499.0	0.50
2	**890.2**	544.5	372.3	**393.6**	67.50	172.3	0.17	496.6	0.50
3	**890.0**	541.5	369.5	**393.8**	67.30	172.0	0.17	496.2	0.50
4	**890.0**	541.8	371.3	**393.2**	67.90	170.5	0.17	496.8	0.50
5	**890.0**	539.3	370.3	**392.8**	67.90	169.0	0.17	497.2	0.50
average	**890.4**	541.8	370.3	**393.2**	67.70	171.5	0.17	497.2	0.50

Table A-9 Calculations for TEST 6

4 connections between manometers P1 and P4													
			for P1-P4					for P2-P3					
Q	Q	U	**hf**	**f 1**	**k_s**	**k_s/D**	**k_s/D * Re**	hf	f 2	k_s	k_s/D	k_s/D * Re	%f
l/sek	m^3/sek	m/sek	**m**	-	**mm**	**-**	**-**	m	-	mm	-	-	
6.28	0.00628	1.67	**0.482**	**0.047**	**1.20**	**0.017**	**1133**	0.169	0.049	1.35	0.019	1277	4%
6.32	0.00632	1.68	**0.479**	**0.046**	**1.14**	**0.016**	**1087**	0.168	0.048	1.27	0.018	1214	4%
6.34	0.00634	1.69	**0.479**	**0.046**	**1.12**	**0.016**	**1069**	0.168	0.047	1.25	0.018	1192	4%
6.28	0.00628	1.67	**0.480**	**0.046**	**1.18**	**0.017**	**1119**	0.166	0.048	1.28	0.018	1212	3%
6.28	0.00628	1.67	**0.480**	**0.046**	**1.18**	**0.017**	**1122**	0.165	0.047	1.25	0.018	1182	2%
6.30	0.00630	1.68	**0.480**	**0.046**	**1.16**	**0.017**	**1106**	0.167	0.048	1.28	0.018	1215	3%

Table A-10 Observed data for TEST 7

Measur.	**P1**	**P 4**	**t**	**P 1-P 4**	**P1-P 4**
no.	mmH_2O	mmH_2O	s	mmH_20	mH_2O
1	833.2	621.6	52.15	211.6	0.212
2	832.8	621.0	52.46	211.8	0.212
3	832.0	620.6	52.34	211.4	0.211
4	831.0	620.4	51.60	210.6	0.211
5	831.0	620.0	51.33	211.0	0.211
average	832.0	620.7	51.98	211.3	0.211

Table A-11 Calculations for TEST 7

Q	**Q**	**U**	f	hf per 1 m	**ks**	**ks/D**	**ks/D * Re**	**hf for T1, T3 (Q1)**	**hf for T1, T3 (Q2)**	hs	K per one connection
l/sek	m³/sek	m/sek	-	m/m (Q1)	**mm**	-	-	**m**	**m**	m	
8.18	0.00818	2.18	0.017	0.060	-0.017	0.000	-21	0.303	0.284	0.007	0.011
8.13	0.00813	2.16	0.017	0.060	-0.015	0.000	-18	0.304	0.275	0.017	0.026
8.15	0.00815	2.17	0.017	0.060	-0.016	0.000	-20	0.303	0.272	0.018	0.028
8.27	0.00827	2.20	0.017	0.060	-0.022	0.000	-27	0.302	0.272	0.019	0.028
8.31	0.00831	2.21	0.017	0.060	-0.023	0.000	-29	0.303	0.253	0.036	0.058
8.21	0.00821	2.18	0.017	0.060	-0.018	0.000	-23	0.303	0.271	0.019	0.030

Table A-12 Observed data for TEST 8

Measur.	**P1**	P2	P 3	**P 4**	t	P 2-P 3	P 2-P 3	P 1-P 4	P 1-P 4
no.	**mmH2O**	mmH2O	mmH2O	**mmH2O**	s	mmH20	mH2O	mmH20	mH2O
1	**874.0**	489.0	348.3	**414.6**	62.80	140.8	0.14	459.4	0.46
2	**873.8**	496.8	351.3	**413.2**	62.90	145.5	0.15	460.6	0.46
3	**874.0**	486.5	348.3	**413.0**	63.20	138.3	0.14	461.0	0.46
4	**874.0**	497.0	351.8	**413.0**	62.40	145.3	0.15	461.0	0.46
5	**873.0**	496.3	347.8	**412.8**	62.90	148.5	0.15	460.2	0.46
average	**873.8**	493.1	349.5	**413.3**	62.84	143.7	0.14	460.4	0.46

Table A-13 Calculations for TEST 8

4 connections between manometers P1 and P4													
				for P1-P4					for P2-P3				
Q	Q	U	**hf**	**f 1**	**ks**	**ks/D**	**ks/D * Re**	hf	f 2	ks	ks/D	ks/D * Re	%f
l/sek	m³/sek	m/sek	**m**	-	**mm**	**-**	**-**	m	-	mm	-	-	
6.79	0.00679	1.81	**0.439**	**0.038**	**0.63**	**0.009**	**648**	0.136	0.035	0.48	0.007	494	8%
6.78	0.00678	1.80	**0.441**	**0.038**	**0.64**	**0.009**	**659**	0.141	0.036	0.55	0.008	561	5%
6.75	0.00675	1.79	**0.441**	**0.038**	**0.67**	**0.010**	**679**	0.133	0.035	0.47	0.007	482	10%
6.84	0.00684	1.82	**0.441**	**0.037**	**0.61**	**0.009**	**632**	0.140	0.035	0.52	0.007	532	5%
6.78	0.00678	1.80	**0.440**	**0.038**	**0.64**	**0.009**	**658**	0.144	0.037	0.59	0.008	602	3%
6.79	0.00679	1.81	**0.440**	**0.038**	**0.64**	**0.009**	**655**	0.139	0.035	0.52	0.008	534	6%

Table A-14Observed data for TEST 9

Measur.	**P1**	P2	P 3	**P 4**	t	P 2-P 3	P 2-P 3	P 1-P 4	P 1-P 4
no.	**mmH2O**	mmH2O	mmH2O	**mmH2O**	s	mmH20	mH2O	mmH20	mH2O
1	**871.6**	469.3	345.3	**471.6**	60.30	124.0	0.12	400.0	0.40
2	**871.0**	467.8	345.0	**471.2**	60.50	122.8	0.12	399.8	0.40
3	**870.0**	467.8	344.3	**471.2**	60.30	123.5	0.12	398.8	0.40
4	**870.0**	467.3	346.0	**471.2**	60.30	121.3	0.12	398.8	0.40
5	**870.0**	470.5	345.0	**471.8**	60.60	125.5	0.13	398.2	0.40
average	**870.5**	468.5	345.1	**471.4**	60.40	123.4	0.12	399.1	0.40

Table A-15 Calculations for TEST 9

4 connections between manometers P1 and P4													
			for P1-P4					for P2-P3					
Q	Q	U	**hf**	**f 1**	**k_s**	**k_s/D**	**k_s/D * Re**	hf	f 2	k_s	k_s/D	k_s/D * Re	%f
l/sek	m³/sek	m/sek	**m**	-	**mm**	**-**	**-**	m	-	mm	-	-	
7.07	0.00707	1.88	**0.378**	**0.031**	**0.31**	**0.004**	**329**	0.119	0.027	0.17	0.002	185	13%
7.05	0.00705	1.87	**0.378**	**0.031**	**0.32**	**0.005**	**336**	0.117	0.027	0.17	0.002	181	13%
7.07	0.00707	1.88	**0.377**	**0.031**	**0.30**	**0.004**	**325**	0.118	0.027	0.17	0.002	181	13%
7.07	0.00707	1.88	**0.377**	**0.031**	**0.30**	**0.004**	**325**	0.116	0.026	0.15	0.002	165	14%
7.04	0.00704	1.87	**0.377**	**0.031**	**0.31**	**0.005**	**334**	0.120	0.027	0.19	0.003	204	11%
7.06	0.00706	1.88	**0.377**	**0.031**	**0.31**	**0.004**	**330**	0.118	0.027	0.17	0.002	183	13%

Table A-16 Observed data for TEST 10

Measur.	**P1**	**P 4**	t	P 1-P 4	P 1-P 4
no.	**mmH2O**	**mmH2O**	s	mmH20	mH2O
1	**895.0**	**299.8**	74.20	595.2	0.60
2	**895.0**	**299.8**	74.10	595.2	0.60
3	**895.0**	**299.8**	74.40	595.2	0.60
4	**895.0**	**299.8**	74.10	595.2	0.60
5	**895.0**	**299.8**	74.30	595.2	0.60
average	**895.0**	**299.8**	74.22	595.2	0.60

Table A-17 Calculations for TEST 10

4 connections				**for P1-P4**			
Q	Q	U	**hf**	**f 1**	**k_s**	**k_s/D**	**k_s/D * Re**
l/sek	m³/sek	m/sek	**m**	-	**mm**	**-**	**-**
5.75	0.00575	1.60	**0.583**	**0.060**	**2.27**	**0.034**	**2066**
5.76	0.00576	1.60	**0.583**	**0.060**	**2.26**	**0.033**	**2055**
5.73	0.00573	1.60	**0.583**	**0.061**	**2.30**	**0.034**	**2087**
5.76	0.00576	1.60	**0.583**	**0.060**	**2.26**	**0.033**	**2055**
5.74	0.00574	1.60	**0.583**	**0.061**	**2.29**	**0.034**	**2076**
5.75	0.00575	1.60	**0.583**	**0.060**	**2.27**	**0.034**	**2068**

Appendix B

Four laser measurements were done for one representative pipe from each setup. The only exception was T10 (paint and sand) were there were two pipes chosen as representative ones and 8 laser runs in total were done. Because the investigating pipes were bended shorter fragments had to be taken into considerations.

The script used to compute laser measurements in R 2.12.0 program:

```
library(graphics)

################
#Set work directory:
################
#Using the laptop:
#setwd("C:/laser")
#Using the K:/:
setwd("C:/laser")
initial.dir<-getwd()

################
#Run script:
################
#source("20101228read_data_test.R")


################
#File name:
###############
#.short
datafile<-"T10_P1-4.short.txt"
outfile<-"T10_P1-4.short.out"
epsfile<-"T10_P1-4.short.eps"



################
#Read the data from the scanner into raw_data:
################
#Using the laptop:
#setwd("C:/laser")
#raw_data<-read.table(datafile, header=TRUE)
#setwd(initial.dir)
#x_r<-raw_data[[1]]
#z_r<-raw_data[[3]]

#Using the K:/:
setwd("C:/laser")
```

```
raw_data<-read.table(datafile, header=TRUE)
setwd(initial.dir)
x_r<-raw_data[[1]]
z_r<-raw_data[[3]]

#A.Testing the code:
#setwd("../../TBM_Hydraulic_Tunnel_Inspections/Data_Scan/Test")
#raw_data<-read.table(datafile, header=TRUE)
#setwd(initial.dir)
#x_r<-raw_data[[1]]
#z_r<-raw_data[[3]]

#B.Testing the code:
#x_r<-seq(0,1000,0.25)
#z_r<-200*sin(x_r*0.001*2*pi)+200*sin(x_r*0.01*2*pi)+200*sin(x_r*0.1*2*pi)+400

#####


######################
#Ordering the data:
######################
sorted_data<-sortedXyData(x_r,z_r)
x_s<-sorted_data[[1]]
z_s<-sorted_data[[2]]-mean(sorted_data[[2]])
z_s2<-sorted_data[[2]]



####################
#Transforming the data onto a fixed grid, delta:
####################
N<-2^(12)
delta<-((max(x_s)-min(x_s))/N)
approx_data<-approx(sorted_data,n=N, method="linear")
x_approx<-approx_data$x
z_approx<-approx_data$y-(mean(approx_data$y))
fre<-1/delta*(0:(N-1))/N
lambda<-1/fre



###################
#Calculating h_sigma:
###################
#Var<-var(z_approx)
Var<-var(z_s)
phi_Nyquist<-1/2/delta
```

```
phi_lowest<-1/N/delta
h_sigma=2*sqrt(2*Var)


#########################
#Fourier transforming the data:
#########################
f<-fft(z_approx, inverse=FALSE)
#ft<-fft(z_approx, inverse=TRUE)/N
#Cxx<-Re(ft*f)
Cxx<-abs(f*Conj(f)/N)


###################
#Find centroidal frequency:
###################
M<-2/delta/N
phi_c<-sum(fre[1:(N/2)]*Cxx[1:(N/2)])/2*M/(sum(Cxx[1:(N/2)])*1/2*M)
#phi_c<-sum(((0:(N/2-1))*Cxx[1:(N/2)]))/4*M^(2)/(sum(Cxx[1:(N/2)])*1/2*M)
max_frebil<-as.integer(4*phi_c*N*delta)



####################
#Find mean range, h_lambda, for different wavelengths, lambda:
####################
lambda_c<-1/phi_c
lambda_bil_c<-as.integer((lambda_c)/(delta))
r<-vector("integer", N-lambda_bil_c)

for (i in 1:(N-(lambda_bil_c))) {
        r[i]<-(max(z_approx[i:(i+lambda_bil_c)]))-(min(z_approx[i:(i+lambda_bil_c)]))
}
h_lambda_c<-sum(r)/(N-(lambda_bil_c))


#Defining j_max>=6:
j_max<-0
for (j in 6:8) {
        if (lambda_bil_c*(j^(3/2)-6^(3/2)+2) <N) {
                j_max<-j}
}


#Calculating h_lambda:
lambda_bil<-vector("integer",j_max)
h_lambda<-vector("integer",j_max)
for (j in 1:5) {
        lambda_bil[j]<-as.integer(lambda_bil_c/(5-j+1))
```

```
	r_lambda<-vector("integer", N-lambda_bil[j])
	for (i in 1:(N-lambda_bil[j])) {
		r_lambda[i]<-(max(z_approx[i:(i+lambda_bil[j])]))-
(min(z_approx[i:(i+lambda_bil[j])]))
	}
	h_lambda[j]<-sum(r_lambda)/(N-(lambda_bil[j]))
}

for (j in 6:(j_max)) {
	lambda_bil[j]<-as.integer(lambda_bil_c*(j^(3/2)-6^(3/2)+2))
	r_lambda<-vector("integer", N-lambda_bil[j])
	for (i in 1:(N-lambda_bil[j])) {
		r_lambda[i]<-(max(z_approx[i:(i+lambda_bil[j])]))-
(min(z_approx[i:(i+lambda_bil[j])]))
	}
	h_lambda[j]<-sum(r_lambda)/(N-(lambda_bil[j]))
}



######################
#Plotting
######################
par(ask=TRUE)
par(mfcol=c(3,1))
par(mai=c(1,1,0.2,1))

sd1_x<-vector("integer",2)
sd1_z<-vector("integer",2)
sd3_z<-vector("integer",2)
sd1_x[1]<-0
sd1_x[2]<-max(x_s)
sd1_z[1]<-mean(z_s)-1/2*h_lambda_c
sd1_z[2]<-mean(z_s)-1/2*h_lambda_c
sd3_z[1]<-mean(z_s)-1/2*h_sigma
sd3_z[2]<-mean(z_s)-1/2*h_sigma

sd2_x<-vector("integer",2)
sd2_z<-vector("integer",2)
sd4_z<-vector("integer",2)
sd2_x[1]<-0
sd2_x[2]<-max(x_s)
sd2_z[1]<-mean(z_s)+1/2*h_lambda_c
sd2_z[2]<-mean(z_s)+1/2*h_lambda_c
sd4_z[1]<-mean(z_s)+1/2*h_sigma
sd4_z[2]<-mean(z_s)+1/2*h_sigma

par(mfg=c(1,1,3,1))
plot(x_s,z_s2, main=datafile, xlab="Length [mm]", ylab="Depth [mm]",type="l")
```

```
points(x_approx,z_approx)
par(lty=3)
lines(sd1_x,sd1_z)
lines(sd2_x,sd2_z)
par(lty=1)
lines(sd1_x,sd3_z)
lines(sd2_x,sd4_z)
par(lty=1)

#######
#Identify points on the graph by leftclicking the mouse over
#the selected point:  To identify outliers:
#par(mfcol=c(1,1))
#plot(x_r,z_r, main="Raw data", xlab="Length [mm]", ylab="Depth [mm]",type="l")
#plot(x_s,z_s, main="Sorted data", xlab="Length [mm]", ylab="Depth [mm]",type="l")
#points(x_r,z_r)
#points(x_s,z_s)
#identify(x_r,z_r)
#identify(x_s,z_s)
########

par(mfg=c(2,1,3,1))
plot(fre[1:(max_frebil)], (Cxx[1:(max_frebil)]), main="Power spectrum", xlab="frequency
[mm-1]", ylab="Cxx", type="l")
arrows(phi_c,0,phi_c,max(Cxx)/2, length = 0.1, angle = 30, code = 1)
text(fre[(max_frebil-1)],max(Cxx)/1.15, "Power spectrum --", pos=2)
text(phi_c,max(Cxx)/1.4, "Centroidal frequency", pos=1)



par(mfg=c(3,1,3,1))
plot(lambda_bil*delta,h_lambda, main="Mean range height / Power spectrum",
xlab="Wave length [mm]", ylab="h_lambda [mm]", type="b", ylim=c(0,max(h_lambda)))
lines(1/fre[2:(N/2-1)], ((Cxx[2:(N/2-1)])/(max(Cxx))*max(h_lambda)))
text(max(lambda_bil)*delta,max(h_lambda)/1.5, "Power spectrum --", pos=2)
text(max(lambda_bil)*delta,max(h_lambda)/1.5-2, "Mean range height -°-", pos=2)
text(lambda_c,h_lambda_c-5, "Centroid", pos=1)
arrows(lambda_c,h_lambda_c,lambda_c,h_lambda_c-5, length = 0.1, angle = 30, code = 1)


#par(mfg=c(3,1,3,1))
#plot(1/fre[1:(max_frebil)], (Cxx[1:(max_frebil)]), xlab="", ylab="", type="l",
yaxes=FALSE)
#axis(4)
#par(ask=FALSE)

#dev.copy2eps("var.eps", width=8, height=11)
#dev.copy2eps(epsfile, width=8, height=11, epsfile)
```

```
#shoot the graphics device down:
#dev.off()



####################
#Calculating the Nikuradse radius, k, using 5 methods: A, B, C, D and E:
####################
kB<-h_sigma
kC<-2*h_sigma
kD<-h_lambda_c
kE<-2*h_lambda_c


###################
#Calculating the energy loss
###################

print("CORRECT THE TUNNEL DIAMETER, d -IN mm")
d<-67.6

r<-d/2/1000
A<-r^2*pi
g<-9.82

print("CORRECT THE kinematic viscosity, ny depending on temperature")
ny<-1.762e-06

print("CORRECT THE DISCHARGE, q -IN m3 S-1")
Q<-0.005748
v<-Q/A
Re<-v*2*r/ny

fA<-(1/(4.285*log10(d/(1000*(sqrt(Var)/1000)^1.66))-8.798))^2
fB<-(1/(4*log10(d/kB)+2.28))^2
fC<-(1/(4*log10(d/kC)+2.28))^2
fD<-(1/(4*log10(d/kD)+2.28))^2
fE<-(1/(4*log10(d/kE)+2.28))^2

#n0 calculated from Boreo and Doandes empirical polynomial:
Std<-sqrt(Var)
n0<-NA
if (Std < 1.5){
        if (Std > 0.5){
        n0<-(-7.062*Std^4+25.721*Std^3-32.132*Std^2+16.861*Std-2.054)/100}}


nA<-(d/4000)^(1/6)*sqrt(fA/(2*g))
nB<-(d/4000)^(1/6)*sqrt(fB/(2*g))
```

```
nC<-(d/4000)^(1/6)*sqrt(fC/(2*g))
nD<-(d/4000)^(1/6)*sqrt(fD/(2*g))
nE<-(d/4000)^(1/6)*sqrt(fE/(2*g))



####################
#Writing to the console
####################
print("%%%%%%%%%%%%")
print("Section:")
print(outfile)
print(date())
print("%%%%%%%%%%%%")
print("Number of datapoints")
print(length(x_r))
print("Spacing between datapoints, delta [mm]=")
print(delta)
print("N=")
print(N)
print("Reynolds tala=")
print(Re)
print("---------------")
print("Nyquist frequency [mm-1]=")
print(phi_Nyquist)
print("Lowest frequency [mm-1]=")
print(phi_lowest)
print("Centroidal frequency [mm-1]=")
print(phi_c)
print("---------------")
print("Signal variance [mm]=")
print(Var)
print("h_sigma [mm]=2*sqrt(2*Var)")
print(h_sigma)
print("---------------")
print("Centroidal wavelength: lambda_c [mm]")
print(lambda_c)
print("h_lambda_c [mm]=")
print(h_lambda_c)
print("---------------")
print("A: Darcy-Weisbach friction factor, f=")
print(fA)
print("B: Darcy-Weisbach friction factor, f=")
print(fB)
print("C: Darcy-Weisbach friction factor, f=")
print(fC)
print("D: Darcy-Weisbach friction factor, f=")
print(fD)
print("E: Darcy-Weisbach friction factor, f=")
```

```
print(fE)
print("--------------")
print("B: Roughness, k=h_sigma [mm]=")
print(kB)
print("C: Roughness, k=2h_sigma [mm]=")
print(kC)
print("D: Roughness, k=h_lambda_c [mm]=")
print(kD)
print("E: Roughness, k=2h_lambda_c [mm]=")
print(kE)
print("--------------")
print("0: Manning number, n")
print(n0)
print("B: Manning number, n")
print(nB)
print("C: Manning number, n")
print(nC)
print("D: Manning number, n")
print(nD)
print("E: Manning number, n")
print(nE)
print("--------------")
print("0: 1/Manning number, M")
print(round(1/n0))
print("A: 1/Manning number, M")
print(round(1/nA))
print("B: 1/Manning number, M")
print(round(1/nB))
print("C: 1/Manning number, M")
print(round(1/nC))
print("D: 1/Manning number, M")
print(round(1/nD))
print("E: 1/Manning number, M")
print(round(1/nE))


######################
#Writing results into the outfile:
######################
sink(outfile)
print("%%%%%%%%%%%")
print("Section:")
print(outfile)
print(date())
print("%%%%%%%%%%%")
print("Number of datapoints")
print(length(x_r))
print("Spacing of datapoints, delta [mm]=")
print(delta)
```

```
print("N=")
print(N)
print("Reynolds tala=")
print(Re)
print("--------------")
print("Nyquist frequency [mm-1]=")
print(phi_Nyquist)
print("Lowest frequency [mm-1]=")
print(phi_lowest)
print("Centroidal frequency [mm-1]=")
print(phi_c)
print("--------------")
print("Signal variance [mm]=")
print(Var)
print("h_sigma [mm]=2*sqrt(2*Var)")
print(h_sigma)
print("--------------")
print("Centroidal wavelength: lambda_c [mm]")
print(lambda_c)
print("h_lambda_c [mm]=")
print(h_lambda_c)
print("--------------")
print("A: Darcy-Weisbach friction factor, f=")
print(fA)
print("B: Darcy-Weisbach friction factor, f=")
print(fB)
print("C: Darcy-Weisbach friction factor, f=")
print(fC)
print("D: Darcy-Weisbach friction factor, f=")
print(fD)
print("E: Darcy-Weisbach friction factor, f=")
print(fE)
print("--------------")
print("B: Roughness, k=h_sigma [mm]=")
print(kB)
print("C: Roughness, k=2h_sigma [mm]=")
print(kC)
print("D: Roughness, k=h_lambda_c [mm]=")
print(kD)
print("E: Roughness, k=2h_lambda_c [mm]=")
print(kE)
print("--------------")
print("0: Manning number, n")
print(n0)
print("A: Manning number, n")
print(nA)
print("B: Manning number, n")
print(nB)
print("C: Manning number, n")
```

```
print(nC)
print("D: Manning number, n")
print(nD)
print("E: Manning number, n")
print(nE)
print("--------------")
print("0: 1/Manning number, M")
print(round(1/n0))
print("A: 1/Manning number, M")
print(round(1/nA))
print("B: 1/Manning number, M")
print(round(1/nB))
print("C: 1/Manning number, M")
print(round(1/nC))
print("D: 1/Manning number, M")
print(round(1/nD))
print("E: 1/Manning number, M")
print(round(1/nE))

sink()
#graphics.off()
##################
#The end
####################
print("tara")
```

Depth – length graphs from first run laser data are outlined below.

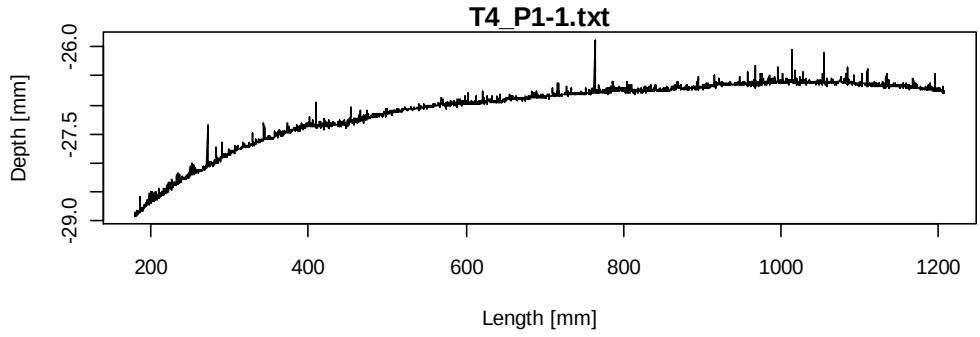

Figure B.1 Depth – length plot for T4 setup, first pipe first run

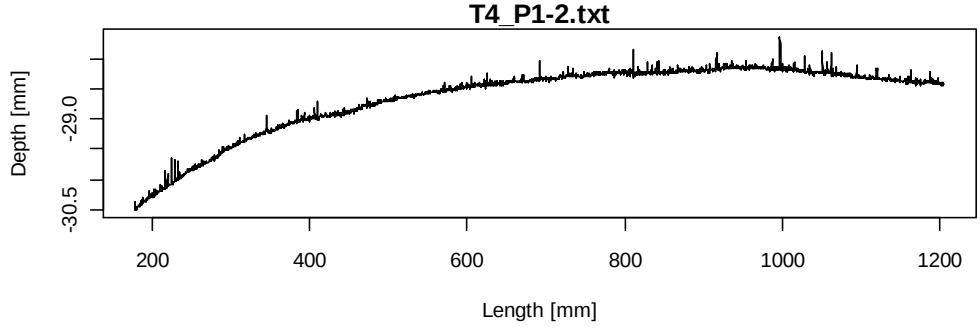

Figure B.2 Depth – length plot for T4 setup, first pipe second run.

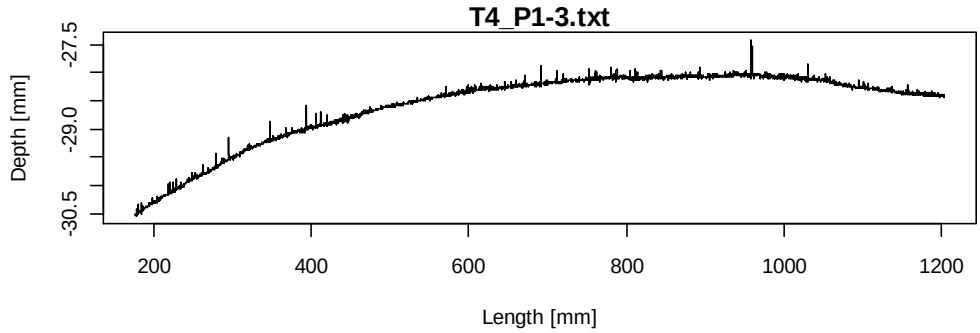

Figure B.3 Depth – length plot for T4 setup, first pipe third run.

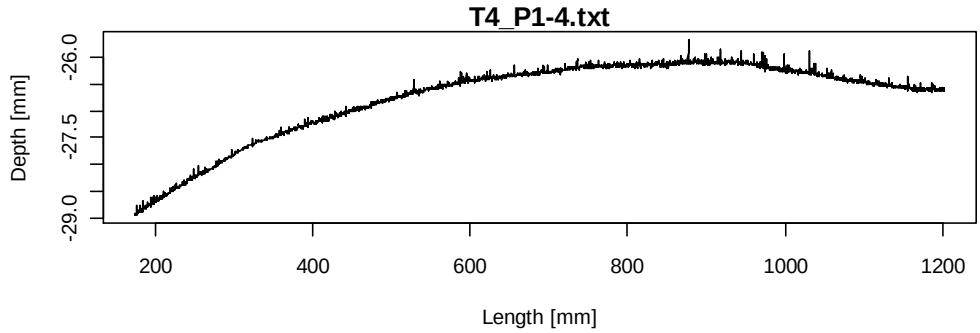

Figure B.4 Depth – length plot for T4 setup, first pipe fourth run.

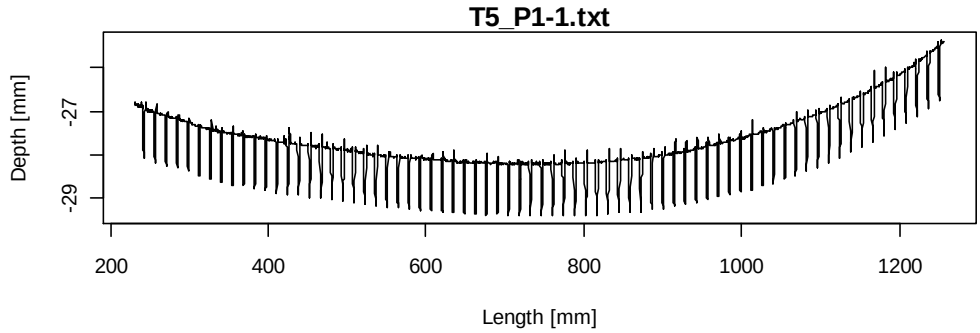

Figure B.5 Depth – length plot for T5 setup, first pipe first run.

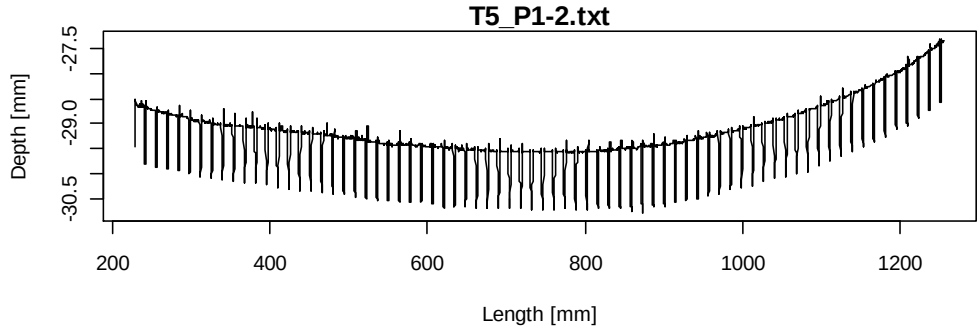

Figure B.6 Depth – length plot for T5 setup, first pipe second run.

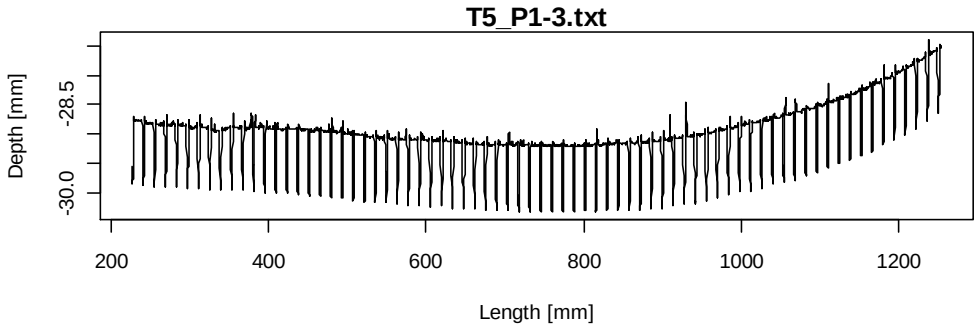

Figure B.7 Depth – length plot for T5 setup, first pipe third run.

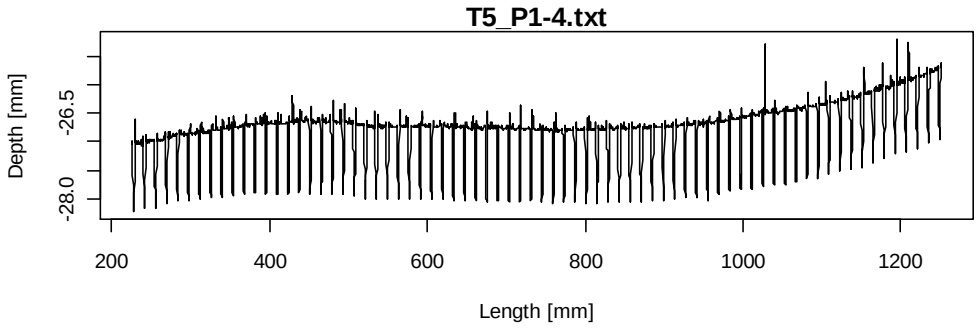

Figure B.8 Depth – length plot for T5 setup, first pipe fourth run.

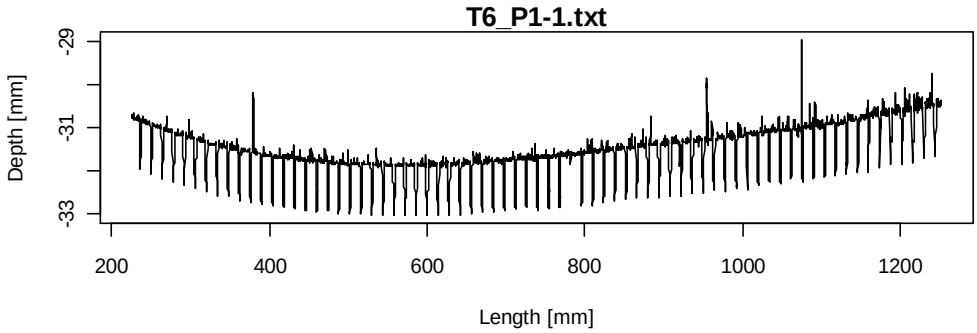

Figure B.9 Depth – length plot for T6 setup, first pipe first run.

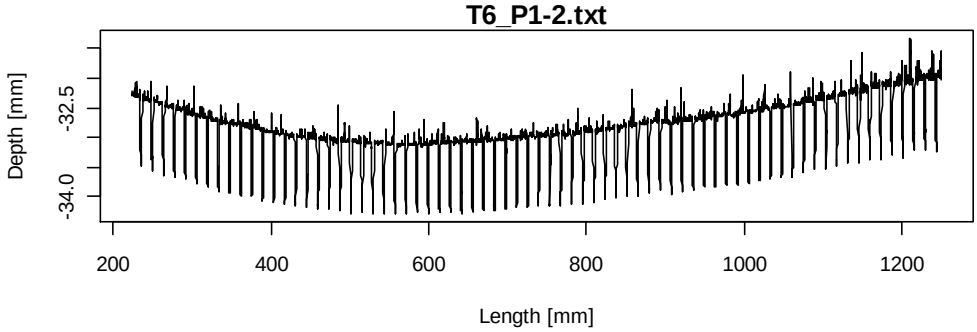

Figure B.10 Depth – length plot for T6 setup, first pipe second run.

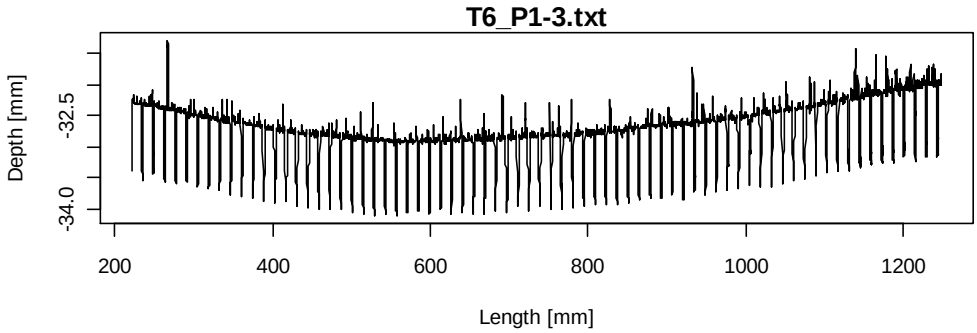

Figure B.11 Depth – length plot for T6 setup, first pipe third run.

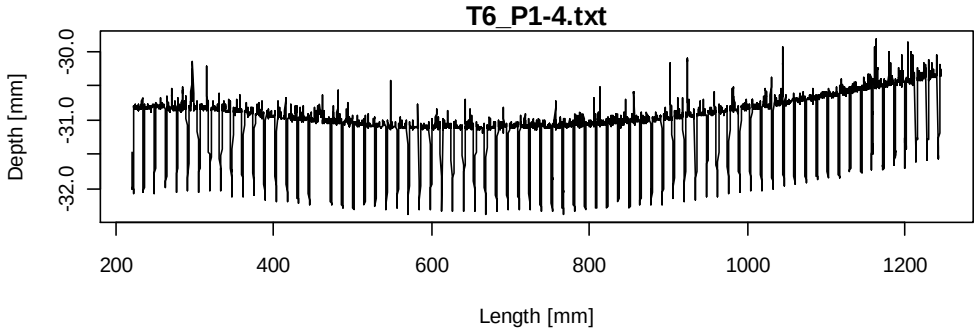

Figure B.12 Depth – length plot for T6 setup, first pipe fourth run.

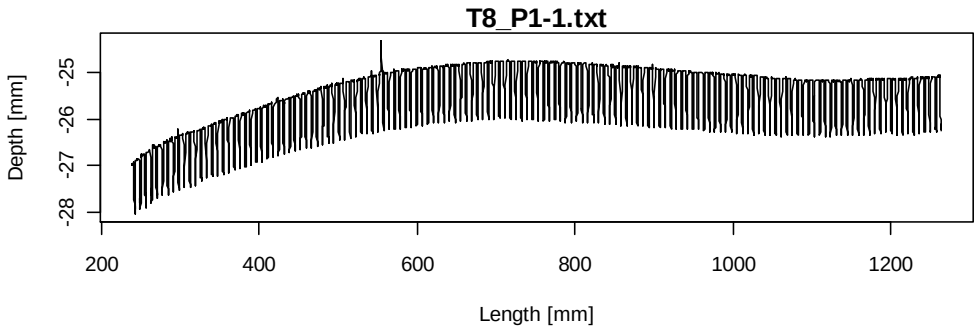

Figure B.13 Depth – length plot for T8 setup, first pipe first run.

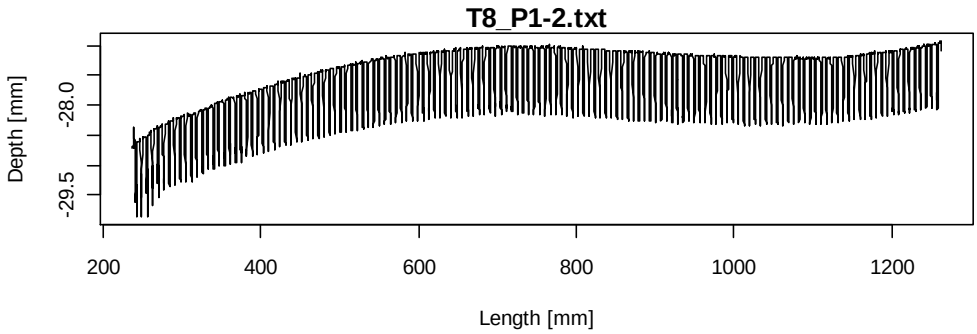

Figure B.14 Depth – length plot for T8 setup, first pipe second run.

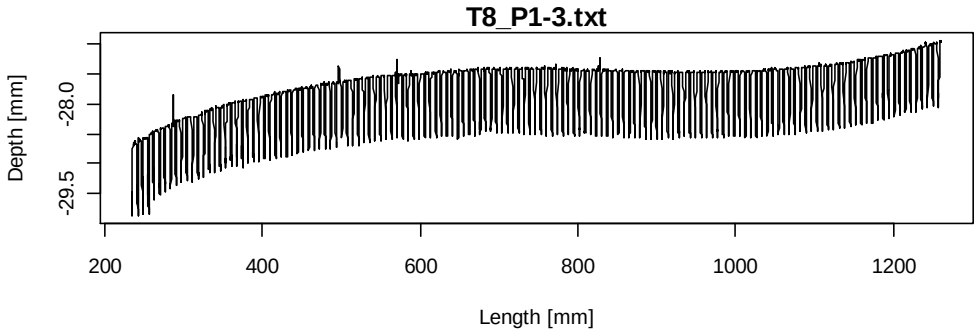

Figure B.15 Depth – length plot for T8 setup, first pipe third run.

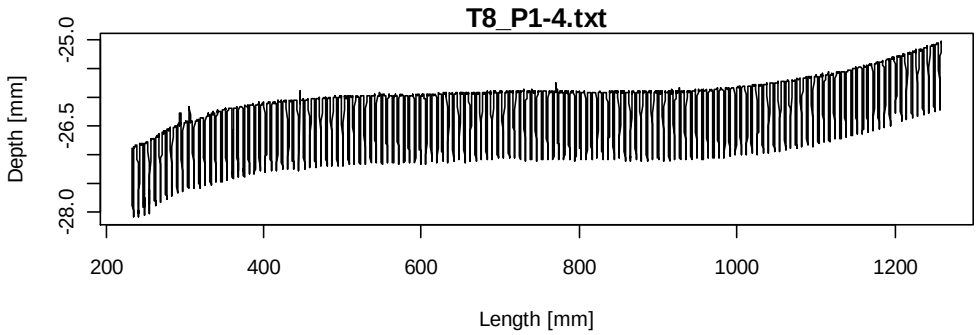

Figure B.16 Depth – length plot for T8 setup, first pipe fourth run.

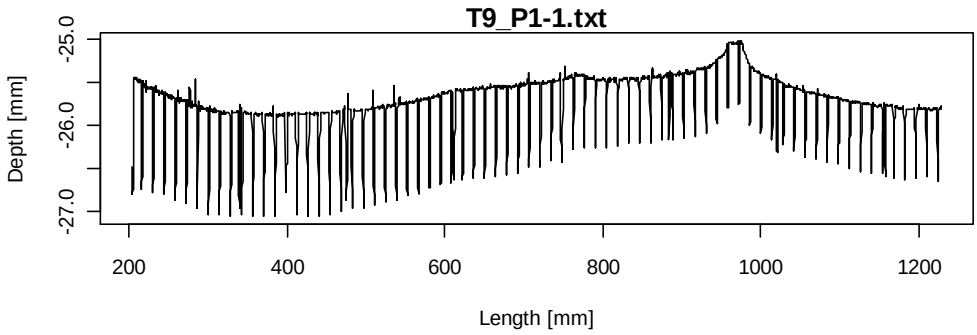

Figure B.17 Depth – length plot for T9 setup, first pipe first run.

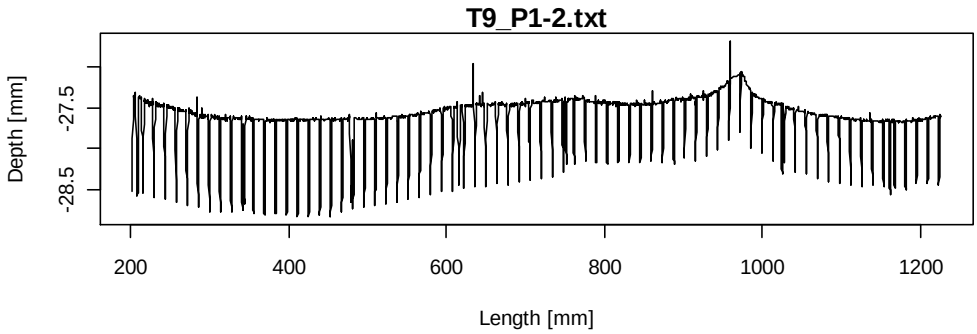

Figure B.18 Depth – length plot for T9 setup, first pipe second run.

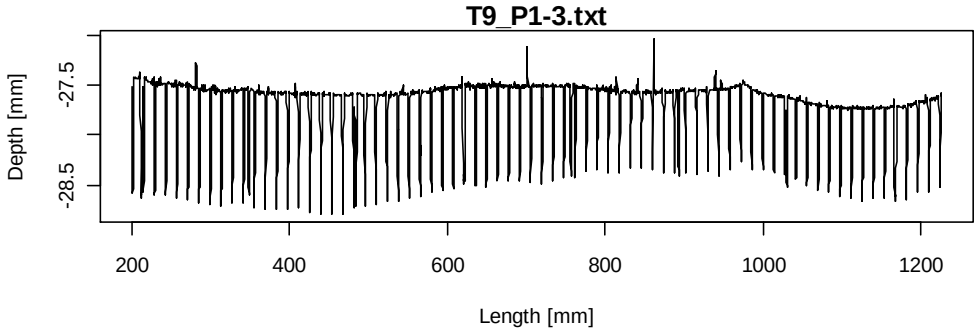

Figure B.19 Depth – length plot for T9 setup, first pipe third run.

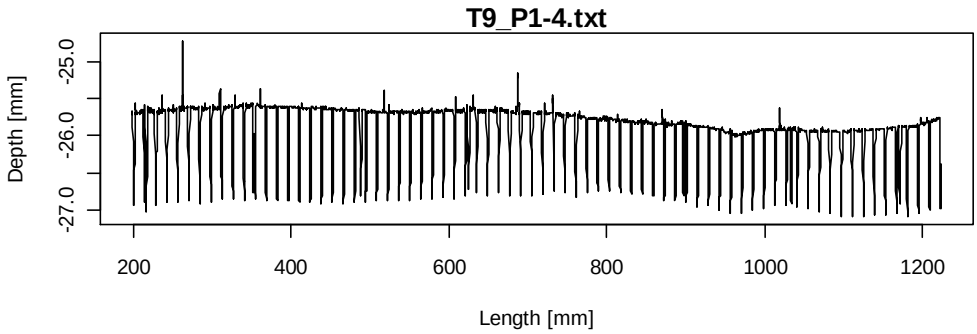

Figure B.20 Depth – length plot for T9 setup, first pipe fourth run.

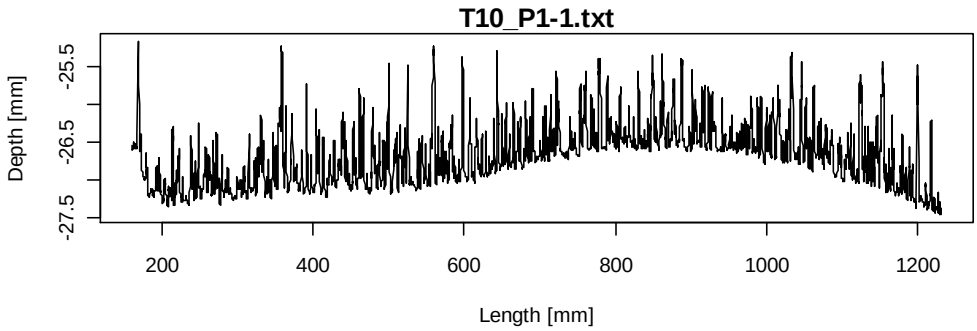

Figure B.21Depth – length plot for T10 setup, first pipe, first run.

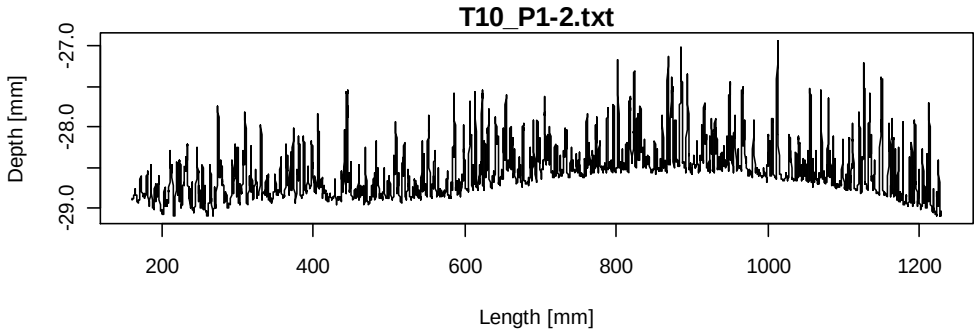

Figure B.22 Depth – length plot for T10 setup, first pipe, second run.

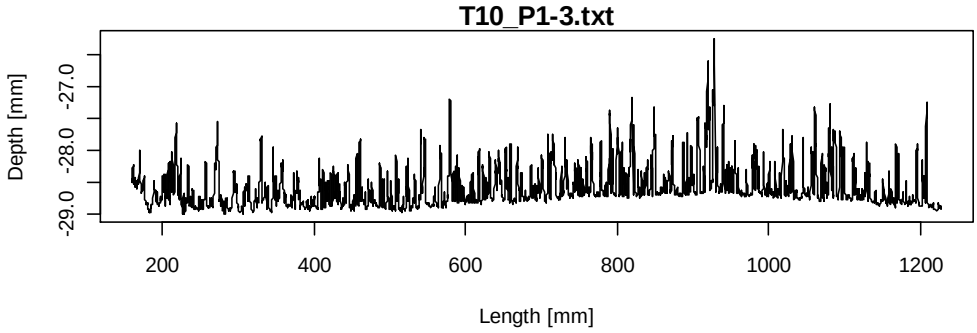

Figure B.23 Depth – length plot for T10 setup, first pipe, third run.

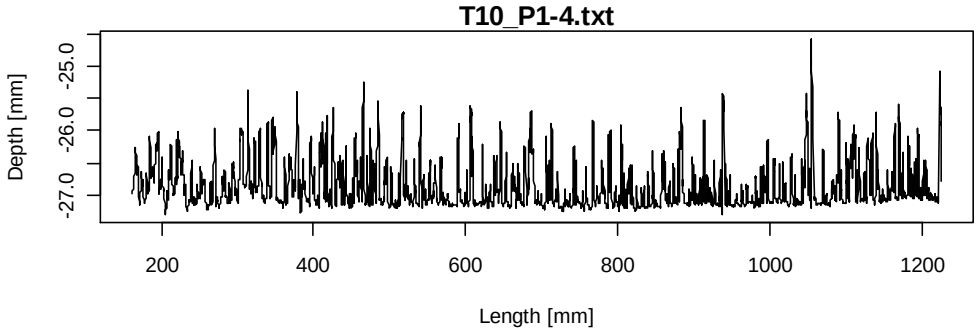

Figure B.24 Depth – length plot for T10 setup, first pipe, fourth run.

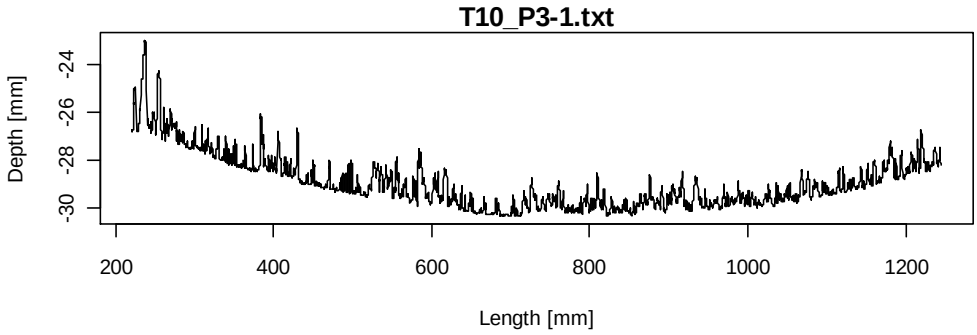

Figure B.25 Depth – length plot for T10 setup, third pipe, first run.

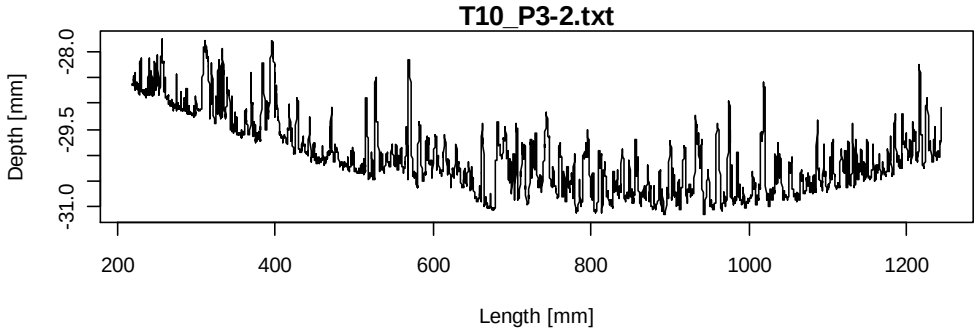

Figure B.26 Depth – length plot for T10 setup, third pipe, second run.

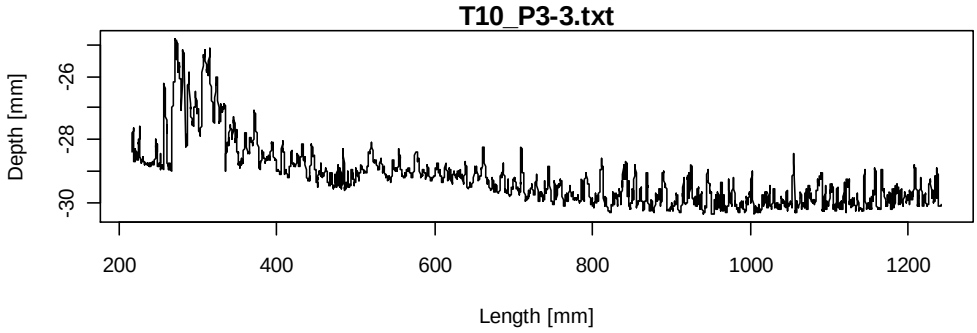

Figure B.27 Depth – length plot for T10 setup, third pipe, third run.

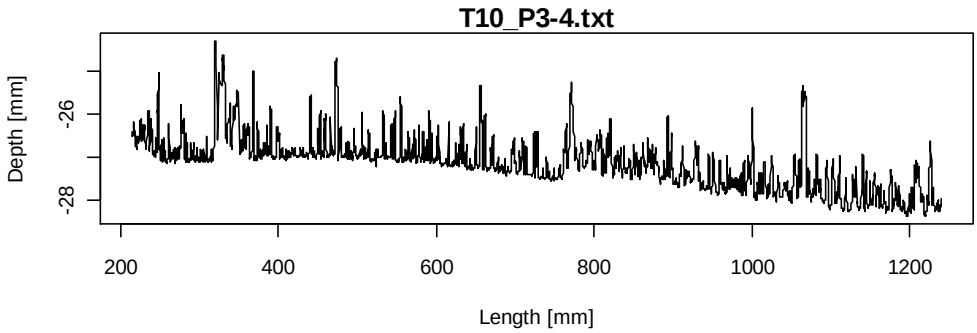

Figure B.28 Depth – length plot for T10 setup, third pipe, fourth run.

Program computations for each setup can be found below.

Table B-1 R program computations for T4.

Section:	Section:	Section:	Section:
T4_P1-1.short.out	T4_P1-2.short.out	T4_P1-3.short.out	T4_P1-4.short.out
Thu Jan 13 18:21:11 2011	Thu Jan 13 18:33:22 2011	Thu Jan 13 18:39:49 2011	Thu Jan 13 18:44:29 2011
Number of datapoints	Number of datapoints	Number of datapoints	Number of datapoints
871	689	802	948
Spacing of datapoints, delta [mm]=	Spacing of datapoints, delta [mm]=	Spacing of datapoints, delta [mm]=	Spacing of datapoints, delta [mm]=
0.02945251	0.02430334	0.02702715	0.03163406
N=	N=	N=	N=
4096	4096	4096	4096
Reynolds tala=	Reynolds tala=	Reynolds tala=	Reynolds tala=
76176.92	76176.92	76176.92	76176.92
----------	----------	----------	----------
Nyquist frequency [mm-1]=	Nyquist frequency [mm-1]=	Nyquist frequency [mm-1]=	Nyquist frequency [mm-1]=
16.97648	20.5733	18.49992	15.80575
Lowest frequency [mm-1]=	Lowest frequency [mm-1]=	Lowest frequency [mm-1]=	Lowest frequency [mm-1]=
0.008289296	0.01004556	0.009033163	0.007717651
Centroidal frequency [mm-1]=	Centroidal frequency [mm-1]=	Centroidal frequency [mm-1]=	Centroidal frequency [mm-1]=
0.5718037	0.5499902	0.541954	0.4150256
----------	----------	----------	----------
Signal variance [mm]=	Signal variance [mm]=	Signal variance [mm]=	Signal variance [mm]=
0.003693331	0.001998966	0.001193163	0.002032476
h_sigma [mm]=2*sqrt(2*Var)	h_sigma [mm]=2*sqrt(2*Var)	h_sigma [mm]=2*sqrt(2*Var)	h_sigma [mm]=2*sqrt(2*Var)
0.1718914	0.1264584	0.09770008	0.1275139
----------	----------	----------	----------
Centroidal wavelength: lambda_c [mm]	Centroidal wavelength: lambda_c [mm]	Centroidal wavelength: lambda_c [mm]	Centroidal wavelength: lambda_c [mm]

1.748852	1.818214	1.845175	2.40949
h_lambda_c [mm]=	h_lambda_c [mm]=	h_lambda_c [mm]=	h_lambda_c [mm]=
0.0911935	0.07805166	0.06666756	0.08892266
---	---	---	---
A: Darcy-Weisbach friction factor, f=	A: Darcy-Weisbach friction factor, f=	A: Darcy-Weisbach friction factor, f=	A: Darcy-Weisbach friction factor, f=
0.003799714	0.003391642	0.003097417	0.003401809
B: Darcy-Weisbach friction factor, f=	B: Darcy-Weisbach friction factor, f=	B: Darcy-Weisbach friction factor, f=	B: Darcy-Weisbach friction factor, f=
0.00620059	0.005710938	0.005342865	0.005723422
C: Darcy-Weisbach friction factor, f=	C: Darcy-Weisbach friction factor, f=	C: Darcy-Weisbach friction factor, f=	C: Darcy-Weisbach friction factor, f=
0.007567637	0.00691156	0.006423901	0.006928184
D: Darcy-Weisbach friction factor, f=	D: Darcy-Weisbach friction factor, f=	D: Darcy-Weisbach friction factor, f=	D: Darcy-Weisbach friction factor, f=
0.005250565	0.005050757	0.00485974	0.00521739
E: Darcy-Weisbach friction factor, f=	E: Darcy-Weisbach friction factor, f=	E: Darcy-Weisbach friction factor, f=	E: Darcy-Weisbach friction factor, f=
0.006302368	0.006040328	0.005791173	0.006258761
---	---	---	---
B: Roughness, k=h_sigma [mm]=	B: Roughness, k=h_sigma [mm]=	B: Roughness, k=h_sigma [mm]=	B: Roughness, k=h_sigma [mm]=
0.1718914	0.1264584	0.09770008	0.1275139
C: Roughness, k=2h_sigma [mm]=	C: Roughness, k=2h_sigma [mm]=	C: Roughness, k=2h_sigma [mm]=	C: Roughness, k=2h_sigma [mm]=
0.3437827	0.2529168	0.1954002	0.2550279
D: Roughness, k=h_lambda_c [mm]=	D: Roughness, k=h_lambda_c [mm]=	D: Roughness, k=h_lambda_c [mm]=	D: Roughness, k=h_lambda_c [mm]=
0.0911935	0.07805166	0.06666756	0.08892266
E: Roughness, k=2h_lambda_c [mm]=	E: Roughness, k=2h_lambda_c [mm]=	E: Roughness, k=2h_lambda_c [mm]=	E: Roughness, k=2h_lambda_c [mm]=
0.182387	0.1561033	0.1333351	0.1778453

0: Manning number, n	0: Manning number, n	0: Manning number, n	0: Manning number, n
NA	NA	NA	NA
A: Manning number, n	A: Manning number, n	A: Manning number, n	A: Manning number, n
0.007073685	0.006683059	0.006386606	0.006693068
B: Manning number, n	B: Manning number, n	B: Manning number, n	B: Manning number, n
0.00903622	0.008672094	0.00838798	0.008681568
C: Manning number, n	C: Manning number, n	C: Manning number, n	C: Manning number, n
0.009982755	0.009540218	0.009197498	0.009551685
D: Manning number, n	D: Manning number, n	D: Manning number, n	D: Manning number, n
0.008315211	0.008155461	0.007999757	0.0082889
E: Manning number, n	E: Manning number, n	E: Manning number, n	E: Manning number, n
0.009110079	0.00891868	0.0087328	0.009078507
0: 1/Manning number, M	0: 1/Manning number, M	0: 1/Manning number, M	0: 1/Manning number, M
NA	NA	NA	NA
A: 1/Manning number, M	A: 1/Manning number, M	A: 1/Manning number, M	A: 1/Manning number, M
141	150	157	149
B: 1/Manning number, M	B: 1/Manning number, M	B: 1/Manning number, M	B: 1/Manning number, M
111	115	119	115
C: 1/Manning number, M	C: 1/Manning number, M	C: 1/Manning number, M	C: 1/Manning number, M
100	105	109	105
D: 1/Manning number, M	D: 1/Manning number, M	D: 1/Manning number, M	D: 1/Manning number, M
120	123	125	121
E: 1/Manning number, M	E: 1/Manning number, M	E: 1/Manning number, M	E: 1/Manning number, M
110	112	115	110

Table B-2 R program computations for T5.

Section: T5_P1-1_short.out Thu Jan 13 18:48:52 2011	Section: T5_P1-2.short.out Thu Jan 13 19:03:22 2011	Section: T5_P1-3.short.out Thu Jan 13 19:07:27 2011	Section: T5_P1-4.short.out Thu Jan 13 19:11:43 2011
Number of datapoints	Number of datapoints	Number of datapoints	Number of datapoints
1059	657	641	1222
Spacing of datapoints, delta [mm]=	Spacing of datapoints, delta [mm]=	Spacing of datapoints, delta [mm]=	Spacing of datapoints, delta [mm]=
0.04473577	0.02668169	0.02695037	0.04861807
N=	N=	N=	N=
4096	4096	4096	4096
Reynolds tala=	Reynolds tala=	Reynolds tala=	Reynolds tala=
70893.1	70893.1	70893.1	70893.1
---	---	---	---
Nyquist frequency [mm-1]=	Nyquist frequency [mm-1]=	Nyquist frequency [mm-1]=	Nyquist frequency [mm-1]=
11.17674	18.73944	18.55262	10.28424
Lowest frequency [mm-1]=	Lowest frequency [mm-1]=	Lowest frequency [mm-1]=	Lowest frequency [mm-1]=
0.005457392	0.009150119	0.009058898	0.005021603
Centroidal frequency [mm-1]=	Centroidal frequency [mm-1]=	Centroidal frequency [mm-1]=	Centroidal frequency [mm-1]=
0.1591526	0.1797462	0.1564106	0.1590452
---	---	---	---
Signal variance [mm]=	Signal variance [mm]=	Signal variance [mm]=	Signal variance [mm]=
0.1882676	0.1811594	0.1628535	0.2052224
h_sigma [mm]=2*sqrt(2*Var)	h_sigma [mm]=2*sqrt(2*Var)	h_sigma [mm]=2*sqrt(2*Var)	h_sigma [mm]=2*sqrt(2*Var)
1.227249	1.203858	1.141415	1.281319
---	---	---	---
Centroidal wavelength: lambda_c [mm]	Centroidal wavelength: lambda_c [mm]	Centroidal wavelength: lambda_c [mm]	Centroidal wavelength: lambda_c [mm]
6.283276	5.5634	6.393427	6.287521
h_lambda_c [mm]=	h_lambda_c [mm]=	h_lambda_c [mm]=	h_lambda_c [mm]=
0.8211818	0.6688233	0.7497546	0.8838098

A: Darcy-Weisbach friction factor, f=	A: Darcy-Weisbach friction factor, f=	A: Darcy-Weisbach friction factor, f=	A: Darcy-Weisbach friction factor, f=
0.009705755	0.00959306	0.00929118	0.009965565
B: Darcy-Weisbach friction factor, f=	B: Darcy-Weisbach friction factor, f=	B: Darcy-Weisbach friction factor, f=	B: Darcy-Weisbach friction factor, f=
0.01160018	0.0115171	0.01129174	0.01178963
C: Darcy-Weisbach friction factor, f=	C: Darcy-Weisbach friction factor, f=	C: Darcy-Weisbach friction factor, f=	C: Darcy-Weisbach friction factor, f=
0.01531495	0.01518902	0.01484844	0.01560286
D: Darcy-Weisbach friction factor, f=	D: Darcy-Weisbach friction factor, f=	D: Darcy-Weisbach friction factor, f=	D: Darcy-Weisbach friction factor, f=
0.01003476	0.009354658	0.009724338	0.01029645
E: Darcy-Weisbach friction factor, f=	E: Darcy-Weisbach friction factor, f=	E: Darcy-Weisbach friction factor, f=	E: Darcy-Weisbach friction factor, f=
0.01297641	0.01198332	0.01252139	0.01336228
B: Roughness, k=h_sigma [mm]=	B: Roughness, k=h_sigma [mm]=	B: Roughness, k=h_sigma [mm]=	B: Roughness, k=h_sigma [mm]=
1.227249	1.203858	1.141415	1.281319
C: Roughness, k=2h_sigma [mm]=	C: Roughness, k=2h_sigma [mm]=	C: Roughness, k=2h_sigma [mm]=	C: Roughness, k=2h_sigma [mm]=
2.454499	2.407717	2.28283	2.562638
D: Roughness, k=h_lambda_c [mm]=	D: Roughness, k=h_lambda_c [mm]=	D: Roughness, k=h_lambda_c [mm]=	D: Roughness, k=h_lambda_c [mm]=
0.8211818	0.6688233	0.7497546	0.8838098
E: Roughness, k=2h_lambda_c [mm]=	E: Roughness, k=2h_lambda_c [mm]=	E: Roughness, k=2h_lambda_c [mm]=	E: Roughness, k=2h_lambda_c [mm]=
1.642364	1.337647	1.499509	1.76762
0: Manning number, n	0: Manning number, n	0: Manning number, n	0: Manning number, n
NA	NA	NA	NA

A: Manning number, n	A: Manning number, n	A: Manning number, n	A: Manning number, n
0.01130537	0.01123955	0.01106129	0.01145569
B: Manning number, n	B: Manning number, n	B: Manning number, n	B: Manning number, n
0.01235955	0.01231521	0.01219413	0.01246007
C: Manning number, n	C: Manning number, n	C: Manning number, n	C: Manning number, n
0.0142013	0.01414279	0.01398333	0.01433416
D: Manning number, n	D: Manning number, n	D: Manning number, n	D: Manning number, n
0.01149539	0.01109901	0.01131619	0.01164432
E: Manning number, n	E: Manning number, n	E: Manning number, n	E: Manning number, n
0.01307217	0.012562	0.01284093	0.0132651
---	---	---	---
0: 1/Manning number, M	0: 1/Manning number, M	0: 1/Manning number, M	0: 1/Manning number, M
NA	NA	NA	NA
A: 1/Manning number, M	A: 1/Manning number, M	A: 1/Manning number, M	A: 1/Manning number, M
88	89	90	87
B: 1/Manning number, M	B: 1/Manning number, M	B: 1/Manning number, M	B: 1/Manning number, M
81	81	82	80
C: 1/Manning number, M	C: 1/Manning number, M	C: 1/Manning number, M	C: 1/Manning number, M
70	71	72	70
D: 1/Manning number, M	D: 1/Manning number, M	D: 1/Manning number, M	D: 1/Manning number, M
87	90	88	86
E: 1/Manning number, M	E: 1/Manning number, M	E: 1/Manning number, M	E: 1/Manning number, M
76	80	78	75

Table B-3 R program computations for T6.

Section:	Section:	Section:	Section:
T6_P1-1.short.out	T6_P1-2.short.out	T6_P1-3.short.out	T6_P1-4.short.out
Thu Jan 13 19:18:26 2011	Thu Jan 13 19:23:21 2011	Thu Jan 13 19:26:55 2011	Thu Jan 13 19:32:05 2011

Number of datapoints	Number of datapoints	Number of datapoints	Number of datapoints
585	721	806	980
Spacing of datapoints, delta [mm]=	Spacing of datapoints, delta [mm]=	Spacing of datapoints, delta [mm]=	Spacing of datapoints, delta [mm]=
0.01703042	0.02192686	0.02429348	0.02944719
N=	N=	N=	N=
4096	4096	4096	4096
Reynolds tala=	Reynolds tala=	Reynolds tala=	Reynolds tala=
65797.23	65797.23	65797.23	65797.23
---	---	---	---
Nyquist frequency [mm-1]=	Nyquist frequency [mm-1]=	Nyquist frequency [mm-1]=	Nyquist frequency [mm-1]=
29.35923	22.80309	20.58165	16.97955
Lowest frequency [mm-1]=	Lowest frequency [mm-1]=	Lowest frequency [mm-1]=	Lowest frequency [mm-1]=
0.01433556	0.01113432	0.01004964	0.008290795
Centroidal frequency [mm-1]=	Centroidal frequency [mm-1]=	Centroidal frequency [mm-1]=	Centroidal frequency [mm-1]=
0.166908	0.1615834	0.1672935	0.1849782
---	---	---	---
Signal variance [mm]=	Signal variance [mm]=	Signal variance [mm]=	Signal variance [mm]=
0.1533759	0.162687	0.1602187	0.1696299
h_sigma [mm]=2*sqrt(2*Var)	h_sigma [mm]=2*sqrt(2*Var)	h_sigma [mm]=2*sqrt(2*Var)	h_sigma [mm]=2*sqrt(2*Var)
1.107704	1.140831	1.132144	1.16492
---	---	---	---
Centroidal wavelength: lambda_c [mm]	Centroidal wavelength: lambda_c [mm]	Centroidal wavelength: lambda_c [mm]	Centroidal wavelength: lambda_c [mm]
5.991326	6.188754	5.977519	5.406042
h_lambda_c [mm]=	h_lambda_c [mm]=	h_lambda_c [mm]=	h_lambda_c [mm]=
0.7521324	0.8902919	0.8848526	0.776133
---	---	---	---
A: Darcy-Weisbach friction factor, f=	A: Darcy-Weisbach friction factor, f=	A: Darcy-Weisbach friction factor, f=	A: Darcy-Weisbach friction factor, f=

0.009127491
B: Darcy-Weisbach friction factor, f=
0.01116779
C: Darcy-Weisbach friction factor, f=
0.01466176
D: Darcy-Weisbach friction factor, f=
0.009734896
E: Darcy-Weisbach friction factor, f=
0.01253682

B: Roughness, k=h_sigma [mm]=
1.107704
C: Roughness, k=2h_sigma [mm]=
2.215407
D: Roughness, k=h_lambda_c [mm]=
0.7521324
E: Roughness, k=2h_lambda_c [mm]=
1.504265

0: Manning number, n
NA
A: Manning number, n
0.01096342
B: Manning number, n

0.00928835
B: Darcy-Weisbach friction factor, f=
0.0112896
C: Darcy-Weisbach friction factor, f=
0.01484523
D: Darcy-Weisbach friction factor, f=
0.01032303
E: Darcy-Weisbach friction factor, f=
0.01340158

B: Roughness, k=h_sigma [mm]=
1.140831
C: Roughness, k=2h_sigma [mm]=
2.281662
D: Roughness, k=h_lambda_c [mm]=
0.8902919
E: Roughness, k=2h_lambda_c [mm]=
1.780584

0: Manning number, n
NA
A: Manning number, n
0.0110596
B: Manning number, n

0.009246216
B: Darcy-Weisbach friction factor, f=
0.01125781
C: Darcy-Weisbach friction factor, f=
0.0147973
D: Darcy-Weisbach friction factor, f=
0.01030074
E: Darcy-Weisbach friction factor, f=
0.01336861

B: Roughness, k=h_sigma [mm]=
1.132144
C: Roughness, k=2h_sigma [mm]=
2.264287
D: Roughness, k=h_lambda_c [mm]=
0.8848526
E: Roughness, k=2h_lambda_c [mm]=
1.769705

0: Manning number, n
NA
A: Manning number, n
0.01103449
B: Manning number, n

0.009405005
B: Darcy-Weisbach friction factor, f=
0.0113772
C: Darcy-Weisbach friction factor, f=
0.01497741
D: Darcy-Weisbach friction factor, f=
0.009840572
E: Darcy-Weisbach friction factor, f=
0.01269143

B: Roughness, k=h_sigma [mm]=
1.16492
C: Roughness, k=2h_sigma [mm]=
2.32984
D: Roughness, k=h_lambda_c [mm]=
0.776133
E: Roughness, k=2h_lambda_c [mm]=
1.552266

0: Manning number, n
NA
A: Manning number, n
0.01112884
B: Manning number, n

	0.01212701	0.01219297	0.01217579	0.01224018
C: Manning number, n		C: Manning number, n	C: Manning number, n	C: Manning number, n	
	0.01389515	0.01398182	0.01395923	0.01404393
D: Manning number, n		D: Manning number, n	D: Manning number, n	D: Manning number, n	
	0.01132233	0.01165934	0.01164674	0.01138362
E: Manning number, n		E: Manning number, n	E: Manning number, n	E: Manning number, n	
	0.01284884	0.01328459	0.01326824	0.01292783
---		---	---	---	
0: 1/Manning number, M		0: 1/Manning number, M		0: 1/Manning number, M		0: 1/Manning number, M	
NA		NA		NA			
A: 1/Manning number, M		A: 1/Manning number, M		A: 1/Manning number, M		A: 1/Manning number, M	
	91		90		91		90
B: 1/Manning number, M		B: 1/Manning number, M		B: 1/Manning number, M		B: 1/Manning number, M	
	82		82		82		82
C: 1/Manning number, M		C: 1/Manning number, M		C: 1/Manning number, M		C: 1/Manning number, M	
	72		72		72		71
D: 1/Manning number, M		D: 1/Manning number, M		D: 1/Manning number, M		D: 1/Manning number, M	
	88		86		86		88
E: 1/Manning number, M		E: 1/Manning number, M		E: 1/Manning number, M		E: 1/Manning number, M	
	78		75		75		77

Table B-4 R program computations for T8.

Section:	Section:	Section:	Section:
T8_P1-1.short.out	T8_P1-2.short.out	T8_P1-3.short.out	T8_P1-4.short.out
Thu Jan 13 20:06:51 2011	Thu Jan 13 20:15:02 2011	Thu Jan 13 20:18:52 2011	Thu Jan 13 20:23:09 2011
Number of datapoints	Number of datapoints	Number of datapoints	Number of datapoints
672	825	984	705

Spacing of datapoints, delta [mm]= 0.02424722
N= 4096
Reynolds tala= 70893.1

Nyquist frequency [mm-1]= 20.62092
Lowest frequency [mm-1]= 0.01006881
Centroidal frequency [mm-1]= 0.1976673

Signal variance [mm]= 0.2439564
h_sigma [mm]=2*sqrt(2*Var) 1.397015

Centroidal wavelength: lambda_c [mm] 5.059006
h_lambda_c [mm]= 1.203871

A: Darcy-Weisbach friction factor, f= 0.01051894
B: Darcy-Weisbach friction factor, f=

Spacing of datapoints, delta [mm]= 0.02899353
N= 4096
Reynolds tala= 70893.1

Nyquist frequency [mm-1]= 17.24523
Lowest frequency [mm-1]= 0.00842052
Centroidal frequency [mm-1]= 0.2004169

Signal variance [mm]= 0.1982594
h_sigma [mm]=2*sqrt(2*Var) 1.259395

Centroidal wavelength: lambda_c [mm] 4.9896
h_lambda_c [mm]= 1.060898

A: Darcy-Weisbach friction factor, f= 0.009860324
B: Darcy-Weisbach friction factor, f=

Spacing of datapoints, delta [mm]= 0.03414727
N= 4096
Reynolds tala= 70893.1

Nyquist frequency [mm-1]=
Lowest frequency [mm-1]= 0.007149639
Centroidal frequency [mm-1]= 0.2016684

Signal variance [mm]= 0.190853
h_sigma [mm]=2*sqrt(2*Var) 1.235647

Centroidal wavelength: lambda_c [mm] 4.958634
h_lambda_c [mm]= 1.050477

A: Darcy-Weisbach friction factor, f= 0.009746168
B: Darcy-Weisbach friction factor, f=

Spacing of datapoints, delta [mm]= 0.0243679
N= 4096
Reynolds tala= 70893.1

Nyquist frequency [mm-1]= 20.5188
Lowest frequency [mm-1]= 0.01001895
Centroidal frequency [mm-1]= 0.2152484

Signal variance [mm]= 0.2124838
h_sigma [mm]=2*sqrt(2*Var) 1.303791

Centroidal wavelength: lambda_c [mm] 4.645796
h_lambda_c [mm]= 1.068445

A: Darcy-Weisbach friction factor, f= 0.01007329
B: Darcy-Weisbach friction factor, f=

0.01218372
C: Darcy-Weisbach friction factor, f=
0.01620512
D: Darcy-Weisbach friction factor, f=
0.01151715
E: Darcy-Weisbach friction factor, f=
0.01518909

B: Roughness, k=h_sigma [mm]=
1.397015
C: Roughness, k=2h_sigma [mm]=
2.79403
D: Roughness, k=h_lambda_c [mm]=
1.203871
E: Roughness, k=2h_lambda_c [mm]=
2.407743

0: Manning number, n
NA
A: Manning number, n
0.01176945
B: Manning number, n
0.01266661
C: Manning number, n
0.01460819

0.01171324
C: Darcy-Weisbach friction factor, f=
0.01548664
D: Darcy-Weisbach friction factor, f=
0.01099284
E: Darcy-Weisbach friction factor, f=
0.01439904

B: Roughness, k=h_sigma [mm]=
1.259395
C: Roughness, k=2h_sigma [mm]=
2.518789
D: Roughness, k=h_lambda_c [mm]=
1.060898
E: Roughness, k=2h_lambda_c [mm]=
2.121795

0: Manning number, n
NA
A: Manning number, n
0.01139504
B: Manning number, n
0.01241963
C: Manning number, n
0.01428068

0.01162984
C: Darcy-Weisbach friction factor, f=
0.01535996
D: Darcy-Weisbach friction factor, f=
0.01095342
E: Darcy-Weisbach friction factor, f=
0.01433997

B: Roughness, k=h_sigma [mm]=
1.235647
C: Roughness, k=2h_sigma [mm]=
2.471295
D: Roughness, k=h_lambda_c [mm]=
1.050477
E: Roughness, k=2h_lambda_c [mm]=
2.100953

0: Manning number, n
NA
A: Manning number, n
0.01132889
B: Manning number, n
0.01237534
C: Manning number, n
0.01422215

0.01186733
C: Darcy-Weisbach friction factor, f=
0.01572125
D: Darcy-Weisbach friction factor, f=
0.01102128
E: Darcy-Weisbach friction factor, f=
0.0144417

B: Roughness, k=h_sigma [mm]=
1.303791
C: Roughness, k=2h_sigma [mm]=
2.607581
D: Roughness, k=h_lambda_c [mm]=
1.068445
E: Roughness, k=2h_lambda_c [mm]=
2.136891

0: Manning number, n
NA
A: Manning number, n
0.01151744
B: Manning number, n
0.01250106
C: Manning number, n
0.01438844

D: Manning number, n	D: Manning number, n	D: Manning number, n	D: Manning number, n
0.01231524	0.01203165	0.01201006	0.01204721
E: Manning number, n	E: Manning number, n	E: Manning number, n	E: Manning number, n
0.01414282	0.0137701	0.01374182	0.01379048
----------	----------	----------	----------
0: 1/Manning number, M	0: 1/Manning number, M	0: 1/Manning number, M	0: 1/Manning number, M
NA	NA	NA	NA
A: 1/Manning number, M	A: 1/Manning number, M	A: 1/Manning number, M	A: 1/Manning number, M
85	88	88	87
B: 1/Manning number, M	B: 1/Manning number, M	B: 1/Manning number, M	B: 1/Manning number, M
79	81	81	80
C: 1/Manning number, M	C: 1/Manning number, M	C: 1/Manning number, M	C: 1/Manning number, M
68	70	70	70
D: 1/Manning number, M	D: 1/Manning number, M	D: 1/Manning number, M	D: 1/Manning number, M
81	83	83	83
E: 1/Manning number, M	E: 1/Manning number, M	E: 1/Manning number, M	E: 1/Manning number, M
71	73	73	73

Table B-5 R program computations for T9.

Section:	Section:	Section:	Section:
T9_P1-1.short.out	T9_P1-2.short.out	T9_P1-3.short.out	T9_P1-4.short.out
Sat Jan 15 14:55:11 2011	Sat Jan 15 14:57:10 2011	Sat Jan 15 14:58:03 2011	Sat Jan 15 14:58:54 2011
Number of datapoints	Number of datapoints	Number of datapoints	Number of datapoints
680	1180	1167	1408
Spacing of datapoints, delta [mm]=	Spacing of datapoints, delta [mm]=	Spacing of datapoints, delta [mm]=	Spacing of datapoints, delta [mm]=
0.0315688	0.0536096	0.05357478	0.06082778
N=	N=	N=	N=

4096	4096	4096	4096
Reynolds tala=	Reynolds tala=	Reynolds tala=	Reynolds tala=
73754.3	73754.3	73754.3	73754.3
---	---	---	---
Nyquist frequency [mm-1]=	Nyquist frequency [mm-1]=	Nyquist frequency [mm-1]=	Nyquist frequency [mm-1]=
15.83842	9.326689	9.33275	8.219928
Lowest frequency [mm-1]=	Lowest frequency [mm-1]=	Lowest frequency [mm-1]=	Lowest frequency [mm-1]=
0.007733605	0.004554047	0.004557007	0.004013637
Centroidal frequency [mm-1]=	Centroidal frequency [mm-1]=	Centroidal frequency [mm-1]=	Centroidal frequency [mm-1]=
0.1752544	0.1675341	0.1698708	0.1661533
---	---	---	---
Signal variance [mm]=	Signal variance [mm]=	Signal variance [mm]=	Signal variance [mm]=
0.1689224	0.1614401	0.1681818	0.1965138
h_sigma [mm]=2*sqrt(2*Var)	h_sigma [mm]=2*sqrt(2*Var)	h_sigma [mm]=2*sqrt(2*Var)	h_sigma [mm]=2*sqrt(2*Var)
1.162489	1.136451	1.159937	1.253838
---	---	---	---
Centroidal wavelength: lambda_c [mm]	Centroidal wavelength: lambda_c [mm]	Centroidal wavelength: lambda_c [mm]	Centroidal wavelength: lambda_c [mm]
5.70599	5.968933	5.886827	6.018537
h_lambda_c [mm]=	h_lambda_c [mm]=	h_lambda_c [mm]=	h_lambda_c [mm]=
0.6745803	0.6425702	0.6447634	0.7570214
---	---	---	---
A: Darcy-Weisbach friction factor, f=	A: Darcy-Weisbach friction factor, f=	A: Darcy-Weisbach friction factor, f=	A: Darcy-Weisbach friction factor, f=
0.00939324	0.00926711	0.009380895	0.00983363
B: Darcy-Weisbach friction factor, f=	B: Darcy-Weisbach friction factor, f=	B: Darcy-Weisbach friction factor, f=	B: Darcy-Weisbach friction factor, f=
0.01136839	0.01127359	0.01135914	0.01169379
C: Darcy-Weisbach friction factor, f=	C: Darcy-Weisbach friction factor, f=	C: Darcy-Weisbach friction factor, f=	C: Darcy-Weisbach friction factor, f=

0.01496412
D: Darcy-Weisbach friction factor, f=
0.009381659
E: Darcy-Weisbach friction factor, f=
0.01202248

B: Roughness, k=h_sigma [mm]=
1.162489
C: Roughness, k=2h_sigma [mm]=
2.324977
D: Roughness, k=h_lambda_c [mm]=
0.6745803
E: Roughness, k=2h_lambda_c [mm]=
1.349161

0: Manning number, n
NA
A: Manning number, n
0.01112187
B: Manning number, n
0.01223545
C: Manning number, n
0.0140377
D: Manning number, n
0.01111502
E: Manning number, n

0.01482108
D: Darcy-Weisbach friction factor, f=
0.009230038
E: Darcy-Weisbach friction factor, f=
0.01180288

B: Roughness, k=h_sigma [mm]=
1.136451
C: Roughness, k=2h_sigma [mm]=
2.272902
D: Roughness, k=h_lambda_c [mm]=
0.6425702
E: Roughness, k=2h_lambda_c [mm]=
1.28514

0: Manning number, n
NA
A: Manning number, n
0.01104695
B: Manning number, n
0.01218432
C: Manning number, n
0.01397044
D: Manning number, n
0.01102483
E: Manning number, n

0.01495015
D: Darcy-Weisbach friction factor, f=
0.009240545
E: Darcy-Weisbach friction factor, f=
0.01181808

B: Roughness, k=h_sigma [mm]=
1.159937
C: Roughness, k=2h_sigma [mm]=
2.319875
D: Roughness, k=h_lambda_c [mm]=
0.6447634
E: Roughness, k=2h_lambda_c [mm]=
1.289527

0: Manning number, n
NA
A: Manning number, n
0.01111456
B: Manning number, n
0.01223047
C: Manning number, n
0.01403114
D: Manning number, n
0.01103111
E: Manning number, n

0.01545708
D: Darcy-Weisbach friction factor, f=
0.009756553
E: Darcy-Weisbach friction factor, f=
0.01256848

B: Roughness, k=h_sigma [mm]=
1.253838
C: Roughness, k=2h_sigma [mm]=
2.507677
D: Roughness, k=h_lambda_c [mm]=
0.7570214
E: Roughness, k=2h_lambda_c [mm]=
1.514043

0: Manning number, n
NA
A: Manning number, n
0.01137961
B: Manning number, n
0.01240932
C: Manning number, n
0.01426704
D: Manning number, n
0.01133492
E: Manning number, n

0.01258251	0.01246707	0.01247509	0.01286506
---	---	---	---
0: 1/Manning number, M	0: 1/Manning number, M	0: 1/Manning number, M	0: 1/Manning number, M
NA	NA	NA	NA
A: 1/Manning number, M	A: 1/Manning number, M	A: 1/Manning number, M	A: 1/Manning number, M
90	91	90	88
B: 1/Manning number, M	B: 1/Manning number, M	B: 1/Manning number, M	B: 1/Manning number, M
82	82	82	81
C: 1/Manning number, M	C: 1/Manning number, M	C: 1/Manning number, M	C: 1/Manning number, M
71	72	71	70
D: 1/Manning number, M	D: 1/Manning number, M	D: 1/Manning number, M	D: 1/Manning number, M
90	91	91	88
E: 1/Manning number, M	E: 1/Manning number, M	E: 1/Manning number, M	E: 1/Manning number, M
79	80	80	78

Table B-6 R program computations for T10 first pipe.

Section:	Section:	Section:	Section:
T10_P1-1.short.out	T10_P1-2.short.out	T10_P1-3.short.out	T10_P1-4.short.out
Thu Jan 13 22:19:48 2011	Thu Jan 13 22:20:23 2011	Thu Jan 13 22:21:05 2011	Thu Jan 13 22:21:43 2011
Number of datapoints	Number of datapoints	Number of datapoints	Number of datapoints
1767	1894	2348	5878
Spacing of datapoints, delta [mm]=	Spacing of datapoints, delta [mm]=	Spacing of datapoints, delta [mm]=	Spacing of datapoints, delta [mm]=
0.04876187	0.06098225	0.07336179	0.1710728
N=	N=	N=	N=
4096	4096	4096	4096
Reynolds tala=	Reynolds tala=	Reynolds tala=	Reynolds tala=
61443.26	61443.26	61443.26	61443.26

Nyquist frequency [mm-1]=
10.25391
Lowest frequency [mm-1]=
0.005006794
Centroidal frequency [mm-1]=
0.1532915

Signal variance [mm]=
0.1422108
h_sigma [mm]=2*sqrt(2*Var)
1.066624

Centroidal wavelength: lambda_c [mm]
6.523519
h_lambda_c [mm]=
0.9029455

A: Darcy-Weisbach friction factor, f=
0.009001138
B: Darcy-Weisbach friction factor, f=
0.01110898
C: Darcy-Weisbach friction factor, f=
0.01457335
D: Darcy-Weisbach friction factor, f=

Nyquist frequency [mm-1]=
8.199107
Lowest frequency [mm-1]=
0.00400347
Centroidal frequency [mm-1]=
0.1643616

Signal variance [mm]=
0.07632262
h_sigma [mm]=2*sqrt(2*Var)
0.7813968

Centroidal wavelength: lambda_c [mm]
6.084148
h_lambda_c [mm]=
0.5518917

A: Darcy-Weisbach friction factor, f=
0.007559437
B: Darcy-Weisbach friction factor, f=
0.009943639
C: Darcy-Weisbach friction factor, f=
0.01284255
D: Darcy-Weisbach friction factor, f=

Nyquist frequency [mm-1]=
6.815537
Lowest frequency [mm-1]=
0.003327899
Centroidal frequency [mm-1]=
0.1346346

Signal variance [mm]=
0.07191065
h_sigma [mm]=2*sqrt(2*Var)
0.7584756

Centroidal wavelength: lambda_c [mm]
7.427509
h_lambda_c [mm]=
0.6014464

A: Darcy-Weisbach friction factor, f=
0.007439973
B: Darcy-Weisbach friction factor, f=
0.00984186
C: Darcy-Weisbach friction factor, f=
0.01269332
D: Darcy-Weisbach friction factor, f=

Nyquist frequency [mm-1]=
2.922733
Lowest frequency [mm-1]=
0.001427116
Centroidal frequency [mm-1]=
0.1563622

Signal variance [mm]=
0.1668541
h_sigma [mm]=2*sqrt(2*Var)
1.15535

Centroidal wavelength: lambda_c [mm]
6.395406
h_lambda_c [mm]=
0.8016804

A: Darcy-Weisbach friction factor, f=
0.009438015
B: Darcy-Weisbach friction factor, f=
0.01144131
C: Darcy-Weisbach friction factor, f=
0.01507432
D: Darcy-Weisbach friction factor, f=

0.01046107	0.008845853	0.009099738	0.01003252
E: Darcy-Weisbach friction factor, f=	E: Darcy-Weisbach friction factor, f=	E: Darcy-Weisbach friction factor, f=	E: Darcy-Weisbach friction factor, f=
0.01360606	0.01124962	0.01161473	0.01297312
---	---	---	---
B: Roughness, k=h_sigma [mm]=	B: Roughness, k=h_sigma [mm]=	B: Roughness, k=h_sigma [mm]=	B: Roughness, k=h_sigma [mm]=
1.066624	0.7813968	0.7584756	1.15535
C: Roughness, k=2h_sigma [mm]=	C: Roughness, k=2h_sigma [mm]=	C: Roughness, k=2h_sigma [mm]=	C: Roughness, k=2h_sigma [mm]=
2.133248	1.562794	1.516951	2.310699
D: Roughness, k=h_lambda_c [mm]=	D: Roughness, k=h_lambda_c [mm]=	D: Roughness, k=h_lambda_c [mm]=	D: Roughness, k=h_lambda_c [mm]=
0.9029455	0.5518917	0.6014464	0.8016804
E: Roughness, k=2h_lambda_c [mm]=	E: Roughness, k=2h_lambda_c [mm]=	E: Roughness, k=2h_lambda_c [mm]=	E: Roughness, k=2h_lambda_c [mm]=
1.805891	1.103783	1.202893	1.603361
---	---	---	---
0: Manning number, n	0: Manning number, n	0: Manning number, n	0: Manning number, n
NA	NA	NA	NA
A: Manning number, n	A: Manning number, n	A: Manning number, n	A: Manning number, n
0.0108449	0.009938521	0.009859678	0.01110497
B: Manning number, n	B: Manning number, n	B: Manning number, n	B: Manning number, n
0.01204798	0.01139855	0.01134007	0.01222686
C: Manning number, n	C: Manning number, n	C: Manning number, n	C: Manning number, n
0.01379929	0.01295396	0.01287848	0.01403447
D: Manning number, n	D: Manning number, n	D: Manning number, n	D: Manning number, n
0.01169136	0.01075095	0.01090414	0.01144938
E: Manning number, n	E: Manning number, n	E: Manning number, n	E: Manning number, n
0.01333347	0.012124	0.01231917	0.01301965
---	---	---	---
0: 1/Manning number, M	0: 1/Manning number, M	0: 1/Manning number, M	0: 1/Manning number, M

NA	NA	NA	NA
A: 1/Manning number, M	A: 1/Manning number, M	A: 1/Manning number, M	A: 1/Manning number, M
92	101	101	90
B: 1/Manning number, M	B: 1/Manning number, M	B: 1/Manning number, M	B: 1/Manning number, M
83	88	88	82
C: 1/Manning number, M	C: 1/Manning number, M	C: 1/Manning number, M	C: 1/Manning number, M
72	77	78	71
D: 1/Manning number, M	D: 1/Manning number, M	D: 1/Manning number, M	D: 1/Manning number, M
86	93	92	87
E: 1/Manning number, M	E: 1/Manning number, M	E: 1/Manning number, M	E: 1/Manning number, M
75	82	81	77

Table B-7 R program computations for T10 third pipe.

Section:	Section:	Section:	Section:
T10_P3-1.short.out	T10_P3-2.short.out	T10_P3-3.short.out	T10_P3-4.short.out
Thu Jan 13 21:15:32 2011	Thu Jan 13 21:18:38 2011	Thu Jan 13 21:22:05 2011	Thu Jan 13 21:25:40 2011
Number of datapoints	Number of datapoints	Number of datapoints	Number of datapoints
2404	1719	2173	1249
Spacing of datapoints, delta [mm]=	Spacing of datapoints, delta [mm]=	Spacing of datapoints, delta [mm]=	Spacing of datapoints, delta [mm]=
0.06829836	0.04879297	0.06094172	0.03661958
N=	N=	N=	N=
4096	4096	4096	4096
Reynolds tala=	Reynolds tala=	Reynolds tala=	Reynolds tala=
61443.26	61443.26	61443.26	61443.26
----------	----------	----------	----------
Nyquist frequency [mm-1]=	Nyquist frequency [mm-1]=	Nyquist frequency [mm-1]=	Nyquist frequency [mm-1]=
7.32082	10.24738	8.20456	13.6539

Lowest frequency [mm-1]=	Lowest frequency [mm-1]=	Lowest frequency [mm-1]=	Lowest frequency [mm-1]=
0.003574619	0.005003603	0.004006133	0.006666942
Centroidal frequency [mm-1]=	Centroidal frequency [mm-1]=	Centroidal frequency [mm-1]=	Centroidal frequency [mm-1]=
0.104691	0.1057858	0.1410363	0.1441952
---	---	---	---
Signal variance [mm]=	Signal variance [mm]=	Signal variance [mm]=	Signal variance [mm]=
0.1441166	0.1978554	0.1193341	0.166184
h_sigma [mm]=2*sqrt(2*Var)	h_sigma [mm]=2*sqrt(2*Var)	h_sigma [mm]=2*sqrt(2*Var)	h_sigma [mm]=2*sqrt(2*Var)
1.073747	1.258111	0.9770737	1.153027
---	---	---	---
Centroidal wavelength: lambda_c [mm]	Centroidal wavelength: lambda_c [mm]	Centroidal wavelength: lambda_c [mm]	Centroidal wavelength: lambda_c [mm]
9.551916	9.453066	7.090371	6.935042
h_lambda_c [mm]=	h_lambda_c [mm]=	h_lambda_c [mm]=	h_lambda_c [mm]=
0.914027	1.099737	0.8340877	0.7786028
---	---	---	---
A: Darcy-Weisbach friction factor, f=	A: Darcy-Weisbach friction factor, f=	A: Darcy-Weisbach friction factor, f=	A: Darcy-Weisbach friction factor, f=
0.009036359	0.009939882	0.008555706	0.009426628
B: Darcy-Weisbach friction factor, f=	B: Darcy-Weisbach friction factor, f=	B: Darcy-Weisbach friction factor, f=	B: Darcy-Weisbach friction factor, f=
0.01113611	0.01181241	0.01076066	0.01143276
C: Darcy-Weisbach friction factor, f=	C: Darcy-Weisbach friction factor, f=	C: Darcy-Weisbach friction factor, f=	C: Darcy-Weisbach friction factor, f=
0.01461412	0.01563754	0.01405178	0.01506139
D: Darcy-Weisbach friction factor, f=	D: Darcy-Weisbach friction factor, f=	D: Darcy-Weisbach friction factor, f=	D: Darcy-Weisbach friction factor, f=
0.01050657	0.01123441	0.01017232	0.00993131
E: Darcy-Weisbach friction factor, f=	E: Darcy-Weisbach friction factor, f=	E: Darcy-Weisbach friction factor, f=	E: Darcy-Weisbach friction factor, f=

0.01367357	0.01476204	0.01317898	0.01282446
---	---	---	---
B: Roughness, k=h_sigma [mm]=	B: Roughness, k=h_sigma [mm]=	B: Roughness, k=h_sigma [mm]=	B: Roughness, k=h_sigma [mm]=
1.073747	1.258111	0.9770737	1.153027
C: Roughness, k=2h_sigma [mm]=	C: Roughness, k=2h_sigma [mm]=	C: Roughness, k=2h_sigma [mm]=	C: Roughness, k=2h_sigma [mm]=
2.147494	2.516222	1.954147	2.306055
D: Roughness, k=h_lambda_c [mm]=	D: Roughness, k=h_lambda_c [mm]=	D: Roughness, k=h_lambda_c [mm]=	D: Roughness, k=h_lambda_c [mm]=
0.914027	1.099737	0.8340877	0.7786028
E: Roughness, k=2h_lambda_c [mm]=	E: Roughness, k=2h_lambda_c [mm]=	E: Roughness, k=2h_lambda_c [mm]=	E: Roughness, k=2h_lambda_c [mm]=
1.828054	2.199475	1.668175	1.557206
---	---	---	---
0: Manning number, n	0: Manning number, n	0: Manning number, n	0: Manning number, n
NA	NA	NA	NA
A: Manning number, n	A: Manning number, n	A: Manning number, n	A: Manning number, n
0.0108661	0.0113964	0.01057316	0.01109827
B: Manning number, n	B: Manning number, n	B: Manning number, n	B: Manning number, n
0.01206268	0.01242356	0.01185759	0.01222229
C: Manning number, n	C: Manning number, n	C: Manning number, n	C: Manning number, n
0.01381858	0.01429425	0.0135501	0.01402845
D: Manning number, n	D: Manning number, n	D: Manning number, n	D: Manning number, n
0.01171676	0.0121158	0.01152888	0.01139148
E: Manning number, n	E: Manning number, n	E: Manning number, n	E: Manning number, n
0.01336651	0.01388834	0.01312254	0.01294484
---	---	---	---
0: 1/Manning number, M	0: 1/Manning number, M	0: 1/Manning number, M	0: 1/Manning number, M
NA	NA	NA	NA
A: 1/Manning number, M	A: 1/Manning number, M	A: 1/Manning number, M	A: 1/Manning number, M
92	88	95	90

B: 1/Manning number, M	83	B: 1/Manning number, M	80
C: 1/Manning number, M	72	C: 1/Manning number, M	70
D: 1/Manning number, M	85	D: 1/Manning number, M	83
E: 1/Manning number, M	75	E: 1/Manning number, M	72

B: 1/Manning number, M	84	B: 1/Manning number, M	82
C: 1/Manning number, M	74	C: 1/Manning number, M	71
D: 1/Manning number, M	87	D: 1/Manning number, M	88
E: 1/Manning number, M	76	E: 1/Manning number, M	77

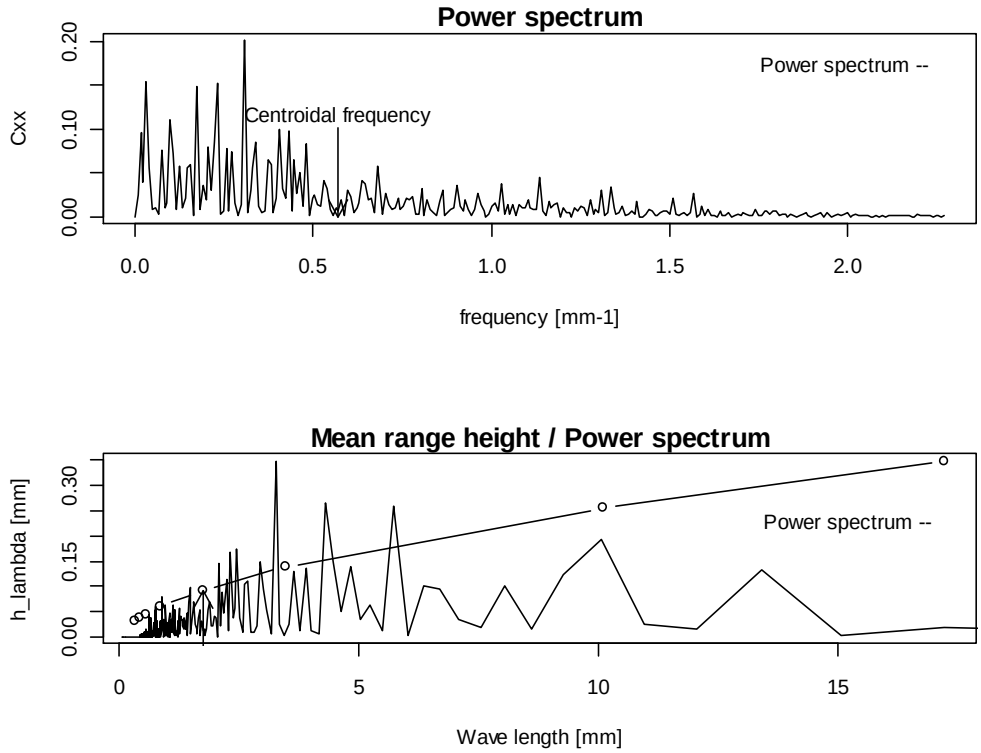

Figure B.29 Power spectrum and mean range height plots for T4, first run.

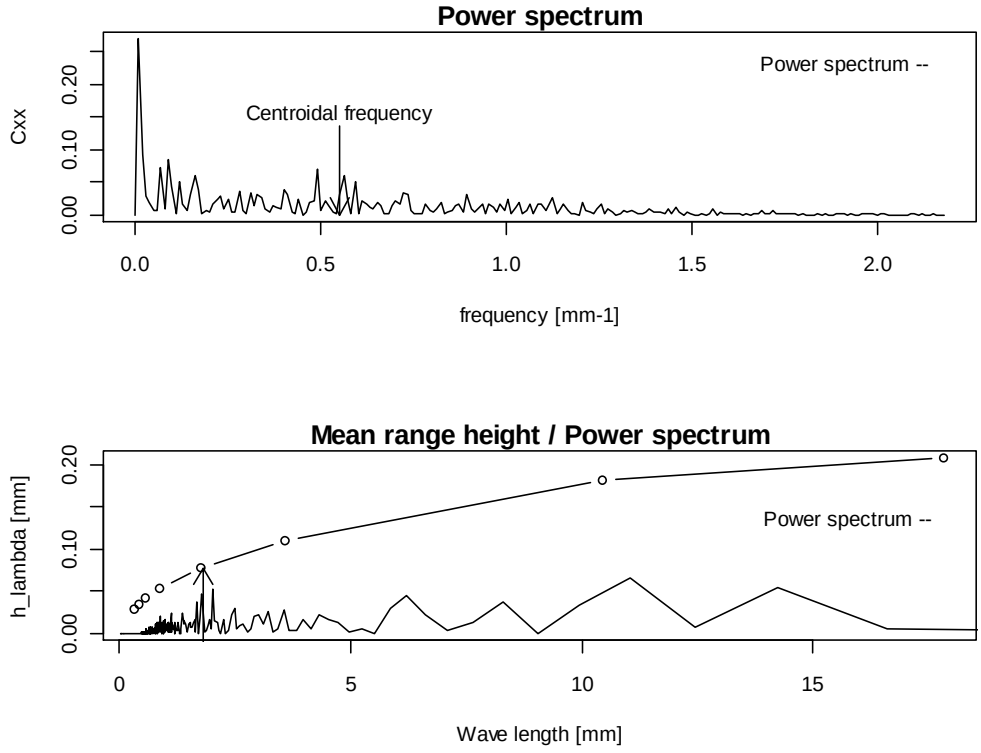

Figure B.30 Power spectrum and mean range height plots for T4, second run.

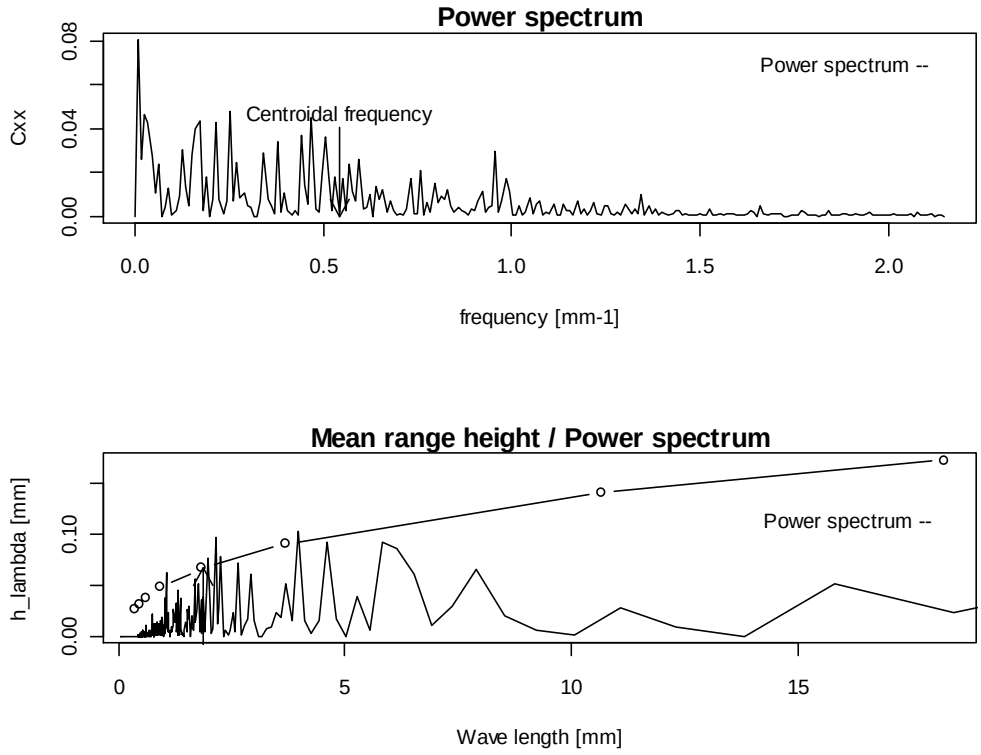

Figure B.31 Power spectrum and mean range height plots for T4, third run.

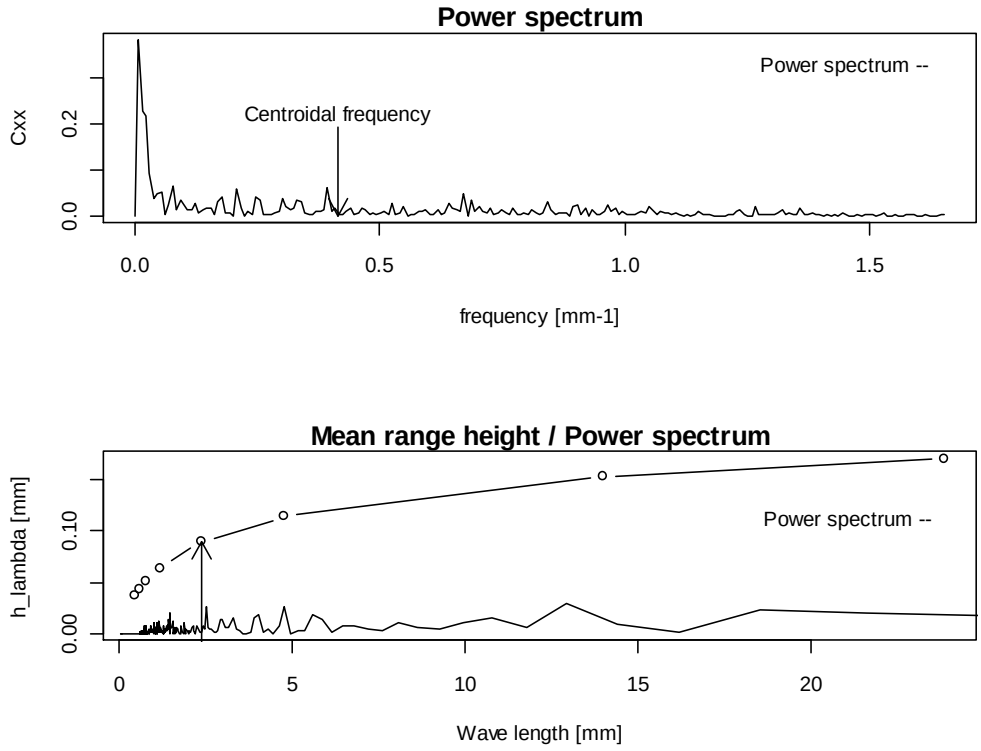

Figure B.32 Power spectrum and mean range height plots for T4, fourth run.

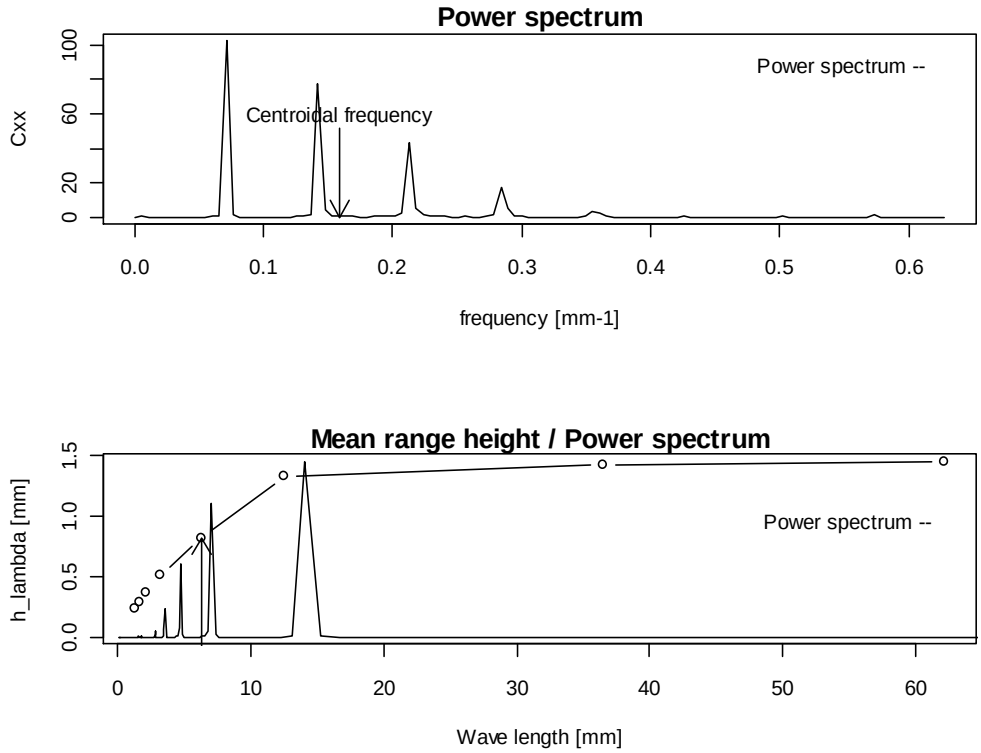

Figure B.33 Power spectrum and mean range height plots for T5, first run.

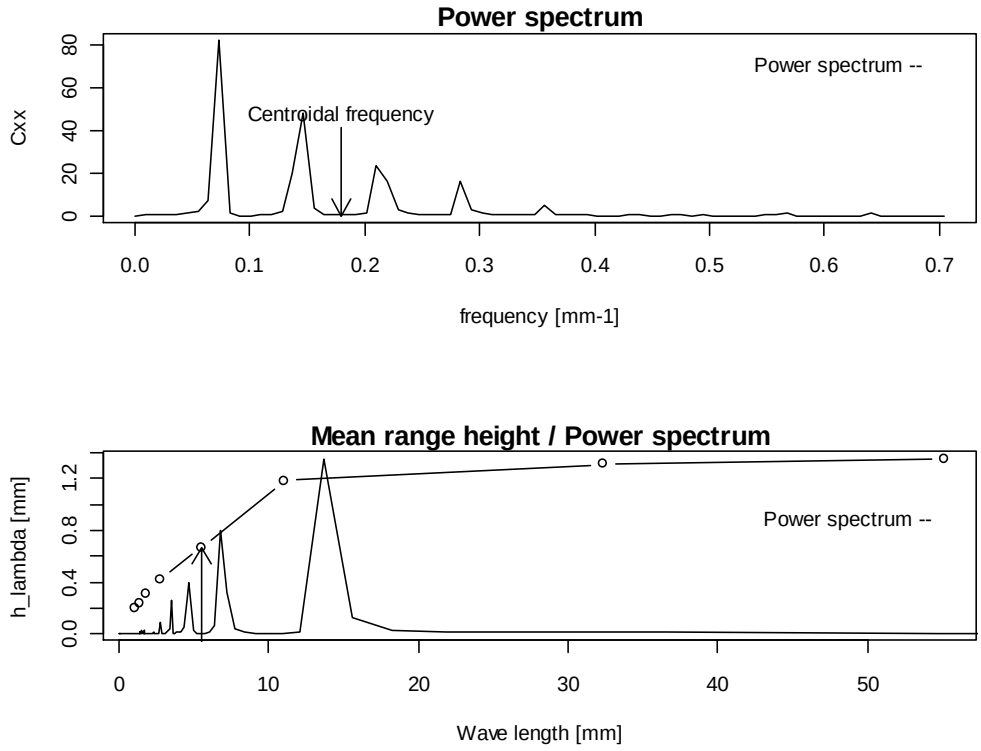

Figure B.34 Power spectrum and mean range height plots for T5, second run.

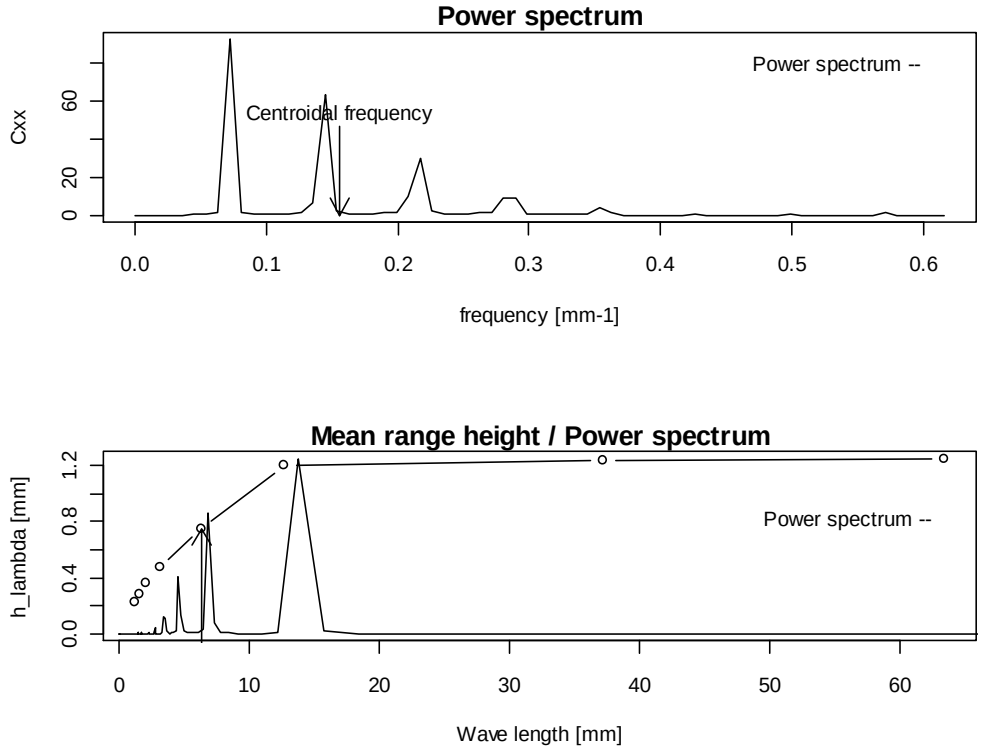

Figure B.35 Power spectrum and mean range height plots for T5, third run.

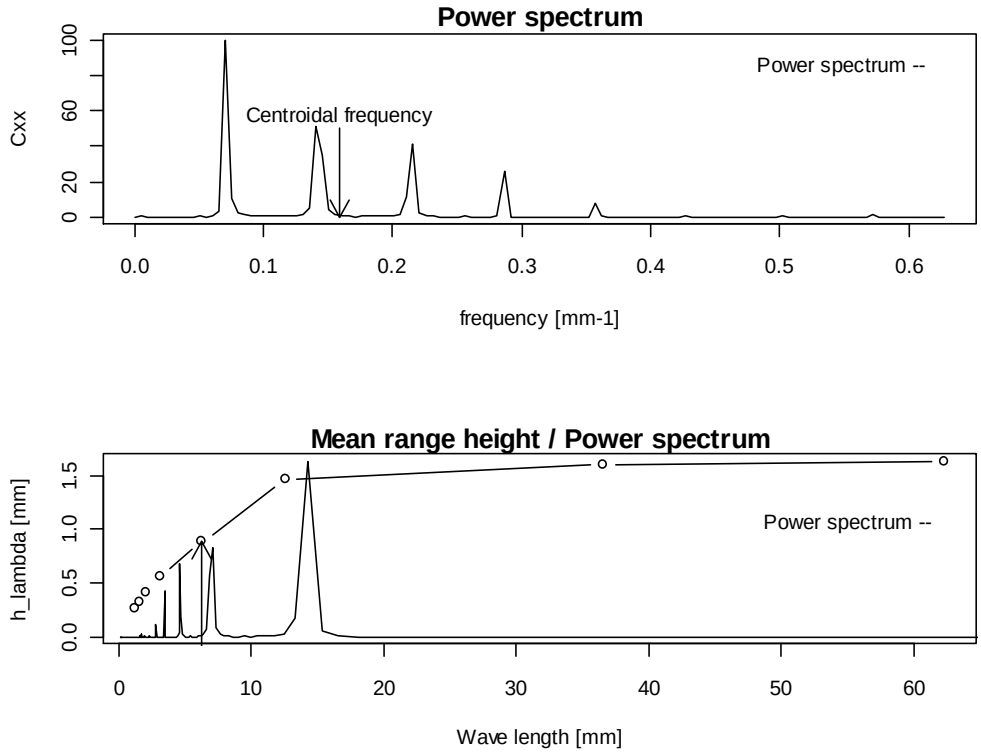

Figure B.36 Power spectrum and mean range height plots for T5, fourth run.

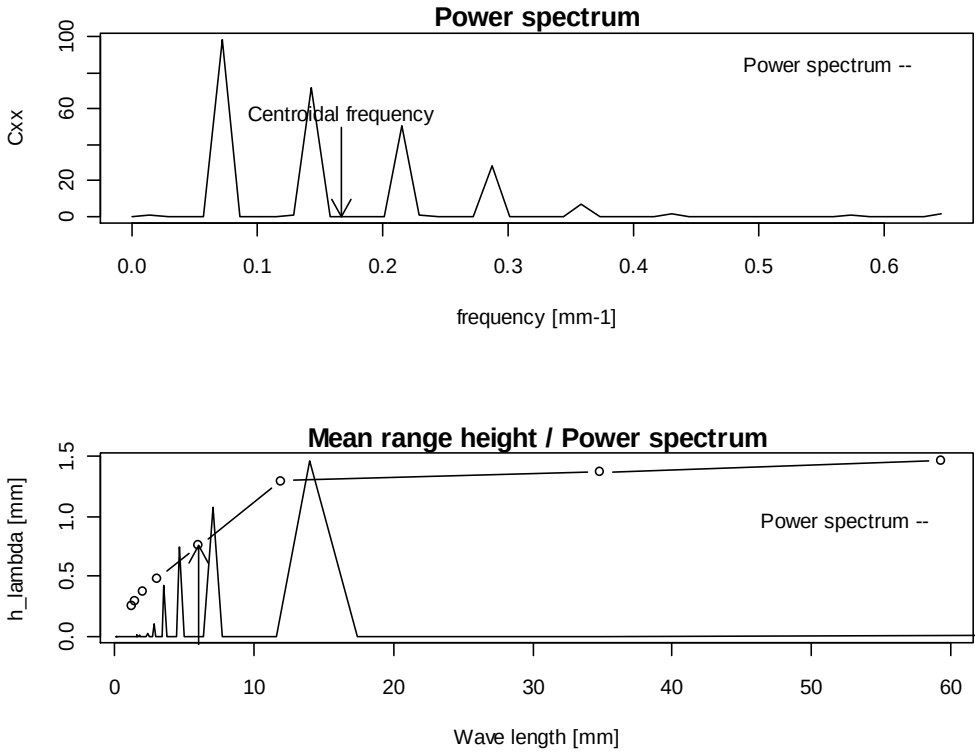

Figure B.37 Power spectrum and mean range height plots for T6, first run.

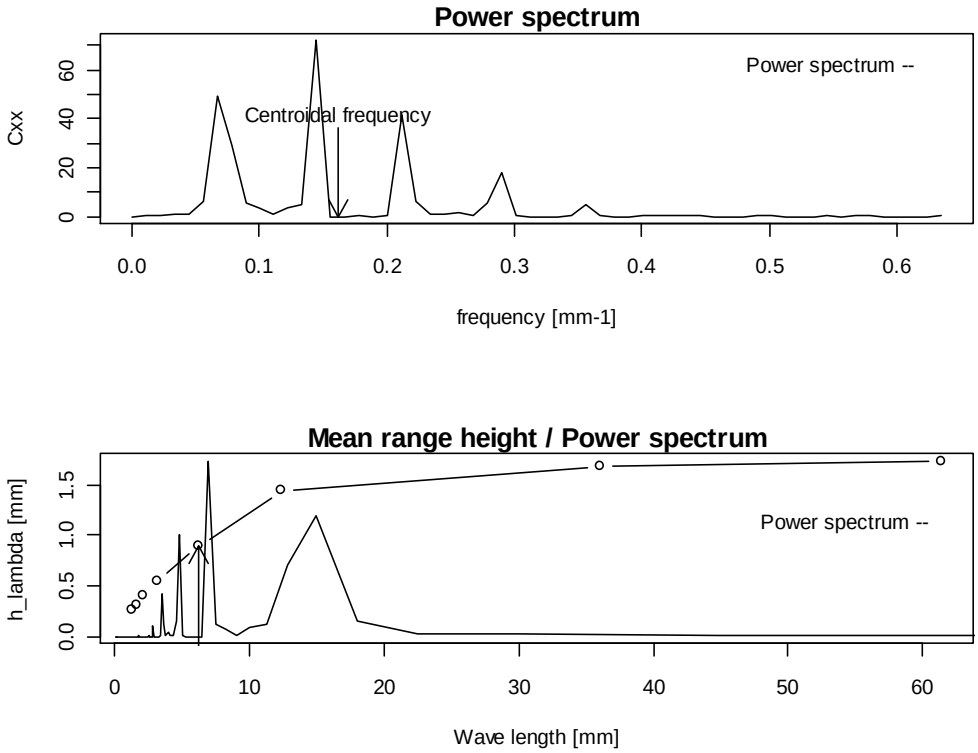

Figure B.38 Power spectrum and mean range height plots for T6, second run.

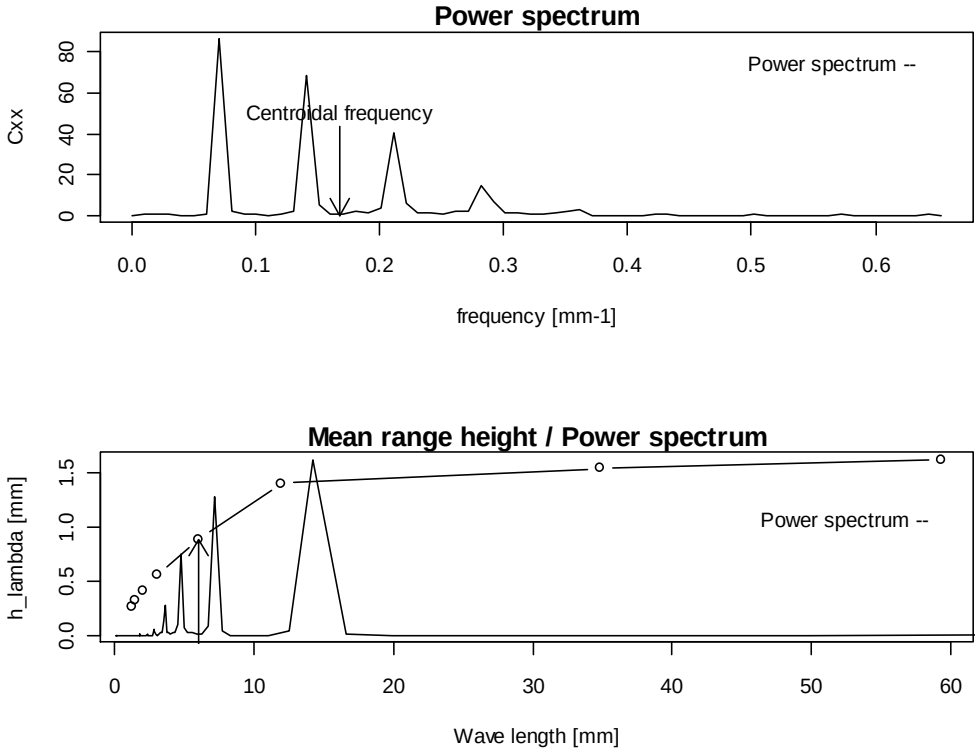

Figure B.39 Power spectrum and mean range height plots for T6, third run.

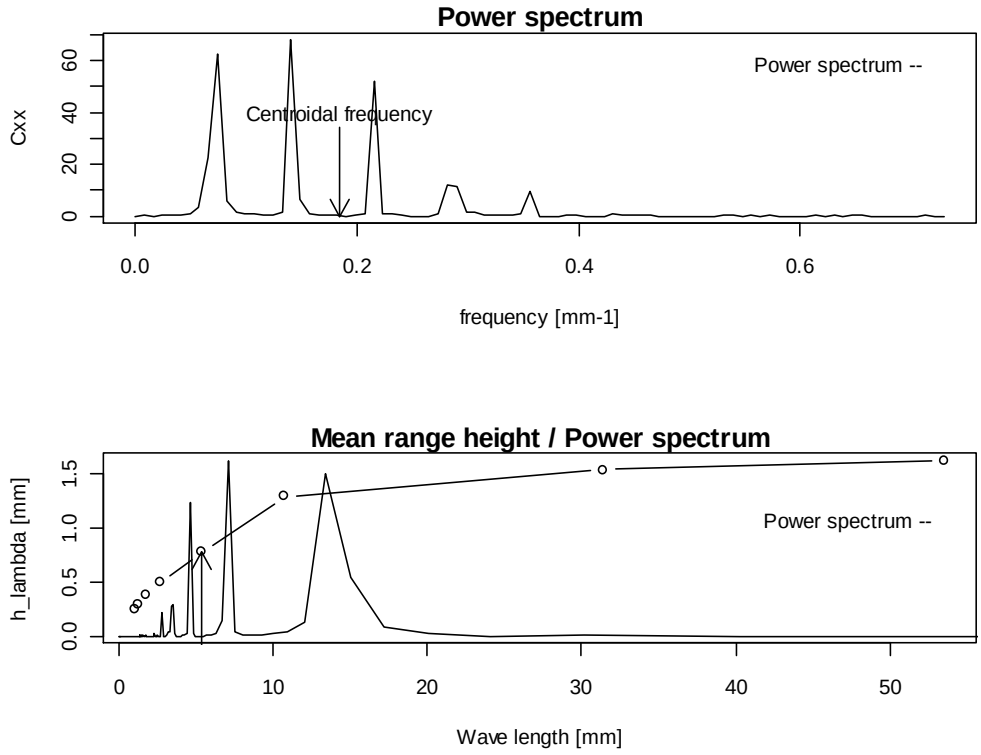

Figure B.40 Power spectrum and mean range height plots for T6, fourth run.

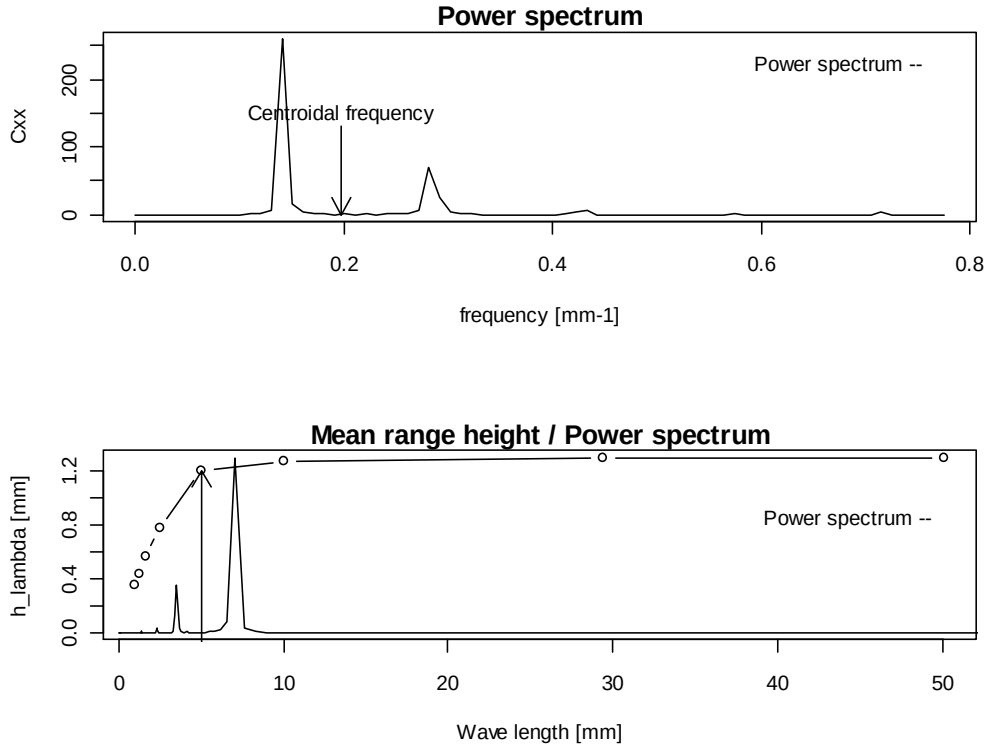

Figure B.41 Power spectrum and mean range height plots for T8, first run.

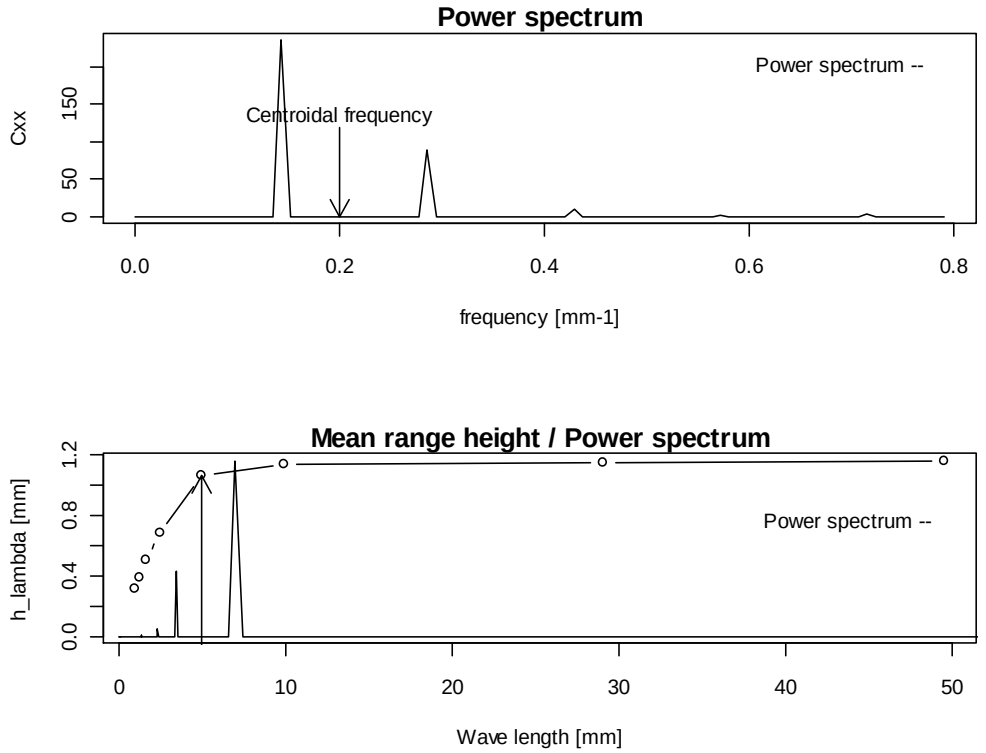

Figure B.42 Power spectrum and mean range height plots for T8, second run.

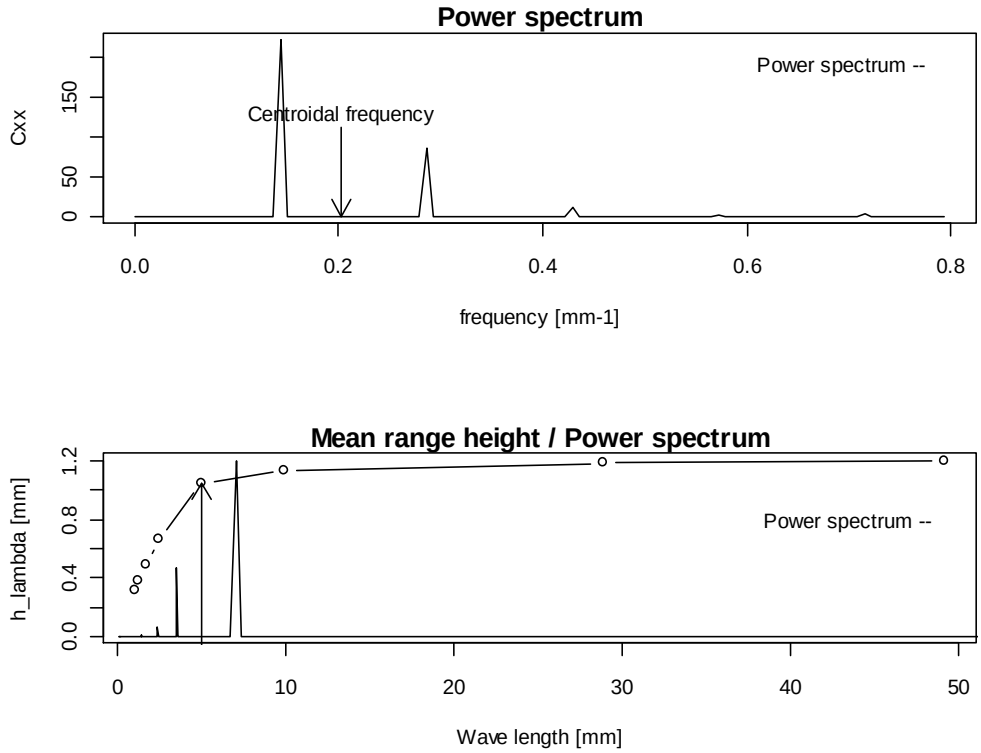

Figure B.43 Power spectrum and mean range height plots for T8, third run.

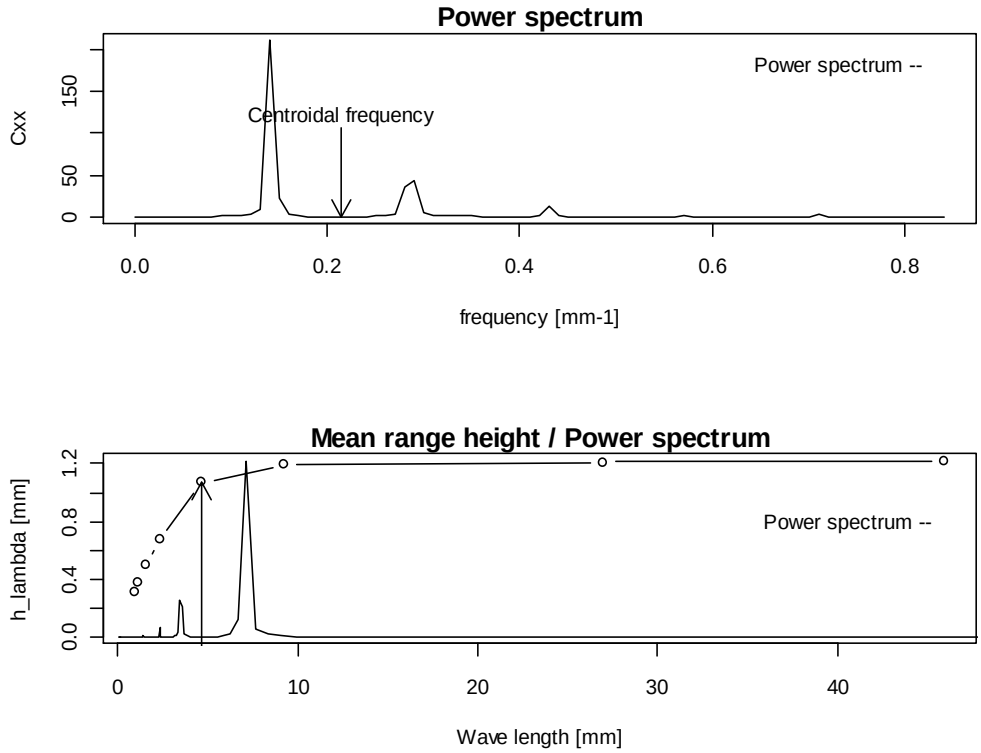

Figure B.44 Power spectrum and mean range height plots for T8, fourth run.

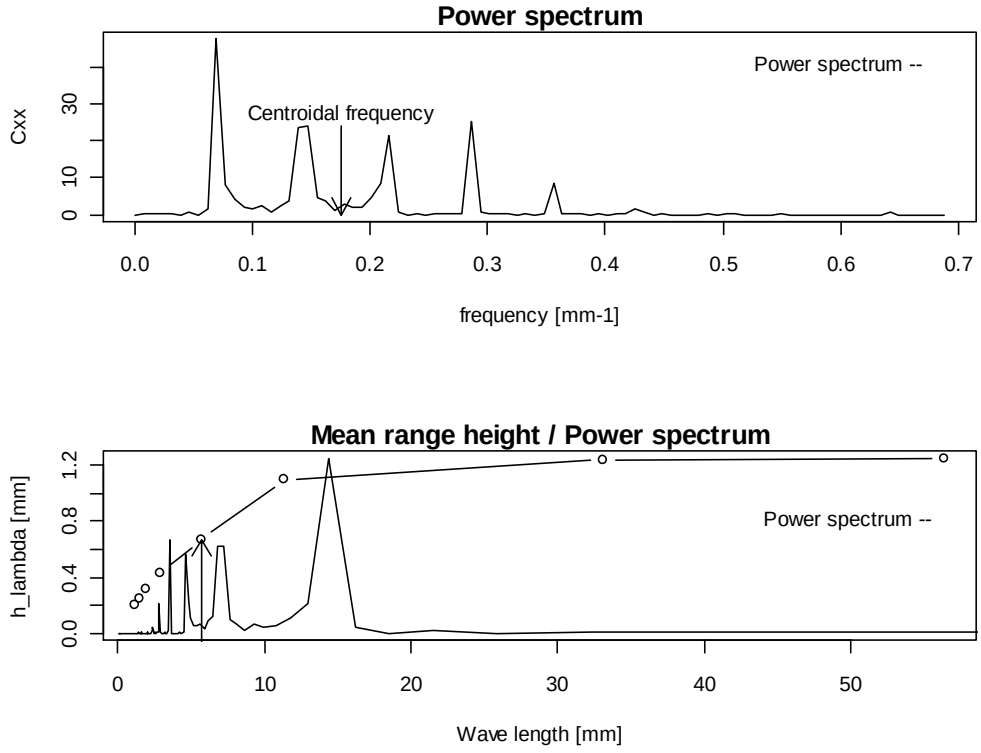

Figure B.45 Power spectrum and mean range height plots for T9, first run.

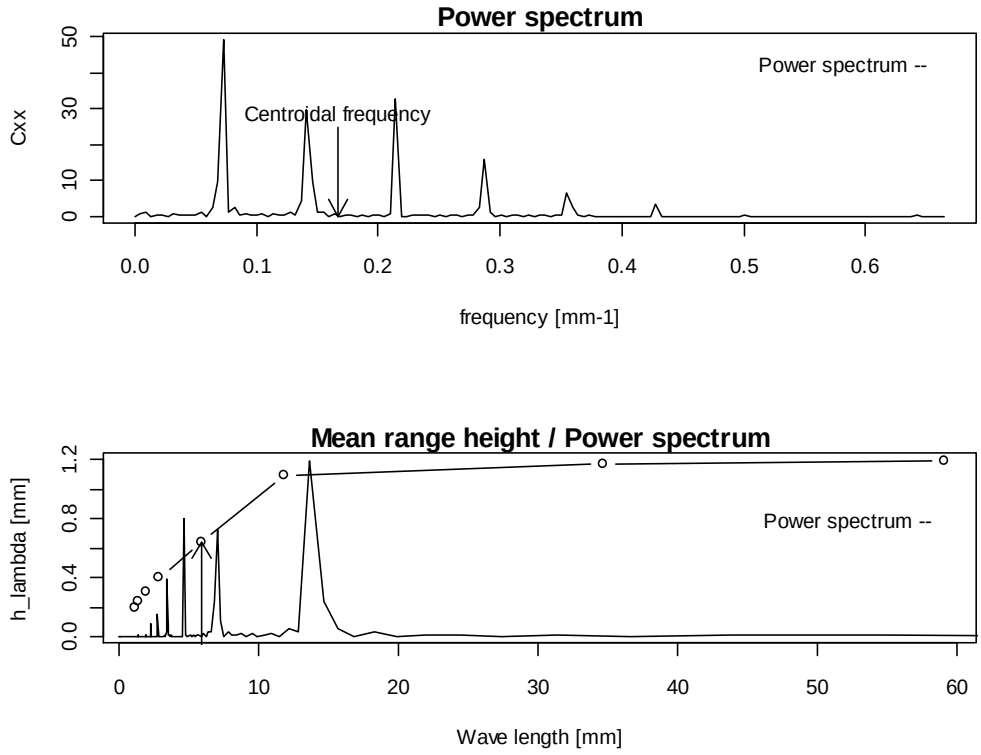

Figure B.46 Power spectrum and mean range height plots for T9, second run.

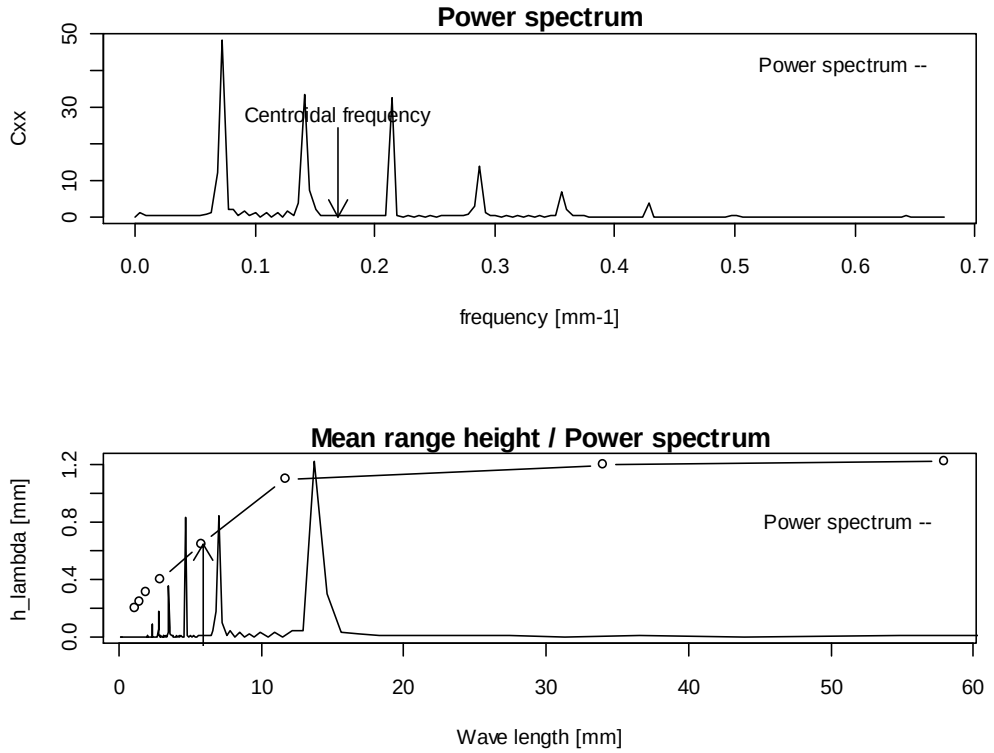

Figure B.47 Power spectrum and mean range height plots for T9, third run.

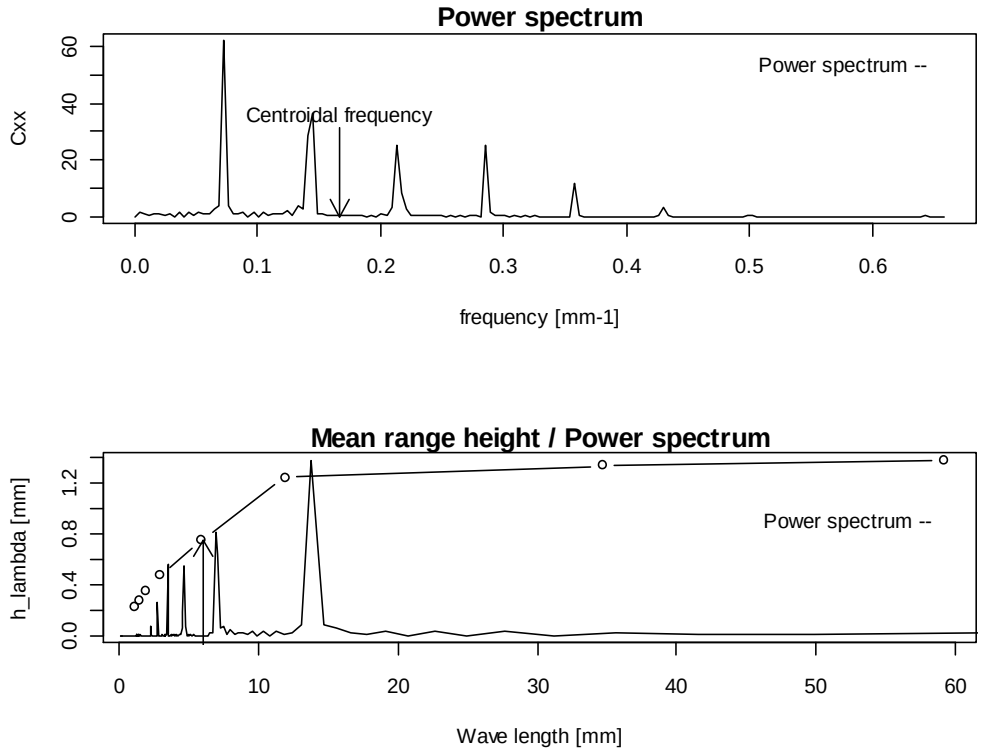

Figure B.48 Power spectrum and mean range height plots for T9, fourth run.

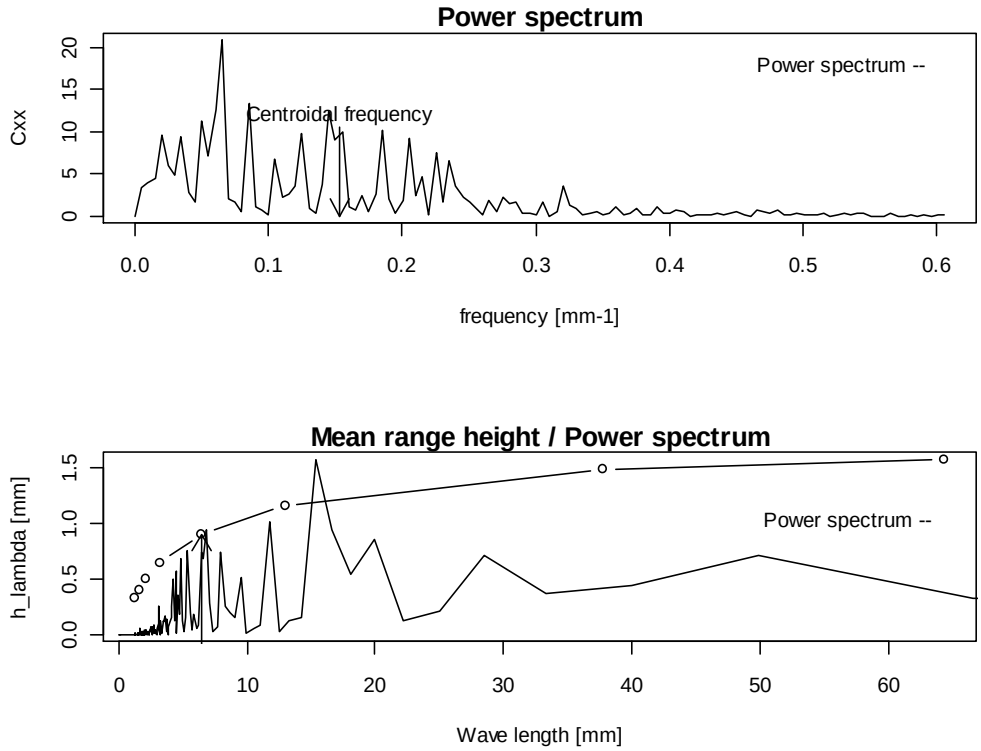

Figure B.49 Power spectrum and mean range height plots for T10, first pipe, first run.

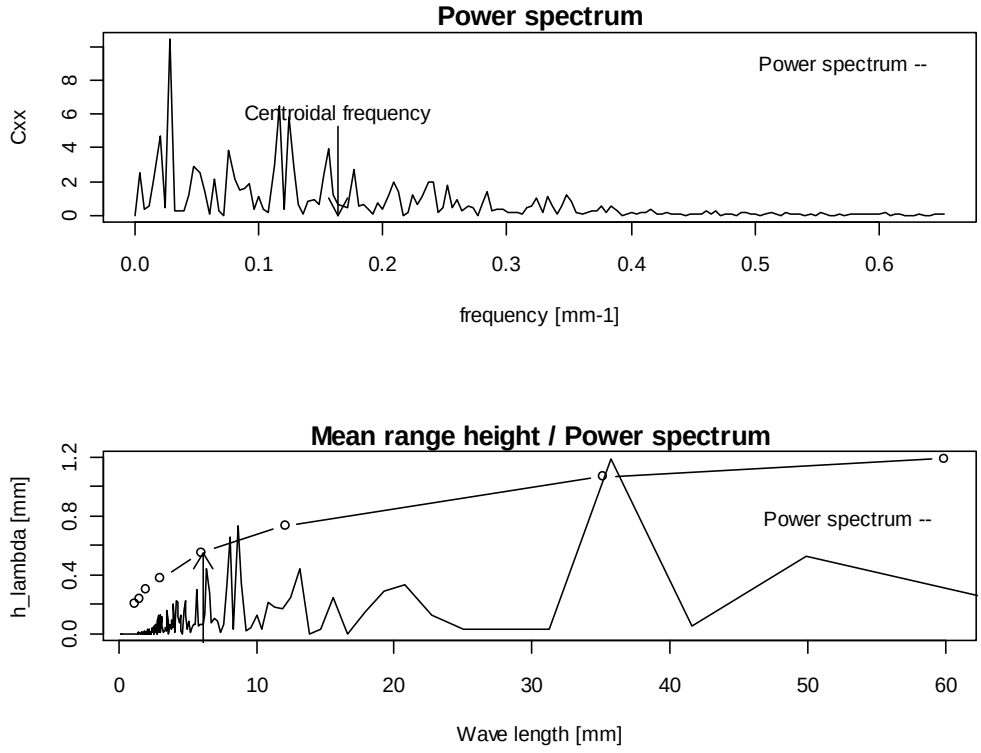

Figure B.50 Power spectrum and mean range height plots for T10, first pipe, second run.

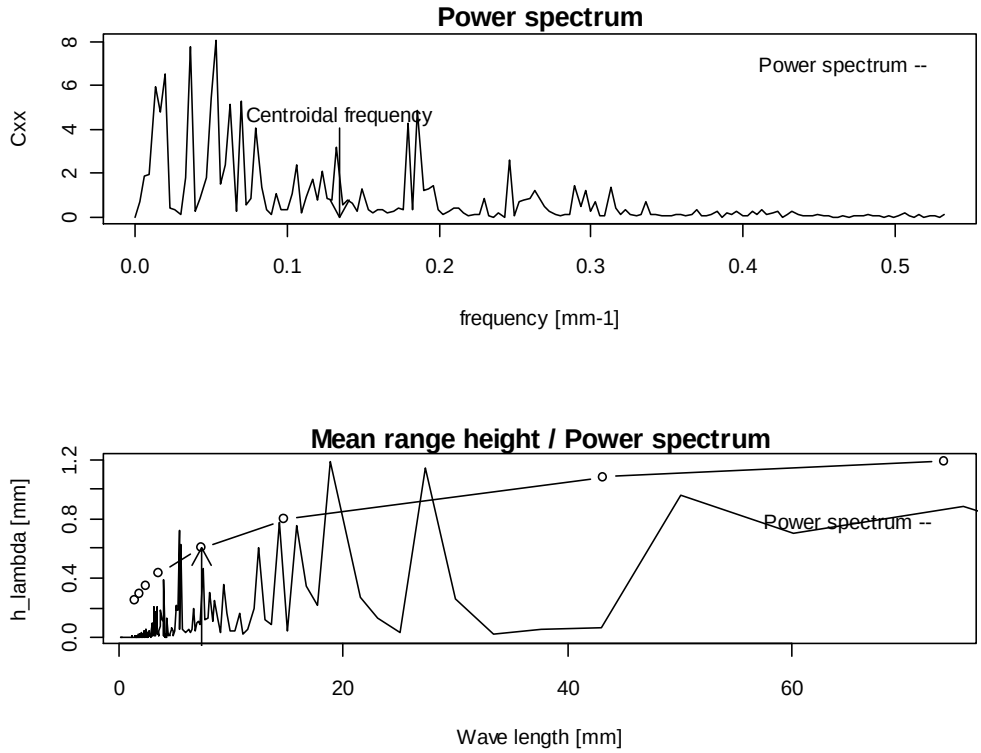

Figure B.51 Power spectrum and mean range height plots for T10, first pipe, third run.

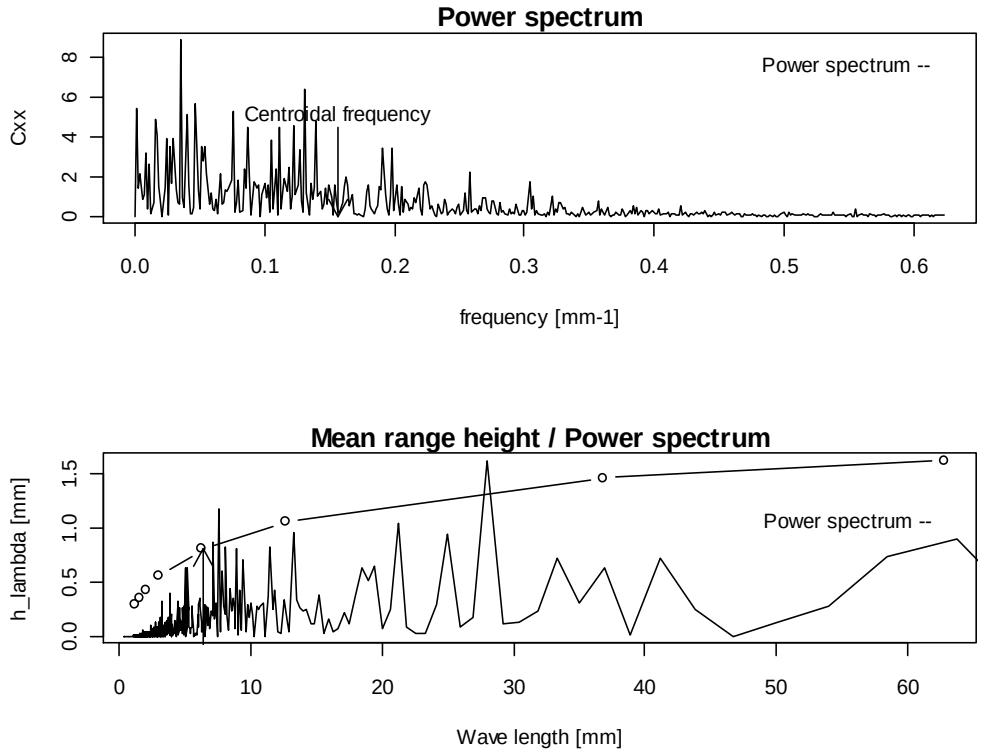

Figure B.52 Power spectrum and mean range height plots for T10, first pipe, fourth run.

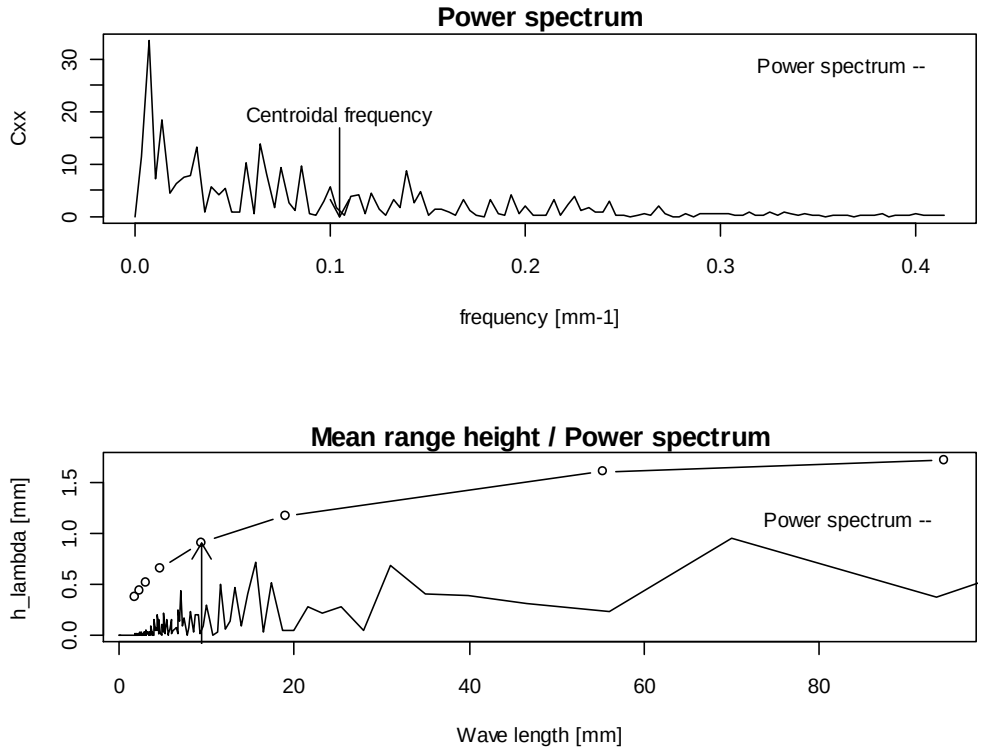

Figure B.53 Power spectrum and mean range height plots for T10, third pipe, first run.

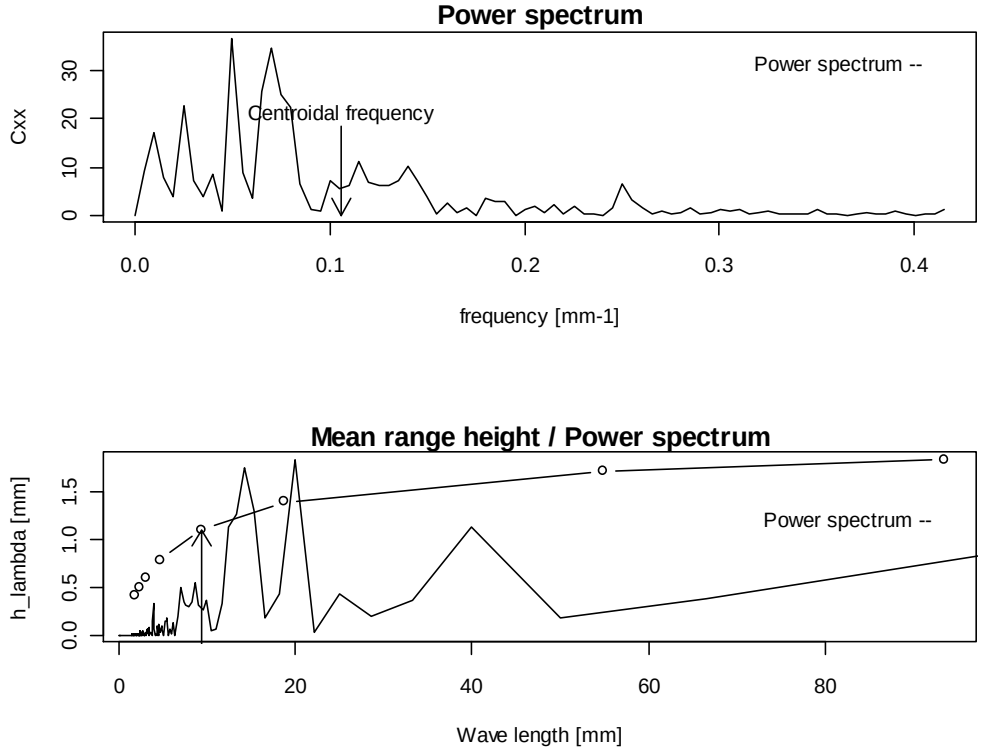

Figure B.54 Power spectrum and mean range height plots for T10, third pipe, second run.

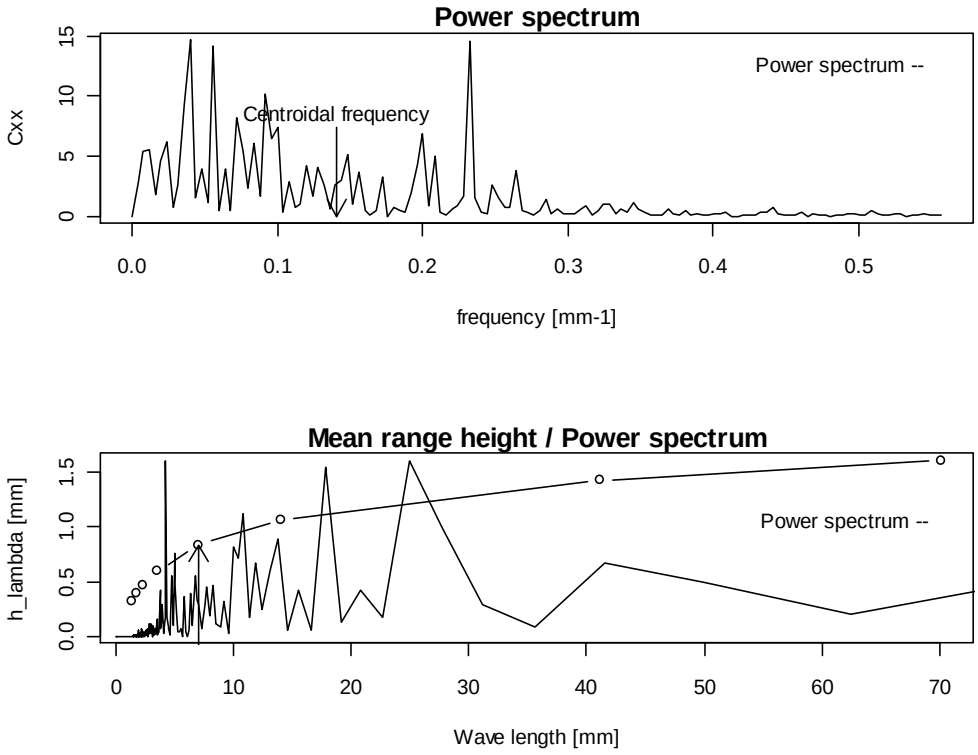

Figure B.55 Power spectrum and mean range height plots for T10, third pipe, third run.

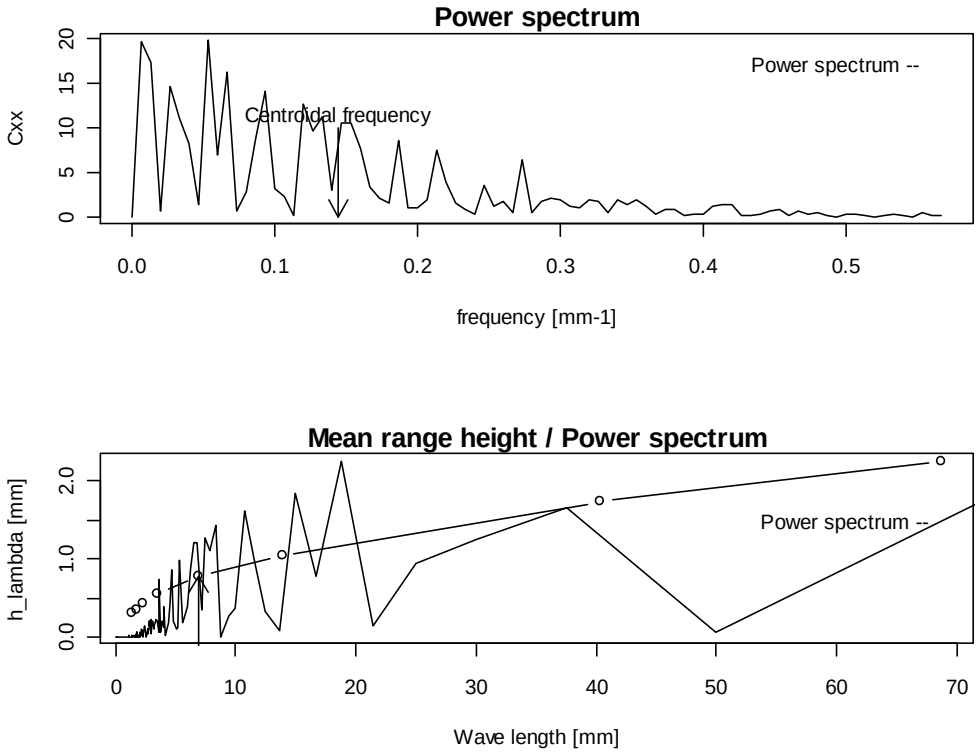

Figure B.56 Power spectrum and mean range height plots for T10, third pipe, fourth run.